Effects of intergenerational transmission of small intestinal bacteria cultured from stunted Bangladeshi children with enteropathy

Kali M. Pruss[1,2]†, Clara Kao[1,2]†, Alexandra E. Byrne[1,2], Robert Y. Chen[1,2], Blanda Di Luccia[1,2,3], Laura Karvelyte[3], Reyan Coskun[1,2], Mackenzie Lemieux[1,2], Keshav Nepal[1,2], Daniel M. Webber[1,2], Matthew C. Hibberd[1,2], Yi Wang[1,2], Dmitry A. Rodionov[4], Andrei L. Osterman[4], Marco Colonna[3], Christian Maueroder[5], Kodi Ravichandran[3], Michael J. Barratt[1,2], Tahmeed Ahmed[6] and Jeffrey I. Gordon[1,2]*

[1]The Edison Family Center for Genome Sciences and Systems Biology, Washington University School of Medicine; St. Louis, MO 63110, USA

[2]The Newman Center for Gut Microbiome and Nutrition Research, Washington University School of Medicine; St. Louis, MO 63110, USA

[3]Division of Immunobiology, Department of Pathology and Immunology, Washington University School of Medicine; St. Louis, MO 63110, USA

[4]Infectious and Inflammatory Disease Center, Sanford Burnham Prebys Medical Discovery Institute, La Jolla, CA 92037 USA

[5]Inflammation Research Centre, VIB, and the Department of Biomedical Molecular Biology, Ghent University, Ghent, Belgium

[6]International Center for Diarrhoeal Disease Research, Bangladesh (icddr,b); Dhaka 1212, Bangladesh

†These authors contributed equally to this work.

*Corresponding author email: jgordon@wustl.edu

Environmental enteric dysfunction (EED), a small intestinal disorder found at a high prevalence in stunted children, is associated with gut mucosal barrier disruption and decreased absorptive capacity[1–4]. To test the hypothesis that intergenerational transmission of a perturbed small intestinal microbiota contributes to undernutrition by inducing EED[5], we characterized two consortia of bacterial strains cultured from duodenal aspirates from stunted Bangladeshi children with EED – one of which induced local and systemic inflammation in female gnotobiotic mice. Offspring of dams colonized with the inflammatory consortium exhibited impaired prenatal and postnatal growth, as well as immunologic changes phenocopying features of EED in children. Dam-to-pup transmission of the inflammatory consortium produced, in recently weaned offspring, alterations in (i) inter-cellular signaling pathways related to intestinal epithelial cell renewal, barrier integrity and immune function plus (ii) glial- and endothelial-neuronal signaling pathways that regulate neural growth, angiogenesis and inflammation in the cerebral cortex. Cohousing of mice harboring the inflammatory or non-inflammatory consortia and subsequent screening of candidate disease-promoting bacterial isolates identified *Campylobacter concisus,* an organism typically found in the oral microbiota, as a contributor to enteropathy. The *C. concisus* strain induced, in a host nitric oxide synthase (NOS)-dependent manner, pro-inflammatory cytokine signaling. Moreover, host-derived nutrients generated by NOS augmented *C. concisus* growth. This preclinical model should facilitate identification of small intestinal microbiota-targeted therapeutics for (intergenerational) undernutrition.

Undernutrition is a significant global health challenge. Numerous epidemiologic studies indicate that stunting in mothers is associated with low birth weight and postnatal linear growth faltering (stunting) in their offspring[6,7]. Stunting in infants and children is accompanied by increased risk of infection, metabolic/hormonal imbalances later in life[8], as well as neurodevelopmental/cognitive abnormalities[9–11].

One hypothesis is that a perturbed small intestinal microbiota[2] contributes to undernutrition by inducing environmental enteric dysfunction (EED)[1,12–14] and subsequent transmission of the maternal small intestinal microbiota to offspring perpetuates intergenerational EED[5]. Evidence that the small intestinal microbiota contributes to the pathogenesis of EED comes in part from the Bangladeshi EED (BEED) study, in which stunted children who had failed to respond to a nutritional intervention underwent esophago-gastroduodenoscopy (EGD)[2,15]. Almost all (95%) of these children displayed histopathologic evidence of EED[2]. Sequencing bacterial 16S rRNA amplicons generated from duodenal aspirates collected during EGD revealed a 'core' group of 14 taxa (amplicon sequence variants, ASVs) that were present in >80% of the children. The absolute abundances of these taxa, not typically classified as enteropathogens, were significantly negatively correlated with linear growth (length-for-age Z score, LAZ) and positively correlated with levels of duodenal mucosal proteins involved in immunoinflammatory responses[2].

Deciphering the role of the small intestinal microbiota in the pathogenesis of EED has been hampered by several factors. For example, EGD is limited to the proximal intestine and carries potential risks, precluding, for ethical reasons, its use in healthy children to define what constitutes a 'normal' small intestinal microbiota. In addition, the volume of fluid and biomass of microbes that can be retrieved from the lumen of the small intestine with EGD is small, limiting the number of ways the material can be employed for downstream analyses. Moreover, preclinical studies are necessary to define mechanisms and establish causal relationships between members of the microbiota and EED. Current mouse models rely on either provision of a low-protein diet, which has not been explicitly defined as a causative factor for EED in humans, and/or administration of a single pathogen or a broad inflammatory insult (e.g. treatment with LPS)[16–19]. While these models are valuable for understanding effects of protein restriction on immunity and the virulence mechanisms of enteric pathogens, they do not simulate the complexity of small intestinal bacterial community dynamics and interactions with the host that likely play a role in pathophysiology of EED in humans.

In the current study, we sought to model maternal-to-offspring transmission of different small intestinal bacterial consortia from children in the BEED study that elicit discordant intestinal and systemic inflammatory responses in gnotobiotic mice. Our goal was to use these consortia to obtain insights about

host cellular and molecular responses and to identify bacteria that have a causal role in pathology associated with EED.

Results

Development of inflammatory and non-inflammatory EED-derived bacterial consortia

In a previous pilot study[2], a collection of 184 bacterial isolates cultured from the duodenal aspirates of children in the BEED study were pooled and introduced by oral gavage directly into adult germ-free mice fed a diet formulated based on foods consumed by children living in Mirpur, Bangladesh, the urban slum where the clinical study was performed ('Mirpur-18' diet, **Supplementary Table 1a**). Compared to controls gavaged with intact cecal contents from conventionally-raised mice (conventionalized animals, CONV-D), the duodenal aspirate-derived culture collection induced an enteropathy characterized by (i) patchy immunoinflammatory infiltrates in the small intestine, (ii) increased duodenal crypt depth, (iii) reduced expression of tight junction proteins and increased expression of genes involved in anti-microbial defense (*Reg3β* and *Reg3γ*) in the duodenum, and (iv) elevated levels of matrix metalloproteinase 8 (MMP8) in serum as well as along the length of the small intestine[2].

We sought to reduce the complexity of the 184-member bacterial consortium derived from the EED donors. To do so, we chose a representative of each bacterial species (based on sequencing full-length 16S rRNA amplicons, **Supplementary Table 1b**) and pooled these 39 isolates into a 'species-representative subset consortium'. These two consortia were gavaged into separate groups of just-weaned 4-5-week-old germ-free mice (n=5 animals/group) fed the Mirpur-18 diet. Mice colonized with all 184 isolates gained significantly less weight over 28 days than mice colonized with the species-representative subset (**Extended Data Fig. 1a, Supplementary Table 2a**). Serum levels of insulin-like growth factor 1 (IGF-1) were significantly correlated with body mass at 9 and 28 days after colonization across all animals (**Extended Data Fig. 1b**), although there were no statistically significant differences between treatment groups (**Supplementary Table 2b**). Leptin levels were diminished compared to CONV-D animals, but not significantly different between mice that received the 184-member and species-representative consortia (**Extended Data Fig. 1c, Supplementary Table 2b**). Together, these results suggest that additional factors contributed to the reduced weight gain observed in animals that received the complete consortium.

Sequencing of RNA isolated from the duodenums, jejunums and ileums of these animals followed by gene set enrichment analysis (GSEA) revealed that a large proportion of the gene ontology (GO) categories that were significantly enriched ($q<0.05$) between animals colonized with the full versus subset bacterial consortia were related to immune function, including genes involved in the anti-bacterial defense response and leukocyte activation (**Extended Data Fig. 1d,e**). Levels of the protein lipocalin-2 (LCN2/NGAL; neutrophil gelatinase-associated lipocalin) were also significantly elevated in the serum of mice colonized with the full 184-isolate consortium (**Extended Data Fig. 1f**); previously we had observed that LCN2 levels in the duodenal mucosa of children with EED were strongly correlated with the absolute abundances of the 14 duodenal EED-associated 'core taxa'[2]. Based on the higher levels of intestinal and systemic inflammation in animals colonized with the full consortium of EED-derived bacteria, we named this community 'child small intestinal inflammation-inducing' (cSI-I); the species-representative subset was designated 'child small intestinal non-inflammatory' (cSI-N).

Modeling maternal-offspring transmission of EED donor small intestinal bacterial consortia

As a prelude to determining whether inflammation induced by the cSI-I consortium could be transmitted from dams to their offspring, we performed a diet oscillation experiment. Adult germ-free animals fed a standard mouse diet were colonized with either the cSI-I or cSI-N consortium. Mice were maintained on the standard chow for one week, then given a diet designed to be representative of that consumed by adults residing in the Mirpur district of Dhaka ('Adult Mirpur' diet; **Supplementary Table 1a**), followed by a return to standard diet for one week. LCN2 levels were measured in serum samples obtained at the end of each of the 7-day diet periods (**Extended Data Fig. 1g**). Statistically significant increases in systemic inflammation were documented in both groups of mice when fed Adult Mirpur compared to

standard mouse diet. Moreover, LCN2 levels were significantly higher in mice colonized with cSI-I compared to cSI-N in both diet contexts (**Extended Data Fig. 1h, Supplementary Table 2b**).

Based on these results, germ-free adult female C57Bl/6J mice were placed on the 'Adult Mirpur' diet. Three days later, separate groups of animals (n=4 dams/group) received an oral gavage of the cSI-I or cSI-N consortia, or intact cecal contents from conventionally raised adult C57Bl/6J mice (**Fig. 1a, Extended Data Fig. 2a**). One week after colonization, female mice were mated with germ-free males. Pups born to these dams were weaned onto the 'Mirpur-18' diet (**Supplementary Table 1a**) which they consumed *ad libitum* until euthanasia on postnatal day 37 (P37). To assess the reproducibility and timing of onset of EED features, second and third litters produced by the same dams were euthanized either on P37 or P14, respectively (**Extended Data Fig. 2a,b**).

We identified bacterial members of each consortium that successfully colonized recipient dams and were transmitted to their offspring using long-read shotgun DNA sequencing of cecal contents from dams and P37 pups followed by assembly of metagenome-assembled genomes (MAGs) (n=4 dams and n=22-25 offspring/consortium). We reasoned that this approach would be useful for initial characterization of colonizing members of culture collections where multiple strains of a given species may exist. A total of 51 unique high-quality MAGs (defined as ≥85% complete and ≤5% contaminated based on marker gene analysis, **Supplementary Table 1c**) were generated from cecal contents of dams and P37 offspring harboring either of the two cSI consortia. A total of 25 MAGs from the cSI-I consortium colonized dams and all were represented in their P37 offspring (**Extended Data Fig. 2c**). Twenty-eight MAGs from the cSI-N consortium colonized dams; all 28 also colonized their P37 offspring (threshold criteria for colonization: >0.0001% relative abundance in at least one intestinal segment in at least 50% of animals, **Supplementary Table 1d, Extended Data Fig. 2c**). Based on short-read shotgun sequencing-based calculations of MAG abundances in fecal samples collected from dams, the cSI-I and cSI-N communities remained stable between 4 and 17 weeks after gavage of these cultured consortia even if the animals had one or more litters during this period (P=0.09, PERMANOVA; n=4 dams/group; **Extended Data Fig. 2d,e**).

The absolute abundances of 21 MAGs were significantly higher in at least one intestinal segment of P37 offspring colonized with the cSI-I consortium compared to cSI-N; the taxonomy of 12 of these 21 MAGs corresponded to ASVs we previously identified as 'core taxa' present in >80% of the duodenal microbiota of Bangladeshi children with duodenal mucosal biopsy-diagnosed EED (**Fig. 1b**)[2]. Moreover, analysis of fecal samples collected from the diet oscillation experiment described in **Extended Data Fig. 1g**, disclosed that 19 of these 21 MAGs were significantly higher in cSI-I compared to cSI-N adult mice when fed either Adult Mirpur or standard mouse diets (**Extended Data Fig. 2f,g**). Fewer MAGs were detected in P14 offspring (88% of MAGs that colonized cSI-I dams; 68% of cSI-N MAGs that colonized dams). Of the 21 MAGs with significantly higher absolute abundance in P37 cSI-I offspring compared to their cSI-N counterparts, seven were significantly higher in the cecum and/or colon of P14 offspring (**Extended Data Fig. 3a**).

Effects on prenatal and postnatal growth

We colonized a separate group of adult female mice with the cSI-I or cSI-N consortia two weeks before mating. Pregnant dams were euthanized when placentation just completed (embryonic day 11.5, E11.5) or near the end of gestation (E17.5). Fetal weights were significantly lower in cSI-I compared to cSI-N dams at E17.5 (**Fig. 1c,** n=7-9 dams/group; n=2-10 fetuses/litter), but not at E11.5 (n=9-10 dams/group; n=4-8 fetuses/litter) (**Extended Data Fig. 3b**; **Supplementary Table 2a**). Placental weights were not significantly different between treatment groups at either timepoint (**Extended Data Fig. 3c,d, Supplementary Table 2a**).

Body mass (**Extended Data Fig. 3e**) and serum levels of IGF-1 (**Extended Data Fig. 3f**) were significantly reduced in pre-weaning (P14) offspring of cSI-I dams compared to their cSI-N counterparts (**Supplementary Table 2a,b**). P14 cSI-I pups displayed significantly higher serum levels of the pro-inflammatory proteins LCN2, S100A9 (S100 calcium binding protein A9), CHI3L1 (Chitinase-3-like protein 1), MMP8 (matrix metallopeptidase 8, or neutrophil collagenase), as well as the immune cell chemoattractant CXCL1 (chemokine ligand 1) compared to their cSI-N and CONV-D counterparts

(**Extended Data Fig. 3g-j**; **Supplementary Table 2b**). LCN2, CHI3L1, S100A9 and MMP8 belong to a group of inflammatory proteins whose expression in duodenal mucosal biopsies was significantly positively correlated with the abundances of the 'core' EED-associated bacterial taxa in Bangladeshi children with EED[2]. LCN2, S100A9 and CHI3L1 were similarly elevated in duodenal, ileal and colonic tissue of cSI-I animals (**Extended Data Fig. 3k-m, Supplementary Table 2b**). Thus, systemic and intestinal inflammation were already evident in these animals prior to completion of weaning.

Characterization of enteropathy in P37 offspring of cSI-I dams

Postnatal day 14 represents a critical period of brain development as well as maturation of lymphoid organs and the adaptive immune system. To determine whether the effects of the cSI-I and cSI-N consortia persisted through the weaning period, we assessed offspring on P37, which represents a developmental state more akin to adolescents[20]. Children with EED have villus blunting: histomorphometric analyses of the small intestines of P37 offspring of cSI-I dams revealed significantly diminished duodenal villus height (**Fig. 1d**) and a significantly diminished ratio of villus height to crypt depth in the duodenum and ileum compared to their cSI-N counterparts (**Fig. 1e, Extended Data Fig. 4a**; **Supplementary Table 2c**). Crypt depth in the ileum of P37 cSI-I mice trended towards increased relative to cSI-N animals (P=0.09, Wilcoxon rank-sum). The observed increase in crypt depth is consistent with the notion that there is a proliferative response involving stem and transit-amplifying cells in this model, but one that is insufficient to restore villus height (see '***Proliferative signaling to stem and transit-amplifying cells'*** below).

LCN2 levels in duodenal, ileal and colonic tissue, as well as serum, were significantly elevated in P37 mice born to dams harboring the cSI-I compared to the cSI-N consortium, or to conventionalized (CONV-D) dams (**Figs. 1f,g**). S100A9, MMP8, CXCL1 and IL-17 were similarly elevated in the serum of P37 cSI-I offspring (**Fig. 1h**, **Extended Data Fig. 4b,c**; **Supplementary Table 2b**). As in P14 animals, duodenal, ileal and colonic tissue levels of S100A9 and CHI3L1 were significantly higher in P37 offspring of cSI-I dams (**Extended Data Fig. 4d,e**; **Supplementary Table 2b**). There were no statistically significant differences in the serum levels of these proteins between litters, nor between male and female offspring in the same treatment group (P>0.05, Wilcoxon rank-sum tests).

Compared to P37 cSI-N and CONV-D mice, serum levels of Dickkopf-1 (DKK1), Osteoprotegerin (OPG) and Fibroblast Growth Factor-23 (FGF23) were significantly higher in cSI-I animals, indicating increased osteocyte and bone remodeling activity (P<0.015 for all comparisons, Wilcoxon rank-sum test; **Supplementary Table 2b**). Micro-computed tomography of femurs disclosed significantly increased cortical tissue mineral density in P37 cSI-I versus cSI-N animals (P=0.03, Wilcoxon rank-sum test; n=19-21 mice/group); no significant differences in other cortical and trabecular parameters were found between the three treatment groups (**Supplementary Table 2d**).

Small intestinal tissue acylcarnitines – Plasma acylcarnitines are elevated in a fasting state and have been identified as a biomarker of EED in children[21]. Moreover, fecal acylcarnitines are elevated in the dysbiotic microbial states associated with inflammatory bowel disease[22] and can activate pro-inflammatory signaling cascades[23,24]. We quantified acylcarnitine levels in intestinal tissue instead of plasma to directly examine whether differences in host fatty acid metabolism were produced as a result of colonization with the cSI-I compared to the cSI-N consortium. Several medium and long-chain acylcarnitines were significantly elevated in the intestine of cSI-I compared to cSI-N or CONV-D offspring (**Extended Data Fig. 4f, Supplementary Table 2e**), suggesting that the carnitine shuttle may be impaired in the intestine.

Flow cytometry of immune cell populations in the intestinal lamina propria –The frequency of neutrophils was significantly increased in the duodenum of P37 cSI-I offspring, but not in the ileum or colon (**Fig. 1i**). $CD3^+$ and $CD4^+$ cells were also higher in the duodenum, ileum and colon of cSI-I animals compared to age-matched cSI-N or CONV-D mice (**Extended Data Fig. 4g,h**). Among $CD4^+$ cells, the Th17 population was significantly higher in the duodenum, ileum and colon of cSI-I offspring (**Fig. 1j**), whereas Th1 cells were diminished in their duodenum and Tregs were diminished in their duodenum and colon (**Supplementary Table 2f**); these findings lead us to speculate that a pro-inflammatory cytokine milieu in the intestines of P37 cSI-I offspring promotes Th17 cell differentiation and proliferation.

These protein biomarker, neutrophil, and T cell phenotypes were also evident in dams: the frequencies of duodenal neutrophils, $CD3^+$ cells, $CD4^+$ T cells and Th17 cells were all significantly elevated in cSI-I adult female mice. Th1 cells and Tregs were similarly significantly reduced in cSI-I compared to cSI-N mothers ($P<0.05$ for all comparisons, Wilcoxon rank-sum test; n=5 mice/group; **Supplementary Table 2f**). The observed increases in $CD3^+$ cells and $CD4^+$ T cells in the intestinal tissues of dams and their offspring harboring cSI-I compared to cSI-N consortia are consistent with prior characterization of EED in children as a T-cell mediated enteropathy[13,25].

Characterizing gene expression in the intestine at a tissue and cellular level

Single nucleus RNA-sequencing (snRNA-Seq) – To characterize the responses of different intestinal epithelial cell types to the EED donor-derived bacterial consortia, we performed snRNA-Seq on intact segments of frozen duodenum and ileum harvested from P37 cSI-I and cSI-N mice. A total of 15,135 duodenal nuclei (**Fig. 2a**) and 20,584 ileal nuclei (**Fig. 2b**) collected from 3 littermates/group passed our quality metrics (see *Methods*). Analysis of marker gene expression identified nuclei from epithelial lineages (stem and transit amplifying cells and their enterocyte, goblet, Paneth, enteroendocrine and tuft cell descendants), as well as from mesenchymal lineages (endothelial, smooth muscle, neuronal, immune and interstitial cells of Cajal). Enterocytes comprised the largest proportion of nuclei (**Supplementary Table 3b**) and based on marker gene expression were divided into villus base, mid-villus and villus tip subpopulations. A significantly higher proportion of Paneth cells were present in the duodenum of cSI-I offspring than their cSI-N counterparts (**Supplementary Table 3b**). Increased density[26] of Paneth cells as well as degranulation[27] have both been reported in Zambian children with EED.

'Pseudo-bulk' analysis of differential gene expression in enterocytes positioned at different locations along the crypt-villus axis in both the duodenum and ileum revealed an enhanced epithelial immune response in P37 cSI-I compared to cSI-N mice. Of the 133 GO categories significantly enriched in at least two subpopulations of enterocytes in cSI-I offspring, 35 were involved in bacterial recognition and defense, as well as recruitment/migration and activation of immune cells (**Extended Data Fig. 5a, Supplementary Table 3c**).

Epithelial homeostasis requires a balance of differentiation, programmed cell death, and clearance of dying cells and cellular debris. This process, termed 'efferocytosis', involves recognition and clearance of dying cells by phagocytes, including both professional phagocytes and healthy neighboring intestinal epithelial cells[28–30]. Efferocytosis can be viewed as a process that sits at the interface between regulation of gut epithelial renewal, inflammation and the microbiota[31]. Based on published literature[32–34], we manually curated an 'efferocytosis' gene set composed of 273 genes. This gene set was significantly enriched in cSI-I mid-villus duodenal enterocytes ($P=0.019$, **Extended Data Fig. 5b**). Genes enriched in cSI-I duodenal enterocytes included caspases linked to apoptosis (*Casp3*), genes linked to phosphatidylserine exposure during apoptosis (*Xkr8, ATP11c*), a channel that regulates apoptotic cell communication with the microbiota (*Panx1*), several efferocytotic receptors/recognition mediators (*Mertk, Stab1*, *Mfge8*), as well as cytosolic proteins linked to intracellular signaling during efferocytosis (*Elmo1, Elmo2, Dock1, Crk*, see **Supplementary Table 3c**). These findings suggest that apoptosis and subsequent efferocytosis within the small intestine play a role in shaping the epithelial response to the cSI-I consortium.

Proliferative signaling to stem and transit-amplifying cells – To assess the effects of the SI consortia on epithelial regeneration, we used the algorithm *NicheNet*[35,36] to characterize intercellular signaling in cSI-I versus cSI-N P37 offspring. *NicheNet* surveys expression of known protein ligands by user-designated 'sender' cell types and their cognate receptors within a 'receiver' population. For our analysis, we defined stem and transit amplifying (stem/TA) cells as 'receivers' and all other cell types within the SI as 'senders' (**Fig. 2c**). Bone morphogenetic protein (Bmp), Wnt and Notch signaling are three of the major pathways that mediate cellular proliferation during normal intestinal development, responses to injury and hyperplastic inflammatory responses[37,38]. In the ileum, ligands more highly expressed in cSI-I compared to cSI-N mice included *Wnt3* in Paneth cells (and their receptors *Lrp6, Ryk* and *Bmpr1a* in TA/stem cells, **Extended Data Fig. 6a, Supplementary Table 3c**), as well as Paneth cell

291 *Bmp7* (and its *Bmpr1a* and *Bmpr2* receptors in stem/TA cells). *Bmp6* and *Bmp2,* two other ligands for
292 *Bmpr1a* and *Bmpr2* receptors, were also expressed at higher levels in ileal cSI-I goblet cells (**Fig. 2c,**
293 **Extended Data Fig. 6a**). Expression of *Wnt5a* and the Wnt inhibitor *Dkk2* were significantly diminished
294 in ileal smooth muscle cells (SMCs) in cSI-I mice, as were their receptors in stem/TA cells (*Cftr* and
295 *Ptprk* in the case of *Wnt5a* and *Lrp6* in the case of *Dkk2*) (**Fig. 2c, Extended Data Fig. 6a,**
296 **Supplementary Table 3c**). SMC-derived *Wnt5a* augments Th2 immunity and inhibits cellular
297 proliferation by downregulating expression of *Ctnnb1* (ß-catenin)[39]. Quantification of Ki67, a marker of
298 cellular proliferation, in duodenal and ileal crypts provided additional evidence of increased epithelial
299 regeneration in cSI-I animals (**Fig. 2d, Extended Data Fig. 6b**; **Supplementary Table 2c**).
300 ***Contextualizing intestinal transcriptional responses with proteomic features in duodenal***
301 ***mucosa of children with EED*** – To further assess the degree to which the transcriptional response in
302 enterocytes present in the duodenum and ileum of P37 offspring recapitulates pathophysiologic changes
303 we had documented in the upper gastrointestinal tract of Bangladeshi children with EED[2], we performed
304 GSEA with mouse homologs of duodenal mucosal proteins that were: (i) negatively correlated with
305 length-for-age-Z-score (LAZ) and positively correlated with the levels of core EED bacterial taxa in
306 BEED study participants, or (ii) positively correlated with LAZ in these children and negatively
307 associated with core EED taxa (**Fig. 2e**). Expression of mouse genes homologous to the human duodenal
308 proteins that were negatively associated with growth and positively correlated with the absolute
309 abundances of core taxa were enriched in cSI-I enterocytes in the duodenum (crypt through mid-villus)
310 and in the ileum (crypt and along the length of the villus) (**Fig. 2e**). Genes encoding antimicrobial
311 peptides (*Reg3β* and *Reg3γ*), the pro-inflammatory cytokine *Il18*, the heat-shock protein *Hsp90aa1* and
312 the immune cell chemoattractant *Ccl28* were more highly expressed in all duodenal enterocyte cell types
313 whereas the type-2 immune response regulator *Arg-2* was more highly expressed in cSI-N offspring
314 (**Extended Data Fig. 6c, Supplementary Table 3c**). Together, these results provide evidence that SI
315 enterocytes play an important role in mediating the immune response in offspring of dams colonized with
316 the cSI-I consortium.
317
318 **Immune signaling in the cerebral cortex**
319 Stunting and EED are both associated with cognitive defects in children. In *Supplementary Information*,
320 we describe the effects of the cSI-I consortium on immune cell representation within the meningeal
321 immune compartment and gene expression in the cerebral cortex of P37 offspring. Briefly, mice
322 harboring the cSI-I consortium had (i) significantly elevated levels of neutrophils and inflammatory
323 monocytes in their meninges compared to their cSI-N and CONV-D counterparts; (ii) significantly higher
324 expression in glutamatergic neurons of pro-inflammatory signaling genes and genes involved in
325 generation of reactive nitrogen species; (ii) a transcriptional profile in astrocytes that negatively
326 associated with systemic inflammation, with expression of astrocyte genes involved in angiogenesis,
327 platelet-derived growth factor (PDGF) signaling, and cholecystokinin signaling significantly diminished
328 in cSI-I compared to cSI-N offspring. Moreover, quantification of ultra-sonic vocalizations (USVs), a
329 marker of early postnatal neurodevelopment, in P5-P9 pups and pup retrieval behavior by dams indicated
330 increased distress and perturbed social communication in cSI-I animals.
331
332 **Cohousing to nominate pathology-inducing bacterial strains**
333 To identify bacterial taxa in the two consortia that either confer or ameliorate the immunoinflammatory
334 state described above, we gavaged separate groups of 4-5-week-old germ-free C57Bl/6J mice consuming
335 the Mirpur-18 diet with the cSI-I or cSI-N culture collections. After nine days, half of the animals from
336 each group were cohoused. This experimental group and the non-cohoused cSI-I and cSI-N control
337 groups were then followed for an additional nine days (n=6 or 8 mice/group/experiment, 2 independent
338 experiments; **Fig. 3a**). Cohoused mice and non-cohoused cSI-I controls gained significantly less weight
339 compared to non-cohoused cSI-N controls (linear mixed effects model; **Supplementary Table 2b**).
340 Irrespective of the initial colonization state, serum concentrations of LCN2 and CHI3L1 were
341 significantly higher in cohoused animals compared to non-cohoused cSI-N controls and did not differ
342 significantly from levels of these biomarkers in non-cohoused cSI-I animals (**Fig. 3b, Supplementary**

343 **Table 2b**). Levels of LCN2 and CHI3L1 were also significantly higher in colonic tissue and trended
344 higher in duodenal tissue of cohoused mice compared to non-cohoused cSI-N controls (**Fig. 3c**;
345 **Supplementary Table 2b**).
346 Analogous to P37 offspring from the intergenerational transmission experiments, non-cohoused
347 cSI-I mice and all cohoused animals harbored significantly higher proportions of neutrophils and Th17
348 cells and a reduced percentage of Th1 cells in the small intestine lamina propria compared to non-
349 cohoused cSI-N controls; this was the case regardless of the initial colonizing bacterial consortium (**Figs.**
350 **3d,e**; **Supplementary Table 2f**). Splenic and meningeal neutrophils were similarly elevated in cSI-I and
351 cohoused animals compared to non-cohoused cSI-N mice. **Figs. 3f,g**; **Supplementary Table 2f**). There
352 was no evidence for a mitigating effect of the cSI-N community on pathology in cSI-I colonized mice
353 (**Supplementary Tables 2a,f**). These results suggested either restructuring of strain composition within
354 the cSI-N consortium after cohousing or transfer of bacteria from cSI-I to cSI-N animals, inducing
355 pathology in these formally healthy animals.
356 We performed shotgun sequencing of intestinal contents from animals in all treatment groups,
357 seeking taxa (MAGs) that were significantly more abundant in the intestines of mice in the
358 'inflammatory' experimental groups (i.e., non-cohoused cSI-I controls and cohoused mice) compared to
359 their 'non-inflammatory' counterparts (non-cohoused cSI-N mice). Three MAGs satisfied these criteria:
360 two belonged to the genus *Actinomyces* (*Actinomyces naeslundii* [MAG041], *Actinomyces odontolyticus*
361 [MAG044]) and the other to the genus *Campylobacter* (*Campylobacter concisus* [MAG048]) (**Fig. 3h**;
362 **Supplementary Table 1d**).
363 Compared to cSI-N controls, the absolute abundance of *C. concisus* was significantly higher in
364 the cecum and colon of cohoused animals, regardless of whether the cohoused animals were initially
365 colonized with the cSI-N or cSI-I consortia (**Fig. 3i**). The absolute abundances of both *A. naeslundii* and
366 *A. odontolyticus* were significantly higher in the jejunum, ileum, cecum and colon of cohoused animals
367 compared to non-cohoused cSI-N controls **(Fig. 3i**). The abundances of all three MAGs were equivalent
368 in cohoused animals and non-cohoused cSI-I controls along the length of the small intestine and in the
369 cecum (**Fig. 3i**), suggesting infiltration of these taxa from cSI-I to cSI-N animals during cohousing.
370 Moreover, the absolute abundances of these MAGs were significantly increased along the length of the
371 gut of P37 cSI-I compared to cSI-N offspring in our intergenerational transmission model (**Fig. 3j**;
372 **Supplementary Table 1d**). *C. concisus* and *Actinomyces spp.* are resident members of the oral
373 microbiota[40] and are not typically considered to be pathogens, although some strains have been associated
374 with periodontitis and inflammatory bowel disease[41–43].
375 Four isolates in our clonally-arrayed culture collection matched these three MAGs that were
376 elevated in cohoused animals compared to cSI-N controls with an average nucleotide identity (ANI) score
377 of >99%: two isolates matched the *A. naeslundii* MAG041 (Bg041a, Bg041b), one matched *A.*
378 *odontolyticus* MAG044 (Bg044) and one matched *C. concisus* MAG048 (Bg048) (**Supplementary Table**
379 **4a;** see S**upplementary Table 4b** for results of mcSEED-based *in silico* metabolic reconstructions of
380 these pathology-associated MAGs, their corresponding isolates, and other phylogenetically related
381 species[44,44]).
382
383 **Testing the role of isolates corresponding to pathology-associated MAGs**
384 We directly tested the capacity of these Bangladeshi *C. concisus, A. odontolyticus* and *A. naeslundii*
385 isolates to induce pathology. To do so, germ-free 4-5-week-old C57Bl/6J mice, consuming the Mirpur-18
386 diet, were gavaged with the cSI-N consortium (experimental day 0). On days 9 through 11, mice were
387 gavaged once daily with either (i) a pool of all four isolates, (ii) the *C. concisus* isolate (Bg048) alone,
388 (iii) the two *A. naeslundii* isolates (Bg041a, Bg041b), (iv) the *A. odontolyticus* isolate (Bg044), or (v) a
389 pool of both *Actinomyces* species. Groups of mice initially colonized with the cSI-N or cSI-I consortium
390 were subsequently gavaged with uninoculated (blank) culture medium as negative and positive controls,
391 respectively ('sham' gavage, **Fig. 4a**).
392 Secondary gavage with all isolates combined or with *C. concisus* alone led to an increase in the
393 absolute abundance of *C. concisus*, most notably in the cecum and colon, compared to sham-gavaged cSI-
394 N controls (**Fig. 4b**). The levels of *C. concisus* achieved over the course of the 9 days following its

395 introduction into cSI-N mice were comparable to levels in cSI-I sham-gavaged controls (**Fig. 4b**) as well
396 as in cohoused animals (**Supplementary Table 1d**). In contrast, gavage with the *Actinomyces* species
397 either alone or in concert resulted in a trending, but not statistically significant, increase in absolute
398 abundance along the length of the intestinal tract compared to cSI-N sham-gavaged controls (**Extended**
399 **Data Fig. 7a,b**; **Supplementary Table 1d**).
400 Mice gavaged with *C. concisus* gained significantly less weight than cSI-N sham-gavaged
401 controls or animals gavaged with the *Actinomyces* strains, either alone or together (**Extended Data Fig.**
402 **7c,d**). Colonic inflammation, assessed by tissue levels of LCN2, was significantly higher when all isolates
403 (*C. concisus+A. odontolyticus+A.naeslundii*) were gavaged together into cSI-N mice compared to all
404 other treatment groups, including mice receiving *C. concisus* alone and the cSI-I positive controls (**Fig.**
405 **4c**). This increase in LCN2 levels did not occur in the duodenum (**Extended Data Fig. 7e**). Similar
406 patterns were observed for the biomarker CHI3L1 (**Extended Data Fig. 7f**). These results suggested that
407 in the distal gut, the presence of *A. odontolyticus* and *A. naeslundii* directly or indirectly affected *C.*
408 *concisus* in a manner that increased its capacity to induce inflammation.
409 Systemic inflammation, as quantified by serum LCN2, was significantly higher 9 days after
410 gavage of the pooled strains (*C. concisus+A. odontolyticus+A.naeslundii*) compared to cSI-N controls,
411 but remained lower than in cSI-I mock-gavaged animals (**Fig. 4d**). In a follow-up experiment, serum
412 LCN2 was assessed 35 days after isolate gavage; introduction of either the four isolates together or *C.*
413 *concisus* alone was sufficient to produce LCN2 levels significantly higher than in cSI-N mock-gavaged
414 controls and not significantly different from cSI-I animals (**Fig. 4e**; **Supplementary Table 2a**). Together,
415 these data suggest that, given a sufficient duration of colonization, this Bangladeshi *C. concisus* isolate
416 can induce levels of systemic inflammation comparable to the cSI-I consortium.
417 ***Effects on intestinal gene expression*** - We conducted bulk RNA-Seq of the duodenum and colon
418 to further understand the host response to the presence of *C. concisus*. The results were compared across
419 the three experimental models that we describe in this report: intergenerational dam-to-pup transmission
420 of the cSI-I and cSI-N consortia (P37 offspring), cohousing, and isolate 'add-in' experiments (the latter
421 two characterized at experimental day 18) (**Supplementary Table 3e**). We examined Reactome pathways
422 whose expression was significantly enriched (compared to cSI-N controls) in (i) P37 cSI-I animals, (ii)
423 cohoused and non-cohoused cSI-I controls, and (iii) animals initially colonized with the cSI-N consortium
424 subsequently gavaged with *C. concisus*, *A. odontolyticus*, or *A. naeslundii* individually, both *Actinomyces*
425 species, all isolates together, as well as cSI-I/sham controls.
426 *C. concisus*, either alone or with the *Actinomyces* species, induced a pro-inflammatory
427 transcriptional response in the colon that was not present in the duodenum (**Supplementary Table 3e**).
428 Compared to their cSI-N counterparts, Reactome pathways involved in recruitment and activation of
429 immune cells, reactive oxygen species generation and detoxification, cell death programs, antigen
430 presentation, MAPK signaling, pro-inflammatory cytokines, and toll-like receptor (TLR) signaling were
431 more highly expressed in the colons of P37 cSI-I animals (from the intergenerational transmission
432 experiment), as well as cohoused and non-cohoused cSI-I controls as well as recipients of *C. concisus* (the
433 isolate alone or with *Actinomyces*) (**Fig. 4f**; **Supplementary Table 3e**). Genes involved in cytokine (IL-
434 1) signaling leading to programmed cell death (apoptosis) and immune cell activation (neutrophil
435 degranulation) were induced in the colon following gavage of *C. concisus* alone or in concert with the
436 *Actinomyces* isolates (**Supplementary Table 3e**). Of the 41 immunoinflammatory Reactome pathways
437 that were significantly enriched in the colons of mice gavaged with the three pathology-associated
438 species, only five were enriched in the duodenum (**Supplementary Table 3e)**; none of the 49 Reactome
439 pathways that were enriched in the colon after gavage of *C. concisus* alone were more highly expressed in
440 the duodenum (**Supplementary Table 3e**). The *Actinomyces* isolates, administered alone or together, did
441 not elicit a significant transcriptional response involving Reactome immune pathways, in either the colon
442 or the duodenum (**Fig. 4f, Supplementary Table 3e**). Together, these findings provided evidence that
443 this *C. concisus* isolate, both alone and in concert with the *A. odontolyticus* and *A. naeslundii* strains
444 cultured from the duodenal microbiota of Bangladeshi children with EED, induced an
445 immunoinflammatory gene response that recapitulates aspects of that induced by the full EED donor-
446 derived cSI-I community.

447 ***C. concisus* metabolism and inflammation**
448 Returning to our previously published V4-16S rRNA dataset generated from the duodenal aspirates of
449 children that took part in the BEED study[2], we found that the prevalence of *C. concisus* did not exceed the
450 80% threshold that we had used to define a core set of bacterial taxa in children with EED. Nonetheless,
451 the prevalence of the only *Campylobacter* ASV present (undefined species) was significantly higher in
452 children with 'epithelial damage' defined by histopathologic scoring metrics[2] (**Fig. 5a**, two-sided
453 Fischer's Exact $P = 0.0057$). The absolute abundance of this *Campylobacter* ASV was significantly
454 positively correlated with levels of only one protein in the duodenal mucosa: CD177, also known as
455 human neutrophil antigen 2 (HNA-2) (Pearson correlation, R = 0.694, *P*-adj = 0.00692). CD177/HNA-2
456 plays a critical role in neutrophil transmigration and extravasation during an inflammatory response[45,46].
457 ***Comparative genomic analysis*** – Some strains of *C. concisus* decreased expression of tight
458 junction proteins and increased permeability to FITC-dextran in a cultured human adenocarcinoma-
459 derived, enterocyte-like cell line (HT-29)[47,48]. Searches of the Bangladeshi *C. concisus* Bg048 isolate
460 genome and corresponding MAG048 failed to identify known *C. concisus* virulence factors including *Zot*
461 (Zonula occludens toxin), which has been found in 30% of *C. concisus* strains[49] and reported to disrupt
462 intestinal epithelial tight junctions and augment IL-8 production in HT29 cells[44,47]. Nonetheless, searches
463 within Bg048 and corresponding MAG for homologs to well-described bacterial virulence factors using
464 the Virulence Factor Database (VFDB[50]) identified genes involved in chemotaxis (the chemotaxis
465 regulator *cheY*, flagellar motor switch proteins *fliM* and *fliN*, and flagellum-specific ATP synthase *fliI*)
466 that were conserved with *Campylobacter jejuni* (**Supplementary Table 4a**).
467 We performed a follow-up comparative genomics analysis that included 119 additional *C.*
468 *concisus* strains isolated from individuals with oral and/or gastrointestinal pathology (periodontitis,
469 gastroenteritis, Ulcerative Colitis, Crohn's Disease, Inflammatory Bowel Disease), or healthy controls[51,52]
470 (**Extended Data Fig. 8**). We performed a functional enrichment analysis that focused on functions
471 (Clusters of Orthologous Genes, COGs) or genes that were enriched in isolates obtained from diseased
472 compared to healthy individuals. COG20 functions and pathways, including genes involved in bacterial
473 defense, bacterial cell wall modification, immune signaling/subversion and Type IV pilus assembly, were
474 significantly enriched in the Bg048 strain and other isolates obtained from diseased compared to healthy
475 hosts (**Supplementary Table 4c**). Our analysis also disclosed that genes encoding a nitrate-inducible
476 formate dehydrogenase (*fdnG*) and formate dehydrogenase H (*fdhF*) were unique to the Bg048 isolate
477 (**Extended Data Fig. 8**). In addition, this strain and only one other among the 119 surveyed contained a
478 *selD* (selenide water dikinase) which, through its capacity to produce selenocysteine, may provide the
479 required selenium cofactor for these formate dehydrogenases[53] (**Extended Data Fig. 8**, **Supplementary**
480 **Table 4c**).
481 ***Intestinal epithelial-derived substrates affecting C. concisus Bg048 growth –*** *C. concisus* is
482 known to be non-saccharolytic and have preference for other simple carbon sources (e.g., fumarate,
483 DMSO) and hydrogen gas for growth. Our *in silico* metabolic predictions indicated that *C. concisus*
484 Bg048 has a broad predicted respiratory capacity, including for nitrate, nitrite and nitrous oxide
485 (**Supplementary Table 4b**)[54].
486 To garner clues about substrates that support *C. concisus* growth in the gut, we conducted RNA-
487 seq analyses of the cecal microbial community of mice from our 'add-in' experiment (**Fig. 4**) and of *C.*
488 *concisus* grown *in vitro* under anaerobic conditions in rich medium (Bolton Broth with and without 1%
489 mucin). Compared to growth *in vitro* in both media conditions, genes involved in (i) motility (Flagellin A
490 *flaA* and secreted flagellin *flaC*, flagellar ring proteins *flgI/flgH*, assembly factor f*liW*, biosynthetic
491 proteins *fliQ/fliP*, basal body rod protein *flgC*, motility protein *motB*, chemotaxis proteins *cheW*, *cheA*,
492 *mcpH*), (ii) oxidative stress response (superoxide dismutases, *sodB/sodC*), and (iii) several genes
493 encoding respiratory proteins (dimethyl sulfoxide *dorA_2*, *dmsA_1*, *dmsB*, tetrathionate *ttrA/B*, thiosulfate
494 *phsB*, and fumarate *fdrA/B*, *ifcA_2* reductases; formate dehydrogenases *fdhF_3/fdhF_4, fdhB1_2* and
495 hydrogenlyases *hycD/hycG/hycE*) were more highly expressed in cSI-N/*C. concisus*-colonized mice
496 (**Extended Data Fig. 9a**, **Supplementary Table 5a**).
497 We then compared *C. concisus* gene expression between cSI-I, cSI-N/*C. concisus*, and cSI-N/*C.*
498 *concisus+Actinomyces* mice compared to cSI-N/mock controls (which harbor lower levels of *C. concisus*)

(**Fig. 5b**). The transcript with the largest increase in expression in cSI-N/*C. concisus* mice compared to cSI-N/mock-gavaged animals was a periplasmic nitrate reductase (*napA*, **Figs. 5b,c**). A nitrate import protein (*nrtD*) was also significantly more highly expressed in cSI-N/*C. concisus* mice, suggesting that nitrate may play a role in *C. concisus* virulence (**Fig. 5c**, **Supplementary Table 5b**). Genes involved in (i) motility (*motB*, twitching mobility proteins *pilT_1/pilT_2*, flagellar proteins *flgB, flgG_1/flgG_2, flgH, flgI, flhA, flhB_1/flhB_2, fliG, fliM, fliN, fliP, fliQ, fliR, ylxH*), (ii) redox homeostasis/survival (*sodB*, cytochrome c551 peroxidase *ccpA*, peroxidase *yfeX*, thiol peroxidase *tpx*), and (ii) formate metabolism (*fdhF_1/fdhF_2, hycE*, formate-tetrahydrofolate ligase *fhs*) were also more highly expressed by *C. concisus* in inflammatory conditions (**Fig. 5b, Supplementary Table 5b**).

Having determined that in the context of the cSI-N community *C. concisus* induced an immunoinflammatory response, we tested the hypothesis that *C. concisus* may utilize host substrates that are produced under conditions where there is inflammation and perturbed intestinal epithelial turnover. To do so, we first turned to an *in vitro* tissue culture system in which we cultured mouse- and human-derived colonic epithelial cell lines (CT26 and HTC116, respectively) with or without subsequent induction of cell death (**Fig. 5d**, see *Methods*) and then collected conditioned medium[31]. *C. concisus* growth in the presence of oxygen (5% O_2) was significantly higher in spent medium from live mouse CT26 cells (**Figs. 5e,f**, **Extended Data Figs. 9b-d**) and human HTC116 cells (**Figs. 5g-i, Extended Data Figs. 9e-g**) compared to conditioned medium harvested from cells undergoing apoptosis or to cell culture medium alone. When cultured anaerobically, *C. concisus* growth did not differ in spent medium from cells that were alive or undergoing apoptosis and was diminished compared to growth in cell culture medium alone (**Extended Data Fig. 9h-k**). These findings suggest that changes in *C. concisus* metabolism in the presence of low levels of oxygen, such as those that may occur in the oxidative state of the inflamed gut[55], may underlie a fitness benefit conferred to *C. concisus* through utilization of host-derived substrates.

During an inflammatory response, nitric oxide produced by inducible nitric oxide synthase (iNOS, encoded by *Nos2*) reacts with reactive oxygen species to form nitrate[56]. Other Proteobacteria have been shown to utilize host-derived nitrate[56–58] or other byproducts of iNOS activity[65] to gain a competitive advantage in mouse models[59]. Given the strong up-regulation of nitrate reductase by *C. concisus* in the gut under inflammatory conditions (cSI-I, cSI-N/*C. concisus*, cSI-N/*C. concisus*+*Actinomyces*) compared to noninflammatory states (cSI-N mice) (**Figs. 5b,c**), we examined whether *C. concisus* could utilize host-derived substrates generated through metabolism of nitric oxide.

Nitrate in ileal tissue was significantly higher with addition of *C. concisus* alone (cSI-N/*C. concisus*) compared to cSI-N and cSI-I sham-gavaged controls as well as when *Actinomyces* were present (cSI-N/*C. concisus*+*Actinomyces*) (**Fig. 5j**). Nitrate reductase activity reduces nitrate to nitrite; increased bacterial nitrate reductase activity should result in elevated luminal nitrite. Nitrite in cecal contents trended higher in *C. concisus*-gavaged animals (**Extended Data Fig. 9l**), although the difference was not statistically significant, perhaps due to microbial reduction of nitrite or the short half-life of nitric oxides.

To test whether epithelial cell nitric oxide generation contributed to the increase in *C. concisus* growth in spent medium collected from live cells, we treated HTC116 cells with the non-selective NOS inhibitor N-iminoethyl-L-ornithine (L-NIO)[60]. L-NIO treatment significantly reduced the growth benefit conferred to *C. concisus* in conditioned medium collected from live cells when *C. concisus* was grown in microaerophilic conditions. L-NIO had no effect on microaerophilic growth in conditioned medium collected from apoptotic cells (**Fig. 5k, Extended Data Figs. 9m,n**), nor on anaerobic growth in spent medium from live epithelial cells (**Extended Data Figs. 9o,p**). Together, these results suggest that host nitric oxide metabolism boosts growth of *C. concisus* and may confer an advantage under conditions where low levels of oxygen are present in the gut, as is the case with inflammation.

We subsequently profiled *C. concisus* gene expression during growth under microaerophilic conditions in conditioned medium from live HTC116 cell cultures, or the cell culture medium (DMEM). A putative formate transporter (*focA*), formate dehydrogenase (*fdhB*) and formate hydrogen lyases (*hycE, hycD*) plus a periplasmic nitrate reductase *(napA)*, as well as other genes involved in anaerobic respiration were significantly more highly expressed when grown in the presence of live HTC116 spent medium compared to medium alone (**Fig. 5l, Supplementary Table 5c**). Importantly, the periplasmic nitrate reductase was not significantly differently expressed in *C. concisus* grown in conditioned medium from

HTC116 cells treated with the NOS inhibitor L-NIO compared to medium alone (DMEM) while other genes involved in anaerobic respiration were still differentially expressed in the presence L-NIO, including those involved in formate metabolism (**Supplementary Table 5c**).

C. concisus-induced inflammatory cytokine signaling enhanced by iNOS

To determine the 'type' of immune response elicited by *C. concisus* and whether the host's capacity to produce nitric oxide plays a role, we collected bone marrow, which harbors a large population of diverse immune cells that seed other body sites, from WT and *Nos2*$^{-/-}$ mice and stimulated these cells for 48 hours with live or heat-killed *C. concisus*. ELISA assays established that iNOS was significantly higher after co-culture of wild-type bone marrow cells with live and heat-killed *C. concisus* compared to bacterial medium alone (**Extended Data Fig. 10a,b**). In alignment with our bulk RNA-Seq data of the colon after gavage of *C. concisus* to cSI-N mice (**Fig. 4f)**, IL-1ß secretion was higher in response to heat-killed *C. concisus* and, in a dose-dependent manner, to co-culture with live *C. concisus* compared to medium alone (**Extended Data Fig. 10c,d**). Production of TNF-a (canonical type 1 cytokine), IL-5 (type 2), IL-17 (main cytokine produced by Th17 cells) and IL-22 (type 3 and produced by Th17 cells) were significantly higher after co-culture of wild-type bone marrow cells with live *C. concisus* compared to medium alone (**Extended Data Figs. 10e-j**). In contrast, incubation with heat-killed *C. concisus* elicited a significant increase in IL-5 only (**Extended Data Fig. 10f**). Levels of all five of these cytokines secreted after exposure to live *C. concisus* were significantly lower in bone marrow obtained from *Nos2*$^{-/-}$ compared to WT mice. (**Fig. 6a-e**). In *Nos2*$^{-/-}$ bone marrow cells, production of IL-1ß, TNF-a, and IL-22 were still significantly higher after incubation with live *C. concisus* compared to the medium control (**Extended Data Fig. 10k-m**). However, genetic ablation of iNOS ameliorated the IL-5 and IL-17 responses – levels in cell supernatants were not significantly higher in response to live *C. concisus* compared to medium control (**Extended Data Fig. 10n,o**). Genes involved in MAPK signaling were more highly expressed in the colon of animals gavaged with *C. concisus* (**Fig. 4f**); p38 MAPK signaling was reduced in *Nos2*$^{-/-}$ animals compared to WT, both after exposure to live *C. concisus* and at baseline (**Extended Data Fig. 10p**).

As noted above, when *C. concisus* was grown under microaerophilic conditions in spent medium from live HTC116 cell cultures, a nitrate-inducible formate transporter (*fdnG*) and formate transporter (*focA*) were expressed at significantly higher levels (**Extended Data Fig. 10q**).To determine whether formate plays a role in *C. concisus* virulence, as has been described for other pathogens, including *Campylobacter jejuni*[61–63], we stimulated bone marrow cells with *C. concisus* that had been grown with and without formate. While formate did not increase *C. concisus* growth (**Extended Data Fig. 10r**); (i) live (but not heat killed) *C. concisus* depleted formate when co-cultured with WT or *Nos2*$^{-/-}$ bone marrow cells (**Extended Data Fig. 10s**) and (ii) *C. concisus* pretreated with 10 mM formate significantly increased IL-1β produced by bone marrow cells (**Fig. 6f**). Collectively, these findings point to inter-related pathways involving nitric oxide metabolism, formate, and effector cytokines in the host response to *C. concisus*.

Discussion

Here we describe a preclinical gnotobiotic mouse model of intergenerational transmission of members of the small intestinal microbiota cultured from children with EED that phenocopied several aspects of EED. In the absence of samples from healthy children living in the same environment as those in our clinical study, we generated two bacterial consortia from duodenal aspirates collected from undernourished Bangladeshi children with EED: one encompassing all isolates recovered from the aspirates which induced intestinal and systemic inflammation; the other a subset comprised of one representative strain of each species present in the full collection. This type of 'reverse translation' experiment provided an opportunity to perform analyses that were not possible in children in the BEED study who were the source of the small intestinal bacteria, e.g., immune profiling along the length of the gut and in extraintestinal tissues, snRNA-Seq analysis of gene expression in multiple cell lineages in different regions of the small intestine and brain, as well as a functional assessment of early postnatal behavior.

602 We were able to dissect structure/activity relationships in the human donor small intestinal
603 bacterial consortia by combining results from our dam-to-pup intergenerational transmission model with
604 shorter duration cohousing experiments and cultured isolate 'add-in' experiments. If the cSI-I and cSI-N
605 consortia had contained unique strains, we would have been able to track the provenance of strains as the
606 two consortia mixed in cohoused mice (and define whether strains 'bloomed' or 'invaded'). However, as
607 the same strains were present in both cSI-I and cSI-N, we are unable to distinguish the origin of strains in
608 cohoused animals. Regardless, from the results of our cohousing experiments, we were able to associate
609 three MAGs – *C. concisus*, *A. naeslundii* and *A. odontolyticus*, all members of the oral microbiota – with
610 development of pathology. Follow-up experiments in which these candidate disease-promoting isolates
611 were introduced to gnotobiotic animals colonized with the non-pathology-inducing cSI-N consortium
612 defined *C. concisus* as the primary driver in inducing intestinal inflammation. These experiments will also
613 provide an opportunity for more detailed physiological profiling, including comprehensive energy balance
614 studies, to ascertain the origin of the weight loss phenotype observed in cSI-I mice.
615 Disruption of the intestinal microbiota by taxa that normally reside in the oral microbiota has
616 been implicated in studies of undernutrition and EED[64,65]. Evidence for this process, referred to as
617 'decompartmentalization' of the microbial community, has come from applying culture-independent
618 methods (primarily16S rRNA amplicon sequencing) to feces. As such, there is little information about
619 disease associations with specific strains, or correlations with their genome-encoded functional features.
620 *C. concisus* has been reported to be over-represented in the fecal microbiota of stunted compared
621 to non-stunted children living in South India, and significantly more abundant in the feces of a cohort of
622 stunted children living in sub-Saharan Africa compared to healthy controls[66,67]. In children of the BEED
623 study, the only *Campylobacter* ASV present correlated significantly with duodenal mucosal levels of
624 CD177, a cell surface glycoprotein involved in neutrophil activation, and was significantly more
625 prevalent in children with histopathologic evidence of epithelial damage from their mucosal biopsies. *C.*
626 *concisus* has been described as a typical member of the oral microbiota in healthy individuals (97%
627 prevalence in a cohort of 59 individuals aged 3-80 years)[40], but it has also been associated with gingival
628 disease[41] and inflammatory bowel disease (IBD); its prevalence was higher in mucosal biopsies from IBD
629 patients compared to healthy controls[41,42]. The distinctions between *C. concisus* strains recovered from the
630 oral and intestinal microbiota of healthy individuals versus those with immunoinflammatory conditions
631 remain to be fully defined.
632 It is intriguing that addition of this EED donor-derived *C. concisus* strain to mice harboring the
633 EED duodenal-derived cSI-N consortium of cultured bacteria produced an immunoinflammatory response
634 that was greatest in the colon – at least within the relatively short duration of the cohousing/'add-in'
635 experiments which were conducted in coprophagic mice. These findings prompt the question of what
636 factors allow it (and other members of the oral microbiota) to establish themselves in distal regions of the
637 intestine. The isolate 'add-in' experiments described in this report illustrated how inflammation induced
638 by *C. concisus* occurred in a context-dependent manner; i.e., inflammation in the colon was enhanced in
639 the presence of the *Actinomyces* strains, which themselves were not sufficient to elicit an
640 immunoinflammatory response.
641 Experiments using heat-killed bacterial culture demonstrated that components and/or products of
642 this pathology-inducing Bangladeshi *C. concisus* isolate were able to induce immune signaling *ex vivo.*
643 Our *in vivo* and *in vitro* studies suggested a role for bacterial nitrate and formate metabolism in
644 pathogenesis of this organism. The mechanisms by which host nitric oxide generation and utilization of
645 host-derived substrates by pathogenic members of the microbiota contribute to decompartmentalization of
646 the oral microbiota and development of enteropathy in humans is an important area that warrants further
647 investigation and could have therapeutic implications. Future studies should also include microbial
648 communities from more distal regions of the intestines of individuals with EED to better characterize how
649 biogeographical features of the microbiota relate to the pathophysiology of this enteropathy.
650 Our 'add-in' experiments indicate that *C. concisus* induces higher levels of inflammation after a
651 longer period of colonization – rather than being cleared by the host. Canonical enteric pathogens,
652 including *Salmonella*[31], have been shown to utilize substrates from dying, rather than live, intestinal,
653 epithelial cells, as is the case for *C. concisus*. The question of what are the initiating events that allow a

654 pathogen/pathobiont to first establish itself in a microbial community and induce inflammation is
655 complex. One approach is to use genetic tools to identify the contributing signaling and metabolic
656 pathways in both the microbe and host. Our model provides a justification for and sets the stage for these
657 types of detailed analysis.
658 Endoscopy studies performed as part of the BEED study established that EED is widespread in
659 children as well as undernourished mothers[15,68]; these findings *support* the notion that EED is an
660 intergenerational health problem, at least in some LMICs. Establishing a clinical infrastructure in these
661 areas that allows concomitant sampling of the oral, small intestinal and fecal microbiota of
662 undernourished mothers with EED, as well as healthy mothers without EED, and subsequently creating
663 preclinical models of the type described in this report should provide an opportunity to obtain a more
664 mechanistic understanding of the intricate interplay between the expressed functions of microbial
665 community components, maternal gut health and nutritional status, intestinal adaptations to pregnancy,
666 plus development prior to and following birth. An anticipated outcome of such an effort would be
667 identification of candidate therapeutic targets, including those that may originate in the oral microbiota
668 and reside in the small intestine.
669
670 **Acknowledgements** We thank David O'Donnell, Maria Karlsson and the late Justin Serugo for their
671 invaluable assistance with mouse husbandry, Darya Khantakova and Bishan Bhattarai for assisting with
672 flow cytometry preparation and FACS, Martin Meier for generating libraries for shotgun sequencing and
673 microbial RNA-Seq, and Jessica Hoisington Lopez, MariaLynn Crosby and members of the Genome
674 Technology Access Core at Washington University School of Medicine for sequencing these libraries.
675
676 **Funding –** This work was supported by grants from the Gates Foundation (INV-033564) and the NIH
677 (DK131107). K.M.P. is the recipient of a postdoctoral fellowship from the Helen Hay Whitney
678 Foundation. C.K. is the recipient of a NIH F30 predoctoral MD/PhD fellowship (DK123838). K.S.R is
679 supported by NIH grant AI159551 and a BJC Investigator award.
680
681 **Contributions –** Duodenal aspirates used for generating the culture collections were collected in the
682 BEED study, which was directed by T.A.. K.M.P., C.K., M.J.B., and J.I.G. designed the gnotobiotic
683 mouse experiments which were performed by K.M.P., C.K. and R.Y.C.. Histomorphometric analyses
684 were conducted by C.K. and A.E.B.. Flow cytometry and FACS were performed by B.D. and M.L. and
685 interpreted with input from M.C.. ELISA and Luminex assays of serum and tissue proteins were
686 conducted by C.K., R.Y.C., K.M.P., and K.N.. Shotgun sequencing of community DNA, snRNA-Seq and
687 bulk RNA-Seq of intestinal segments and of brain, and microbial RNA-Seq data were generated and
688 analyzed by K.M.P., C.K., R.Y.C. and Y.W.. MAG assembly and calculations of MAG abundances were
689 performed by C.K., D.M.W. and M.C.H. Long-read shotgun sequencing and assembly of the genomes of
690 the nominated pathology inducing strains from the culture collection were generated by C.K.. A.E.B.
691 designed experiments to assess USVs and performed statistics on quantified metrics. Intestinal epithelial
692 tissue culture experiments were designed by L.K., C.M., and K.R. and conducted by L.K.. *C. concisus*
693 culture and co-culture with immune cell experiments were designed by K.M.P., J.I.G. and M.C., and were
694 conducted and analyzed by K.M.P.. D.R. generated *in silico* metabolic reconstructions of MAGs and
695 cultured bacterial strains. K.M.P. performed the comparative genomics analysis of *C. concisus* strains.
696 K.M.P. and J.I.G. wrote the paper with assistance from C.K., M.J.B, and other co-authors.
697
698 **Competing Interests -** D.R. and A.O. are co-founders of Phenobiome Inc., a company pursuing
699 development of computational tools for predictive phenotype profiling of microbial communities.
700
701 **Data availability –** Datasets generated by (i) shotgun sequencing of DNA isolated from the intestinal
702 contents of gnotobiotic mice and from individual cultured bacterial strains, (ii) snRNA-Seq and bulk
703 RNA-Seq of intestinal tissue and cerebral cortex, and (iii) microbial RNA-Seq of cecal contents harvested
704 from gnotobiotic mice, have been deposited at the European Nucleotide Archive (ENA;
705 https://www.ebi.ac.uk/ena) under accession number ERA22531095.

Ethics and Inclusion – This work was performed as part of a long-standing collaboration investigating the role of the gut microbiota in undernutrition that is covered by a memorandum of understanding, between teams led by Tahmeed Ahmed (International Centre for Diarrhoeal Disease Research, (icddr,b) Bangladesh) and Jeffrey Gordon (Washington University in St Louis, USA). Bacterial isolates used in this study were obtained from duodenal aspirates collected from the previously reported Bangladesh EED study, which was approved by the Ethical Review Committee (ERC) at the icddr,b (protocol no: PR-16007; ClinicalTrials.gov number, NCT02812615). Written informed consent was obtained from each child's parent or guardian to participate and to undergo EGD if the child met the inclusion criteria. Human biospecimens were transferred to Washington University under a Materials Transfer Agreement (MTA). Bacterial isolates cultured and used in this study are the property of icddr,b and are available under MTA upon request to T.A. and J.I.G.

Code Availability – The custom source code for annotation of bacterial genes and prediction of metabolic pathway presence/absence is available at https://github.com/rodionovdima/PhenotypePredictor-2 and has been accessioned at Zenodo (DOI: 10.5281/zenodo.13250652). All other analyses presented utilize published algorithms with their accompanying methods and are referenced as such.

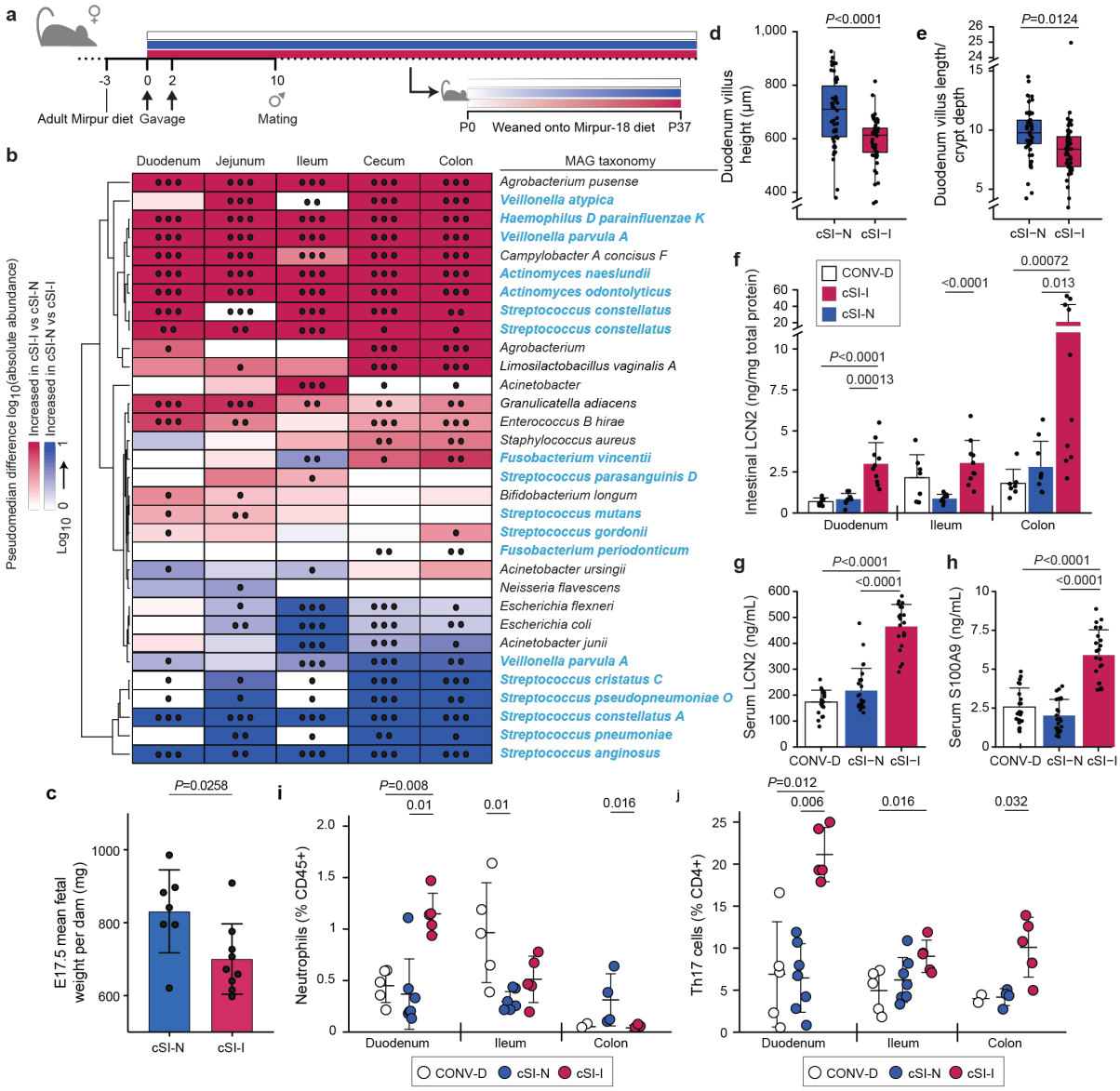

Fig. 1. Dam-to-offspring transmission of bacteria cultured from duodenal aspirates collected from Bangladeshi children with EED. a, Design of intergenerational transmission experiment. **b,** Differential abundances of bacterial MAGs (rows) along the length of the intestine (columns) of P37 pups born to dams harboring cSI-N or cSI-I bacterial consortia (n=21-25 mice/group). MAGs were included in the heatmap if they demonstrated significant differential $\log_{10}$ absolute abundance in at least one of the intestinal locations. MAG taxonomy colored in blue indicates correspondence to ASVs representing 'core taxa' identified in the small intestines of stunted children with EED in the BEED study. •, *P*-adj < 0.05; ••, *P*-adj < 0.01; •••, *P*-adj < 0.001, FDR-corrected Wilcoxon rank-sum tests. **c,** Average fetal mass for a given dam at E17.5. Dams were colonized with the cSI-I or cSI-N consortia for two weeks prior to mating (n=7-9 dams/group; n=2-10 fetuses/litter, unpaired t-test). **d,e,** Villus length (**d**), and ratio of villus length to crypt depth (**e**) in the duodenum of P37 cSI-I compared to cSI-N mice (n=5 animals/group, boxes denote interquartile range). **f,** Levels of lipocalin-2 (LCN2) protein in intestinal tissue from P37 mice (n=7-10 mice/group). **g,h,** Serum levels of LCN2 (**g**), and S100A9 protein (**h**), in P37 pups (n=21-25 mice/group). For **c-e**, n=4-6 litters/group, 3-7 pups/litter. **i,j,** Frequency of neutrophils (**i**), and Th17 cells (**j**), along the length of the gut (n=5-7 mice/group, each point represents an individual animal). For **d-j**, statistics shown are the result of Wilcoxon-rank sum tests. For **c-j**, mean values ± s.d. are shown.

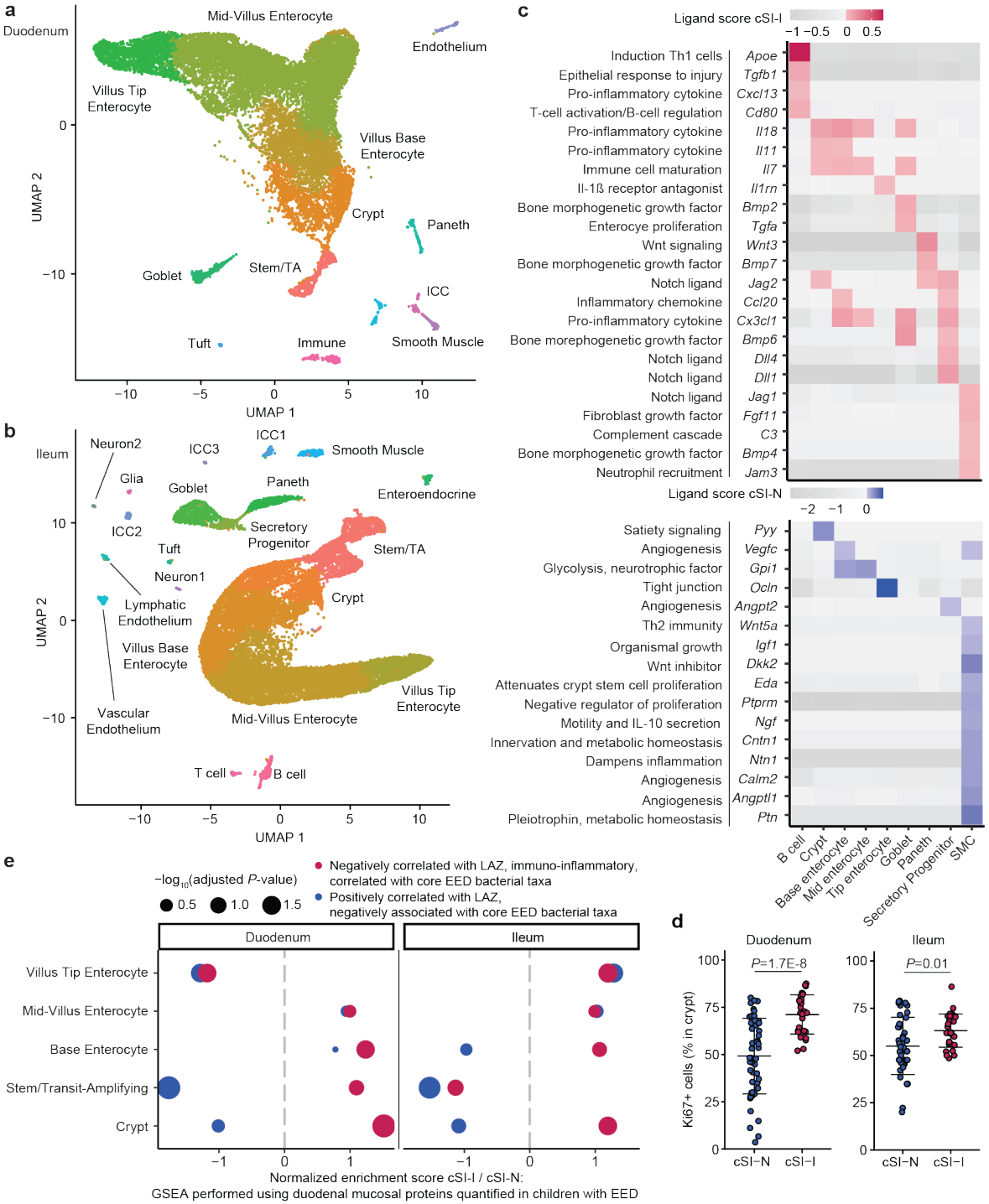

Fig. 2. Increased proliferative signaling in the small intestine of P37 offspring of cSI-I dams. a,b, Uniform manifold and projection (UMAP) plot of single nuclei isolated from the duodenum (**a**), and ileum (**b**) of P37 offspring (n=3 mice/group). **c,** Intercellular signaling from cell populations (columns) to stem/transit amplifying (TA) cells in the ileum. A subset of ligands identified by *NicheNet* are shown that were significantly differentially expressed between cSI-I and cSI-N animals. Annotations for these ligands (left) are based on literature findings. Their paired receptors are shown in **Extended Data Fig. 6a**. Ligands that were more highly expressed in cSI-I mice are shown in red (top of panel); those more highly expressed in cSI-N animals are shown in blue (bottom of panel). **d,** Percent of all cells in a crypt that were

Ki67^{+} in the duodenum (left) or ileum (right) (n=3-5 mice/group; each dot represents a single crypt-villus unit; 10 crypts analyzed per intestinal segment per mouse). *P*-values were determined by Tukey's post-hoc tests; mean values ± s.d. are shown. **e,** Gene set enrichment analysis (GSEA) along the crypt-villus axis, focusing on genes encoding duodenal mucosal proteins whose levels were quantified in children with EED in the BEED study.

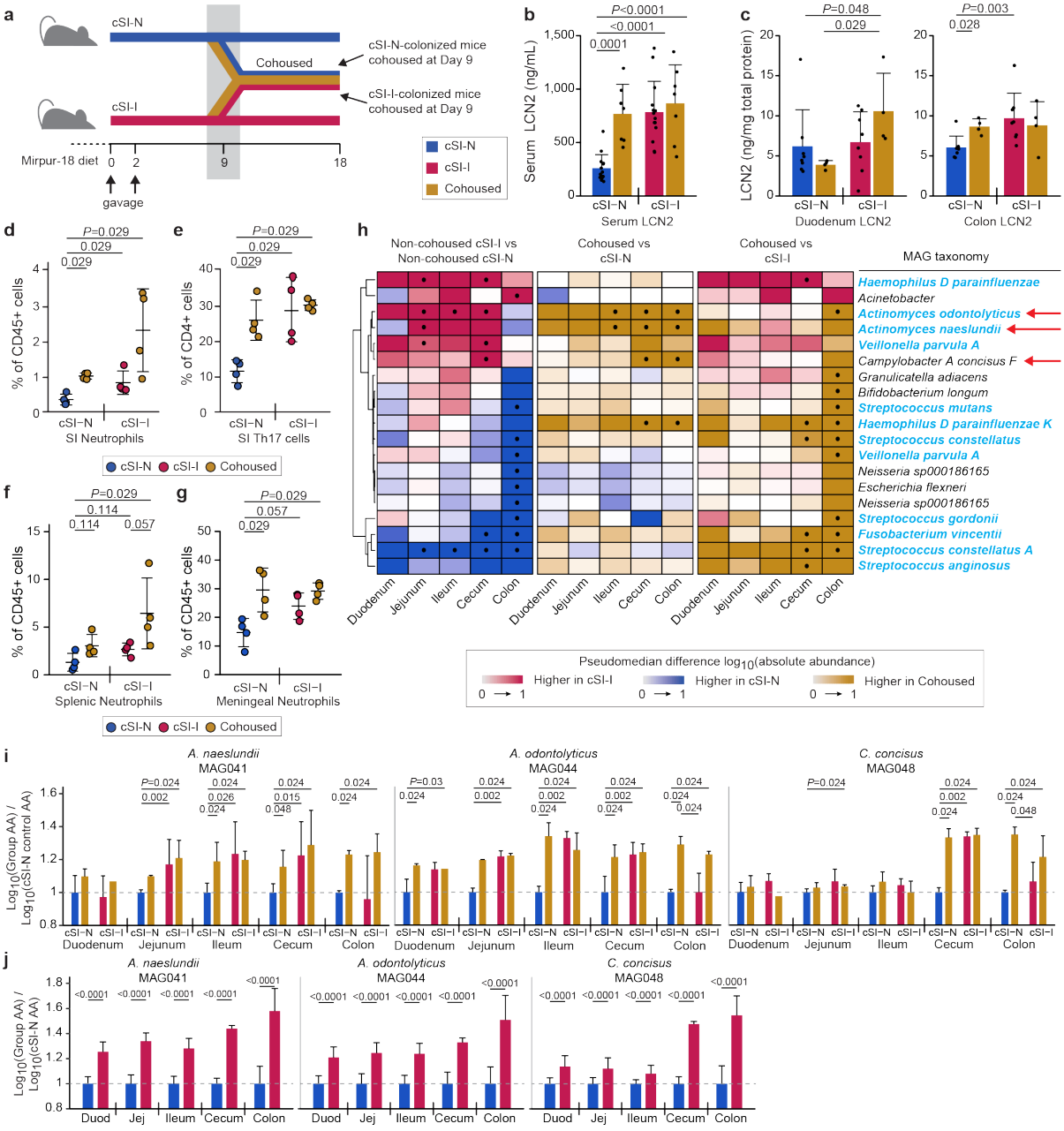

Fig. 3. Identification of bacteria associated with pathology after cohousing. a, Experimental design of cohousing experiment. **b,** Serum levels of LCN2 protein on experimental day 18, 9 days after initiation of cohousing (n=14 mice/control group, n=7 mice/cohoused group). **c,** Intestinal tissue levels LCN2 measured on experimental day 18, 9 days after cohousing (n=8 mice/control group, n=4 mice/cohoused group). **d,e,** Frequency of neutrophils (**d**), and Th17 cells (**e**), in the small intestinal lamina propria (n=4 mice/group; duodenal, jejunal and ileal segments were combined prior to analysis). **f,g,** Frequency of neutrophils in the spleen (**f**), and meninges (**g**) (n=4 mice/group). For panels **d-f**, each point represents an

individual animal; the color code matches that used in panel **a**. **h,** Differences in absolute abundances of MAGs along the length of the gut (n=6 mice/group). MAGs were included if they demonstrated statistically significant differences in their absolute abundance for any comparison between groups in at least one segment of the intestine. MAG taxonomy colored in blue indicates correspondence to ASVs representing 'core taxa' in the duodenal microbiota of stunted Bangladeshi children with EED in the BEED study. The three red arrows point to MAGs defined as 'pathology-associated'. • *P*-adj < 0.05, FDR-corrected Wilcoxon rank-sum. **i,j,** Log_{10} absolute abundances (AA) of the pathology-associated MAGs (MAG041, MAG044 and MAG048) along the length of the intestine in either the cohousing experiment (**i**) or P37 animals from the intergenerational experiment (**j**). Values are expressed relative to cSI-N non-cohoused controls (n=6 mice/control group and n=3/cohoused groups, **i**) or P37 cSI-N offspring in the intergenerational transmission experiment (n=22-25 mice/group, **j**). For **b-j**, *P*-values were determined by Wilcoxon rank-sum test; mean values ± s.d. are shown in **b-g**, **i-j**.

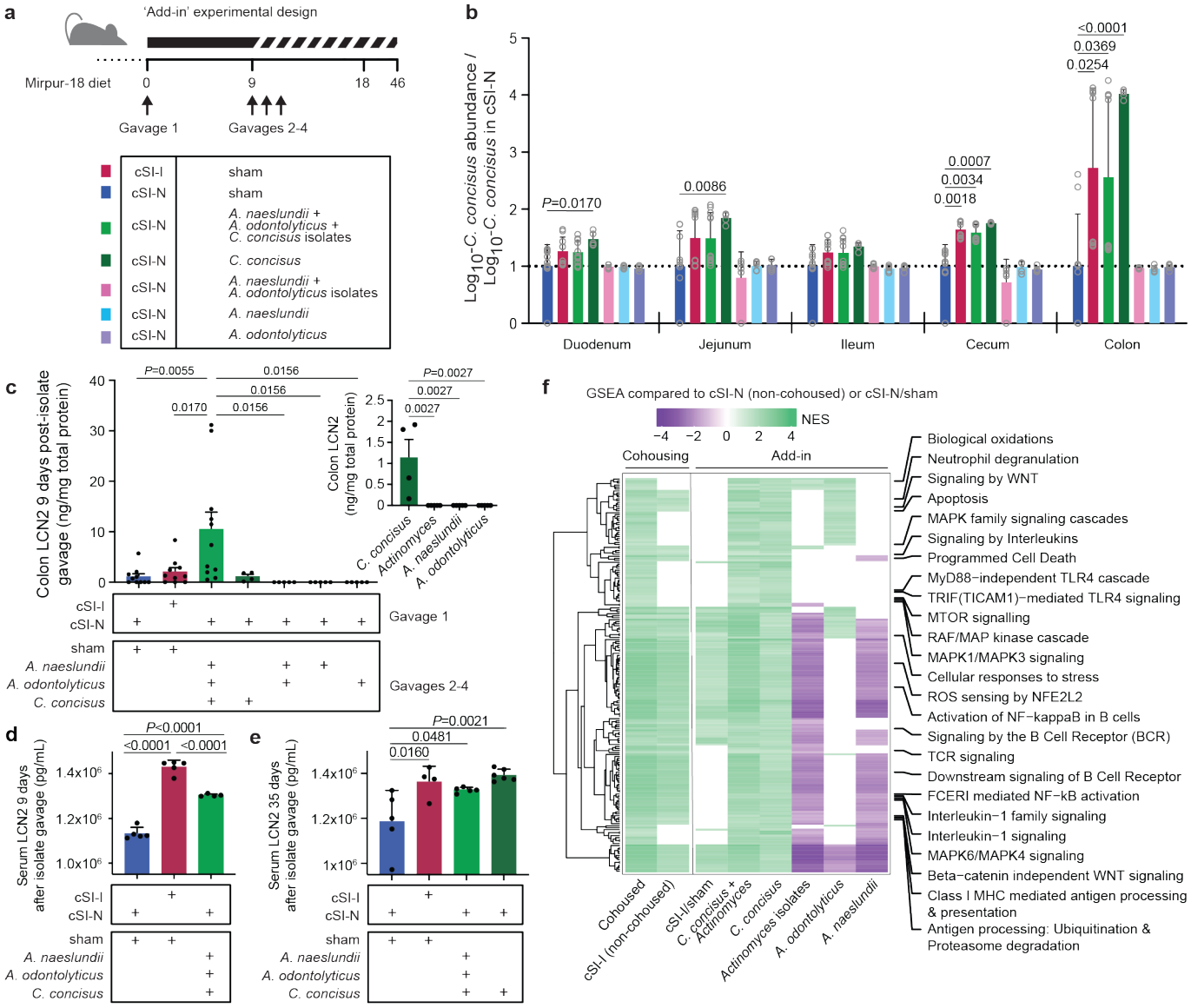

Fig. 4. Direct test of candidate pathology-inducing small intestinal bacterial strains in cSI-N mice. a, Experimental design of 'add-in' experiment. Individual cultured isolates, alone or in combinations, were gavaged once daily on days 9-11 into mice previously colonized with the cSI-N bacterial consortium. **b,**

785 Ratio of the absolute abundance of *C. concisus* strain Bg048 (corresponding to MAG048) shown relative
786 to its absolute abundance in cSI-N/sham controls (a ratio of 1 is indicated by the dotted line; two-way
787 ANOVA with Dunnett's multiple comparisons to cSI-N/sham control; mean values ± s.d. are shown).
788 Colors correspond to the groups shown in panel **a**. **c,** Levels of LCN2 protein in colonic tissue measured
789 on experimental day 18, 9 days after isolate gavage. The inset shows colonic LCN2 levels after addition
790 of the individual isolates alone (one-way ANOVAs with Tukey's multiple comparisons; mean values ±
791 s.e.m. are shown). **d,e,** Serum LCN2 at 9 (**c**), or 35 days (**d**), following isolate gavage (mean ± s.d. shown,
792 one-way ANOVAs with Tukey's multiple comparisons). **f,** Results of bulk-RNA-Seq analysis:
793 normalized enrichment scores (NES) for all Reactome pathways that were significantly enriched in the
794 colon (GSEA *q*-value <0.05) of the indicated treatment groups compared to their respective cSI-N
795 counterparts (non-cohoused cSI-N controls, or cSI-N/sham). Pathways related to the immune system are
796 labeled. Pathways were included in the heatmap if they were significantly enriched with the addition of *C.*
797 *concisus* and in cohoused animals. If a pathway was not significantly enriched, it was assigned a NES
798 score of zero. For panels **b, c, f**, n=5-11 mice/group combined across two independent experiments. For **d**
799 and **e**, n=5 mice/group in a third independent experiment.

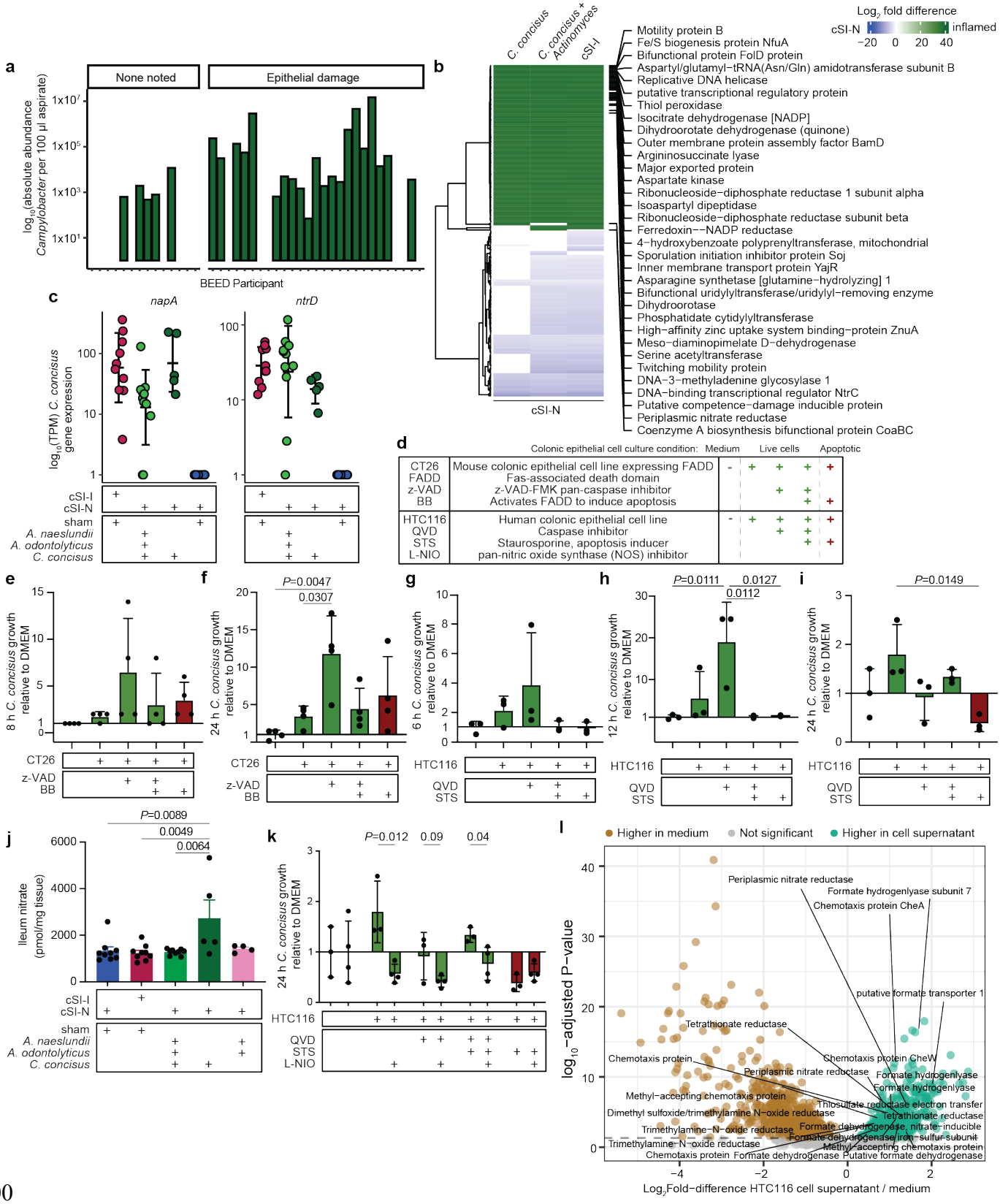

Fig. 5. Host epithelial cell nitrate metabolism boosts *C. concisus* growth *in vitro*. a, Absolute abundance of the *Campylobacter* ASV identified in duodenal aspirates from children in the BEED study.

804 **b,** Heatmap of significantly differentially expressed genes (*DESeq2* Wald test) in the colon between cSI-I
805 and *C. concisus*-gavaged animals ('inflamed') compared to sham-gavaged cSI-N controls. The gene
806 products for the most significantly differentially expressed genes across all three pairwise conditions are
807 labeled. **c,** Expression of *C. concisus* nitrate reductase (*napA*) and nitrate transporter (*ntrD*) 9 days post-
808 isolate gavage, or in cSI-I and cSI-N sham-gavaged controls (tpm, transcripts per million). **d,**
809 Abbreviations of cell lines and treatments used to collect conditioned medium from mouse and human
810 colonic epithelial cells that were live or apoptotic. QVD, Quinoline-Val-Asp-
811 Difluorophenoxymethylketone (caspase inhibitor); L-NIO, N^5-(1-Iminoethyl)-L-ornithine,
812 dihydrochloride (nitric oxide synthase inhibitor). Conditioned medium acquired from live epithelial cells
813 is colored in green; apoptotic cells, in red. **e,f,** Growth of *C. concisus* after 8 (**e**) or 24 hours (**f**) in
814 conditioned medium collected from CT26 mouse colonic epithelial cells that were live (CT26:FADD, z-
815 VAD, z-VAD+BB) or were treated with an inducer of apoptosis (BB). Growth is presented relative to (as
816 a ratio to) growth in cell culture medium (n=4 biological replicates per condition). **g-i,** Growth of *C.*
817 *concisus* after 6 (**g**), 12 (**h**), or 24 (**i**), hours in spent medium collected from HTC116 human colonic
818 epithelial cells that were live (QVD, QVD+STS), or that had been treated with an inducer of apoptosis
819 (STS) relative to growth in cell culture medium (n=3 biological replicates per condition, growth is
820 presented as a ratio to growth in cell culture medium). **j,** Levels of nitrate in homogenized ileal tissue 9
821 days post-isolate gavage. **k,** Comparison of *C. concisus* growth after 24 hours in spent medium collected
822 from live (QVD, QVD+STS) or apoptotic (STS) HTC116 cells that were or were not treated with L-NIO
823 (n=3-4 biological replicates per condition, pairwise t-tests for each ± L-NIO comparison). **l,** *C. concisus*
824 genes that were significantly differentially expressed when cultured in conditioned medium collected
825 from HTC116 cells compared to medium alone (*DESeq2* Wald test). For **c-j**, bars denote mean ± s.d.. For
826 **b-c, j**, n=5-11 mice/group combined across two independent experiments. For **e-j**, *P*-values were
827 determined with one-way ANOVA and Tukey's multiple comparisons.
828

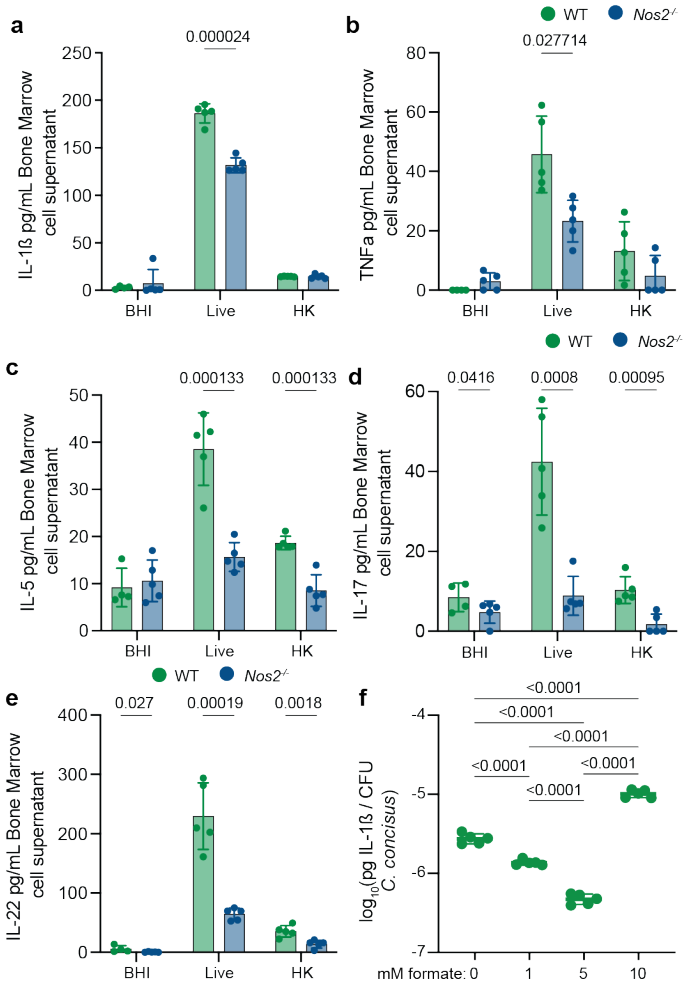

Fig. 6. *C. concisus* elicits cytokine signaling in a *Nos2*-dependent manner. a-e, Bone marrow cells harvested from conventionally-raised wild-type (WT) or iNOS$^{-/-}$ (*Nos2*$^{-/-}$) mice were incubated with live or heat-killed (HK) *C. concisus* for 48 hours and cytokines were quantified in bone marrow cell supernatants (n=4-5 biological replicates per condition, mean ± s.d., multiple unpaired t-tests with two-stage step-up FDR correction). **f,** IL-1ß quantified in bone marrow supernatants after 24 hours incubation with *C. concisus* pre-treated (grown for the 24 hours prior to co-culture) with various concentrations of formate (n=5 biological replicates per condition, mean ± s.d., one-way ANOVA: $F_{(3,16)}$=527.4, P<0.0001, Tukey's multiple comparisons shown).

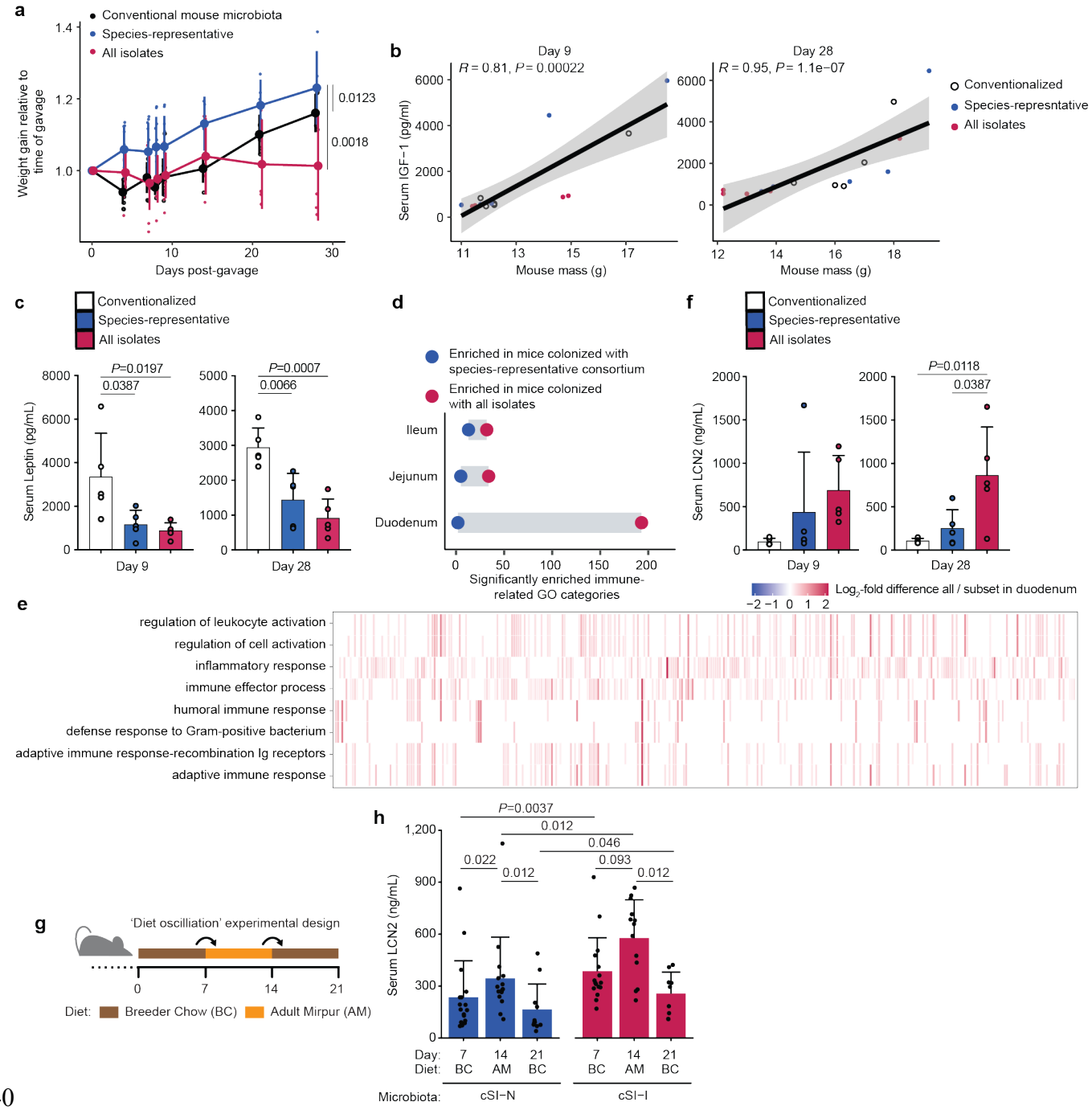

Extended Data Fig. 1. Initial test of the host response to colonization with the cSI-N and cSI-I consortia. a, Weight gain of mice colonized with all 184 isolates cultured from duodenal aspirates obtained from children with EED (cSI-I), or a species-representative set of isolates (cSI-N). A control group of CONV-D mice was colonized with cecal microbiota harvested from conventionally raised animals. All mice were fed Mirpur-18 diet *ad libitum*. Each small point represents the weight gain for an individual mouse; larger points denote the mean, error bars, standard deviation. n=5-10 mice/group, linear mixed effects model (Weight ~ Group*Day + (1|MouseID), *P*-values shown are the result of Tukey's post-hoc tests). **b,** Serum IGF-1 correlates with mouse weight measured 9 (left) or 28 (right) days after colonization (n=5 mice per group per timepoint, linear regression). **c,** Serum leptin levels determined nine (left) or 28 days (right) days post-colonization (n=5 mice per group per timepoint, bars denote mean ±

852 s.d.). **d,** Number of Gene Ontology (GO) categories related to the immune system that were significantly
853 enriched (GSEA q value < 0.05) based on differential gene expression in the small intestine of mice
854 colonized with all isolates (red) versus the species representative subset (blue). Bulk RNA-seq was
855 performed in duodenal, jejunal, and ileal tissue 28 days following gavage (n=5 mice/group). **e,** Expression
856 of genes (columns, un-labeled) that comprise the leading edge of the eight GO categories most
857 significantly enriched in animals colonized with the full consortium (red) compared to the species-
858 representative subset (blue). Bulk RNA-seq of duodenal tissue, 28 days post colonization. **f,** Serum
859 lipocalin-2 (LCN2) levels 9 (left) or 28 days (right) days post-gavage of the consortia (n=5 mice per
860 treatment group per timepoint.). **g,** Design of experiment to test whether systemic inflammation induced
861 by cSI-I consortium is influenced by diet. **h,** Serum levels of LCN2 after mice were fed breeder chow for
862 one week (day 7), Adult Mirpur the following seven days (day 14), and a final week of breeder chow (day
863 21) (Wilcoxon rank-sum tests, n=8-17 mice/group). For **a,c,f,h**, bars denote mean ± s.d.
864

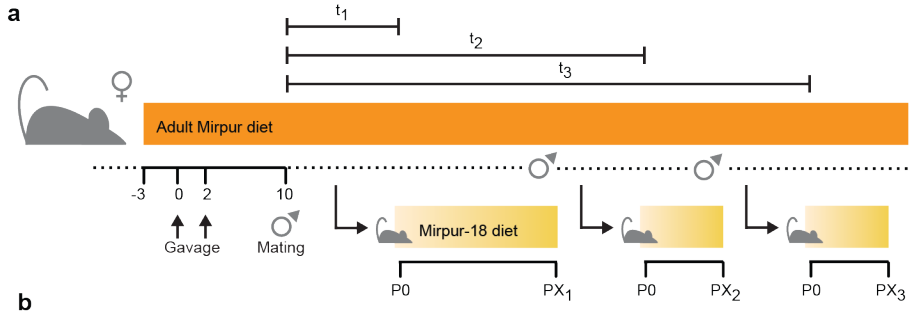

b

Microbiota	Dam	Litter 1			Litter 2			Litter 3		
		t1 (days)	PX1 (age)	Litter size	t2 (days)	PX2 (age)	Litter size	t3 (days)	PX3 (age)	Litter size
CONV-D	1	28	P37	3						
	2	28	P37	3	76	P37	5	115	P14	8
	3	52	P37	7	108	P14	5			
	4	77	P37	3						
cSI-N	1	28	P37	5	78	P37	4			
	2	28	P37	5	76	P37	3			
	3	48	P37	4	96	P14	5			
	4	51	P37	4	96	P14	6			
cSI-I	1	19	P37	4						
	2	34	P37	4	60	P14	3	101	P14	4
	3	34	P37	3	60	P14	3	100	P14	4
	4	45	P37	6	85	P37	5	115	P14	5

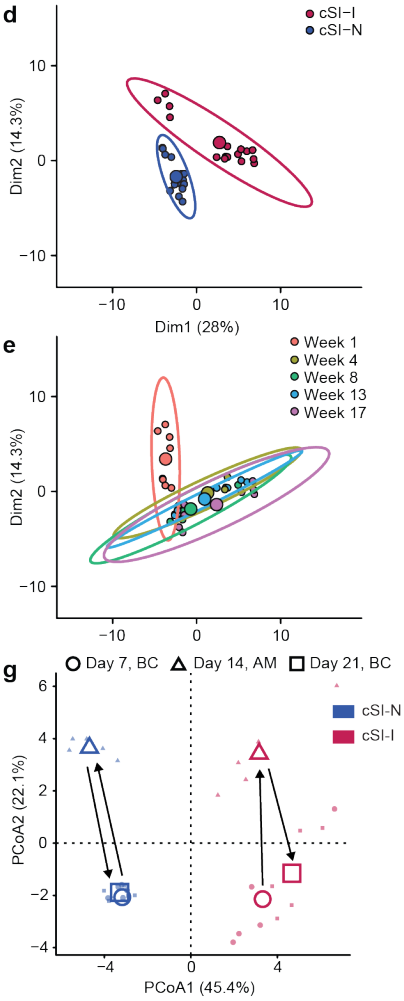

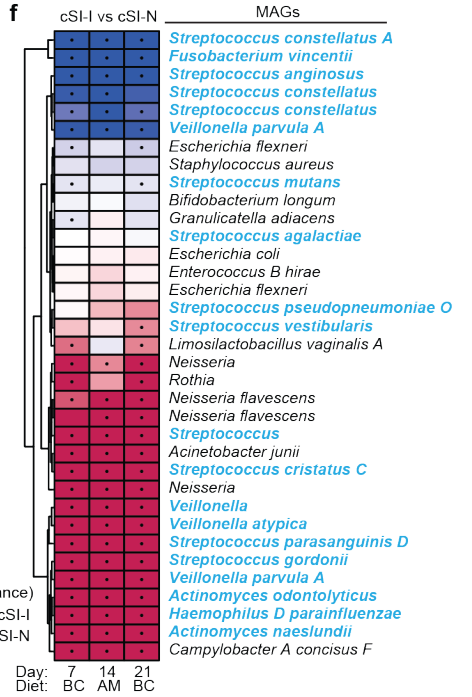

865

866 **Extended Data Fig. 2 Intergenerational transmission of duodenal bacteria. a,** Design of the
867 intergenerational transmission experiment. **b,** Summary of animals collected during intergenerational
868 experiment. Litter sizes and the age of offspring at the time of sample collection are shown for each dam
869 (n=4 dams/group). t_1-t_3 denotes the number of days between first mating and birth of the litter. **c,** MAGs
870 present at >0.001% relative abundance in gavage mixes, dams, and their P14 and P37 offspring. **d,e,**
871 Principal component analysis of MAGs in feces of dams ordinated by their $\log_{10}$ absolute abundance and
872 colored by bacterial consortium (**d**) or timepoint (**e**). The composition of community membership differs
873 significantly between cSI-I and cSI-N dams (**i**, *P*=0.01, PERMANOVA) but is stable after the first week
874 of colonization (**j**, *P*=0.09, PERMANOVA weeks 4 through 17). Each small point represents a fecal
875 sample from one animal. Larger filled circles are the centroids for the ellipses shown, which denote the
876 95% confidence interval. **f,** Detectable MAGs ($\log_{10}$ count > 0) in mice from the 'Diet oscillation
877 experiment' (**Extended Data Fig. 1g**) are included in the heatmap; MAGs that match 'core taxa'
878 described in children with EED are highlighted in blue, as in **Fig. 1b**, MAGs whose absolute abundance
879 differs significantly between cSI-I and cSI-N mice are indicated (•, *P*-adj < 0.05, FDR-corrected
880 Wilcoxon rank-sum). **g,** Principal component analysis of MAGs in feces of mice during the transition
881 from breeder chow (the larger shape denotes the centroid of points for each diet and timepoint, circle) to
882 Adult Mirpur (triangle) and back to breeder chow (square).
883

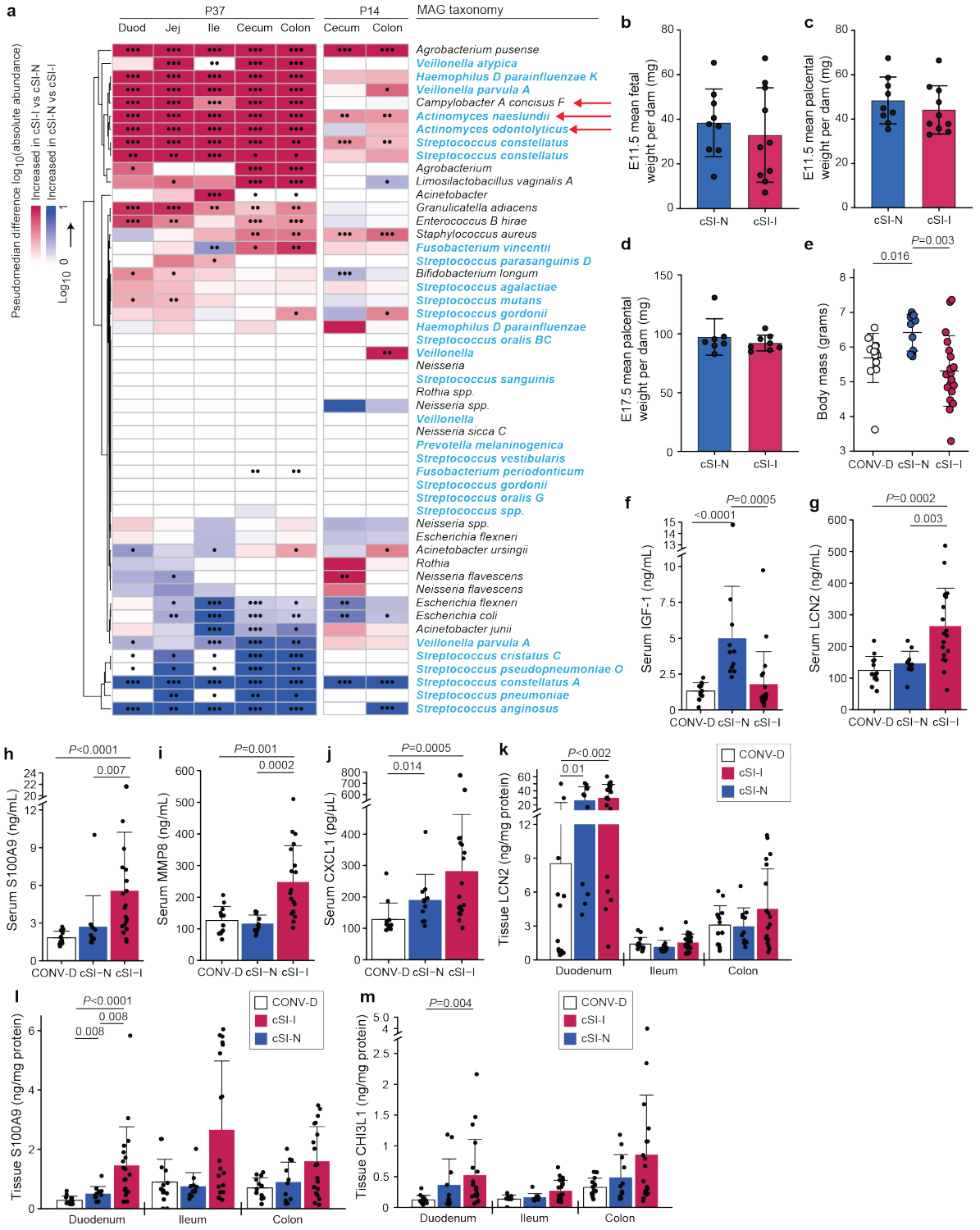

Extended Data Fig. 3. Growth and inflammatory phenotypes of P14 offspring and fetuses. a, MAGs whose absolute abundance differs significantly between P14 cSI-I and cSI-N mice are indicated (•, *P*-adj < 0.05, ••, *P*-adj < 0.01, •••, *P*-adj < 0.001, FDR-corrected Wilcoxon rank-sum). All 51 MAGs are included in the heatmap. **b,** Average masses of fetuses per dam at E11.5, n=9-10 dams/group; n=4-8 fetuses/litter. **c,d,** Average masses of placentas within each dam at E11.5 (**c**) and E17.5 (**d**); n=7-10 dams/group; n=2-10 conceptuses/litter. For **b-d**, *P*-values determined with unpaired t-tests. **e,** Body mass

892 of P14 offspring of dams colonized with the cSI-I consortium (red), cSI-N consortium (blue), or cecal
893 contents from a conventional mouse (CONV-D). Each point represents an individual animal. **f,** Serum
894 levels of IGF-1 in P14 offspring. **g-j,** Serum levels of the inflammation-associated proteins, LCN2 (**g**),
895 S100A9 (**h**), MMP8 (**i**), and CXCL1 (**j**), in P14 offspring. **k-m,** Levels of the inflammation-associated
896 proteins LCN2 (**k**), S100A9 (**l**), and CHI3L1 (**m**) in duodenal, ileal, and colonic tissue of P14 animals.
897 For **a,e-m**, n=11-19 mice/group, 3-8 pups/litter, *P*-values were determined using Wilcoxon rank-sum with
898 Tukey's post-hoc tests. For **b-m**, all panels, mean values ± s.d. are shown.
899

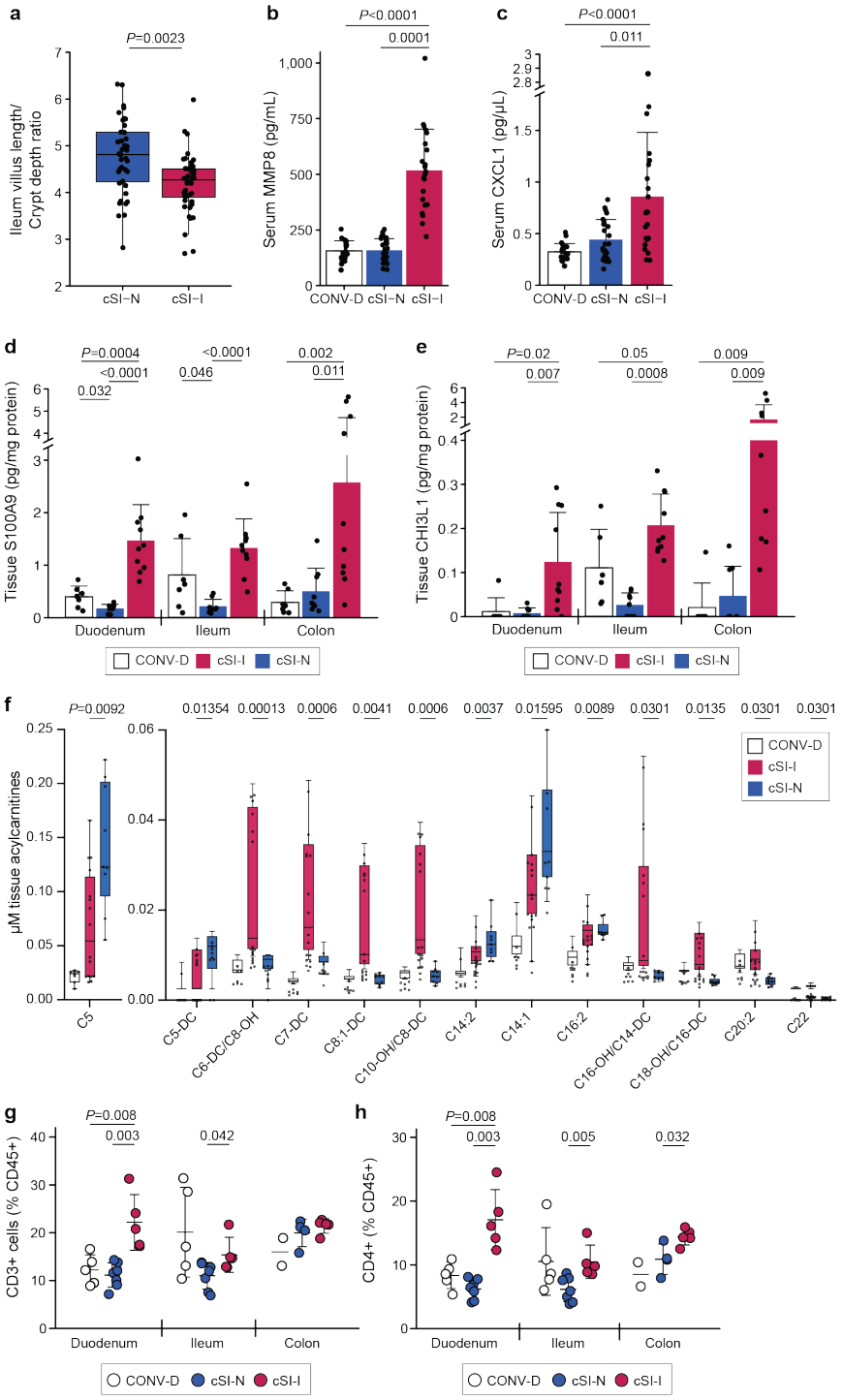

Extended Data Fig. 4. Assessment of EED biomarkers and immune profiling of P37 animals. a, Ratio of villus length to crypt depth in the ileums of cSI-I and cSI-N mice (n=5 mice/group, Wilcoxon rank-sum test; boxes denote interquartile range). **b,c,** Levels of serum MMP8 (**b**), and CXCL1 (**c**), in the P37 offspring of C57Bl/6J dams colonized with the cSI-I or cSI-N consortia, or with mouse microbiota harvested from the cecal contents of conventionally raised (CONV-D) C57Bl/6J mice (n=21-25 mice/group). **d,e,** Levels of S100A9 (**d**), and CHI3L1 (**e**), in the duodenal, ileal, and colonic tissue of P37 animals (n=7-10 animals/group). **f,** Concentration of acylcarnitines in small intestinal tissue of P37 animals. Acylcarnitines shown exhibited a statistically significant difference in levels between cSI-I

versus cSI-N groups (n=7-16 mice/group, Mann-Whitney tests with Benjamini, Krieger, Yekutieli two-stage step up FDR correction, *q*-values shown). **g,h,** Frequency of $CD3^+$ (**g**), and $CD4^+$ (**h**) immune cells in duodenal, ileal and colonic lamina propria (n=4-7 mice/group, except for colonic tissue collected from CONV-D animals for which n=2 and a statistical comparison was excluded). For panels **b-e** and **g-h**, bars denote mean ± s.d. and *P*-values were determined by Wilcoxon rank-sum tests.

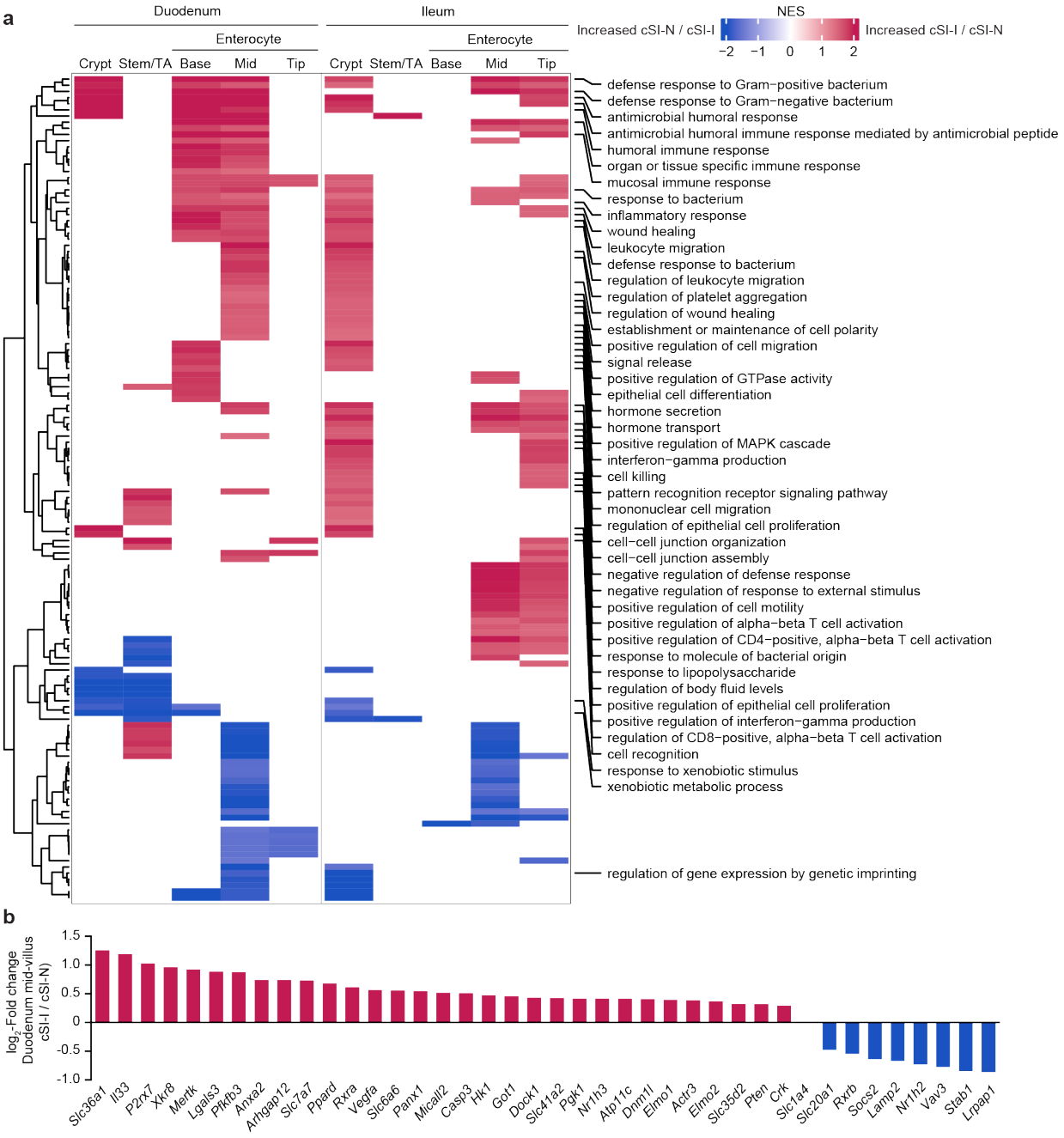

Extended Data Fig. 5. snRNA-Seq differential gene expression in the duodenum and ileum of P37 cSI-I versus cSI-N animals. a, Normalized enrichment scores (NES) for all GO categories (rows) that were significantly enriched ($q < 0.05$, GSEA) in at least two of the indicated cell populations (columns) in either the duodenum (left) or ileum (right). Immune-related GO terms are labeled. If a GO category was non-significant, it was assigned an NES value of 0. **b,** Significantly differentially expressed genes

comprising the 'leading edge' of the efferocytosis gene set in duodenal mid-villus enterocytes (cSI-I versus cSI-N; *P*-adj < 0.05, GSEA). See **Supplementary Table 3c** for annotations.

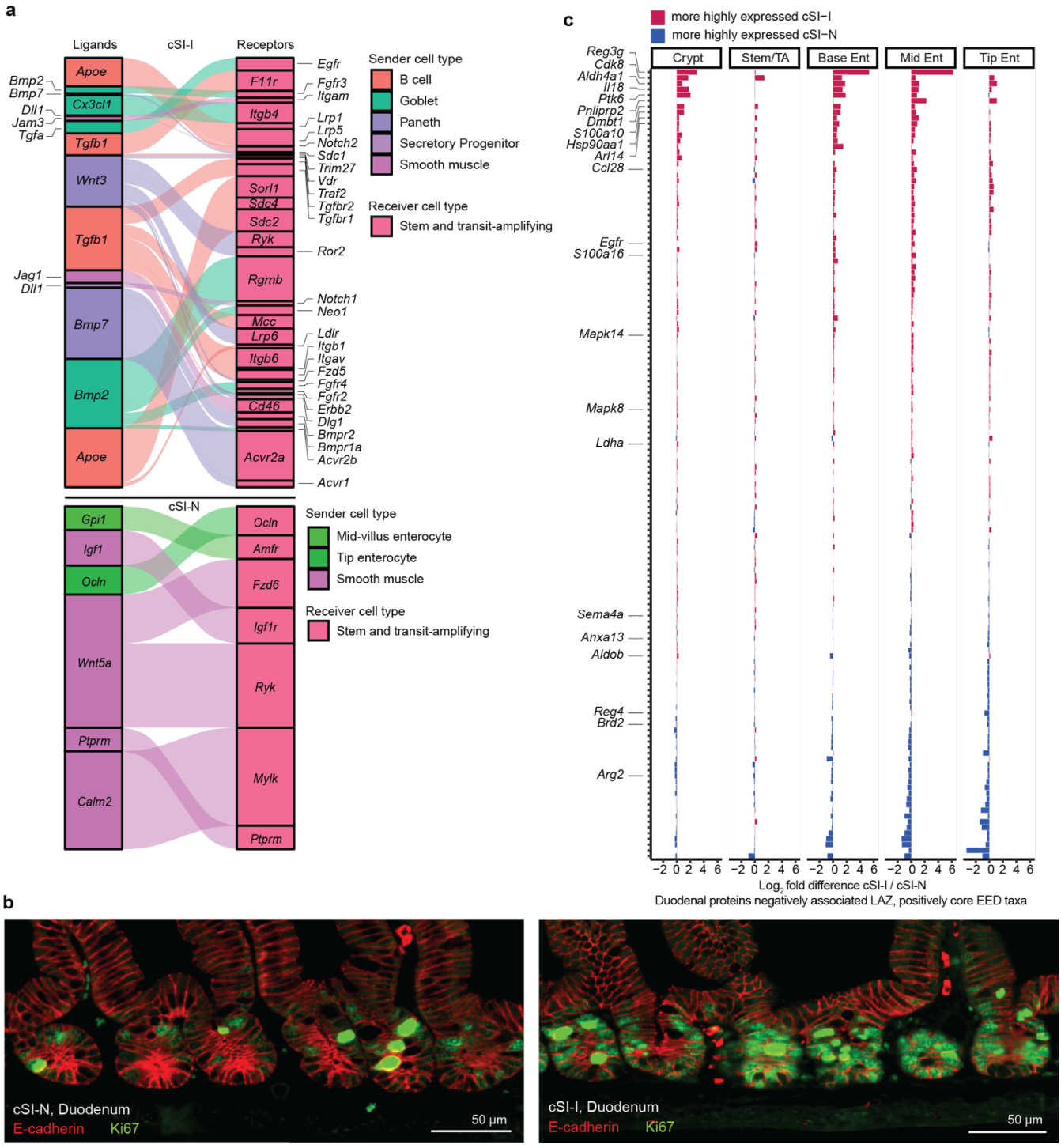

Extended Data Fig. 6. Expression of genes encoding orthologs of proteins quantified in the duodenal mucosa of children with EED and proliferative inter-cellular signaling in P37 animals. a, *NicheNet* analysis of the expression of receptors (right) in stem and transit-amplifying (TA) cells for ligands (left) expressed by various cell types in the ileum of P37 animals. Upper panel – ligands expressed more highly in cSI-I animals; lower panel – ligands expressed more highly in cSI-N animals.

933 Boxes are sized proportionally to the weighted ligand/receptor score, related to **Fig. 2d**. **b,** Representative
934 sections of crypts from the duodenum of cSI-N (left) and cSI-I (right) P37 mice. Sections were stained
935 with antibodies to E-cadherin (red) and Ki67 (green). Scale bar, 50 µm. **c,** Expression of transcripts
936 (rows) in cell populations (columns) in the duodenum of P37 animals that match proteins, quantified in
937 biopsies of the duodenal mucosa of Bangladeshi children with EED, that were (i) negatively correlated
938 with their LAZ and (ii) positively correlated with the absolute abundances of 'core' EED bacterial taxa;
939 the abundances of these taxa were positively correlated with their degree of stunting); related to **Fig. 2c**
940 (see **Supplementary Table 3c** for a list of the mouse homologs of LAZ-associated human proteins).
941

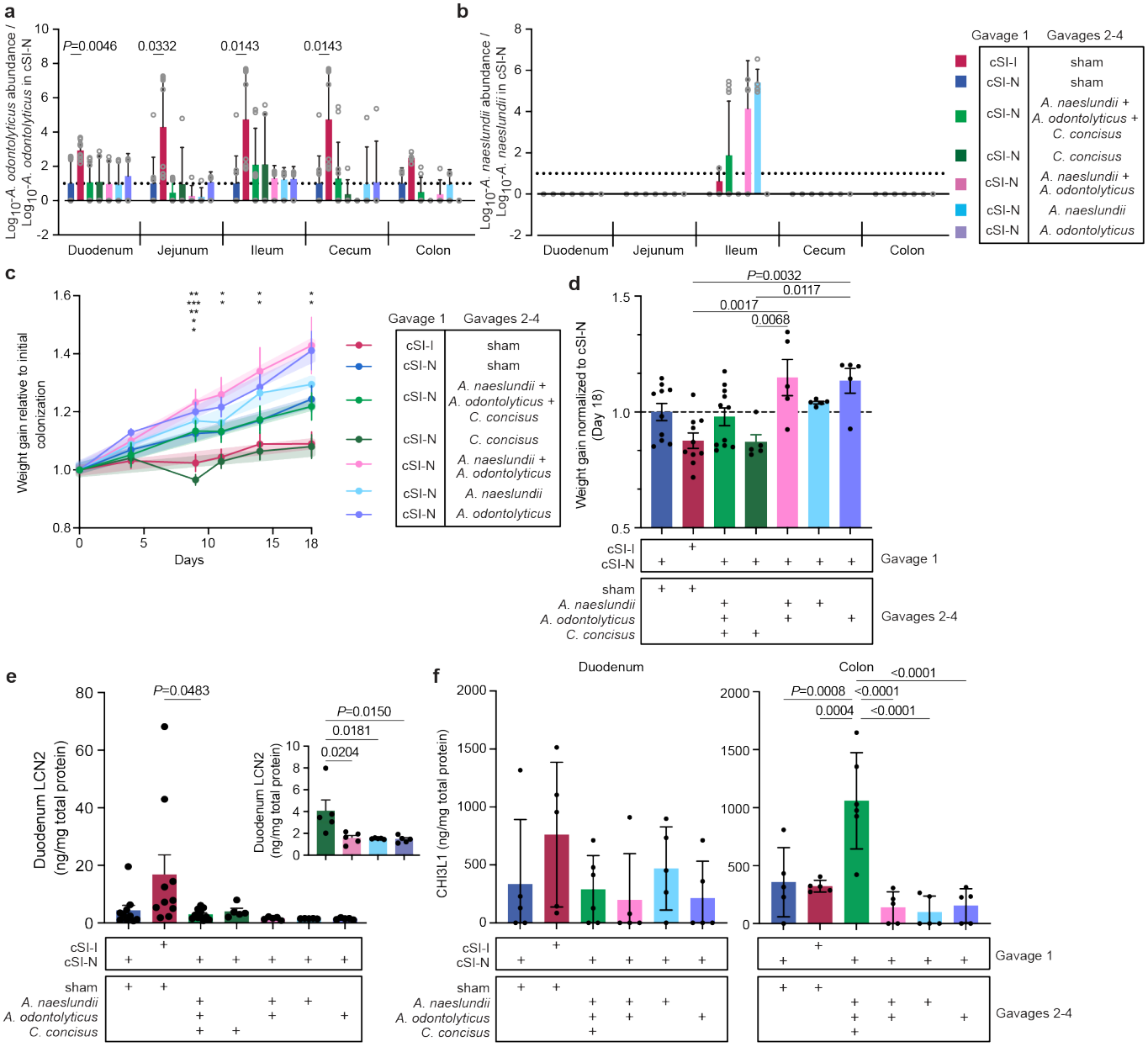

Extended Data Fig. 7. Abundance of *Actinomyces* in isolate 'add-in' experiments and. a,b, Mice were initially colonized with either the cSI-N or cSI-I consortium ('gavage 1'). Gavages 2-4 were performed on experimental days 9 through 11, as in **Fig. 4a**. The absolute abundances of *A. odontolyticus* isolate Bg044 (corresponding to MAG044, panel **a**) and *A. naeslundii* isolate Bg041 (corresponding to MAG041, panel **b**), shown relative to their absolute abundance in the cSI-N/sham-gavaged controls (a ratio of 1 is indicated by dotted line; mixed-effects analysis with Dunnett's multiple comparisons to cSI-N/sham control; mean values ± s.d. are shown.) **c,** Changes in body mass relative to time of colonization in mice in 'add-in' experiments (points and error bars denote mean values ± s.e.m.; shaded, thicker line represents results of linear regression. *P<0.05, **P<0.01, ***P<0.001 for Tukey's multiple comparisons demonstrating significant differences between *C. concisus*-gavaged animals compared to cSI-N/mock, cSI-N/*A.naeslundii*, *A. odontolyticus*, or *Actinomyces* from two-way repeated measures ANOVA; all stats are reported in **Supplementary Table 2b**). **d**, Relative weight gain in isolate-gavaged and cSI-I/mock-gavaged animals relative to weight gain in cSI-N mice (one-way ANOVA with Tukey's post-hoc, mean ± s.e.m.). **e,** Levels of LCN2 protein in duodenal tissue on experimental day 18 (one-way ANOVA with

Tukey's multiple comparisons; mean values ± s.e.m. are shown). The inset shows comparisons between individual isolates. **f,** Tissue levels of CHI3L1 (Chitinase-3-like protein 1) in the duodenum and colon (one-way ANOVA with Tukey's multiple comparisons, n=5-6 mice/group, mean ± s.d. shown). For **a-e**, n=5-11 mice/group combined across two independent experiments.

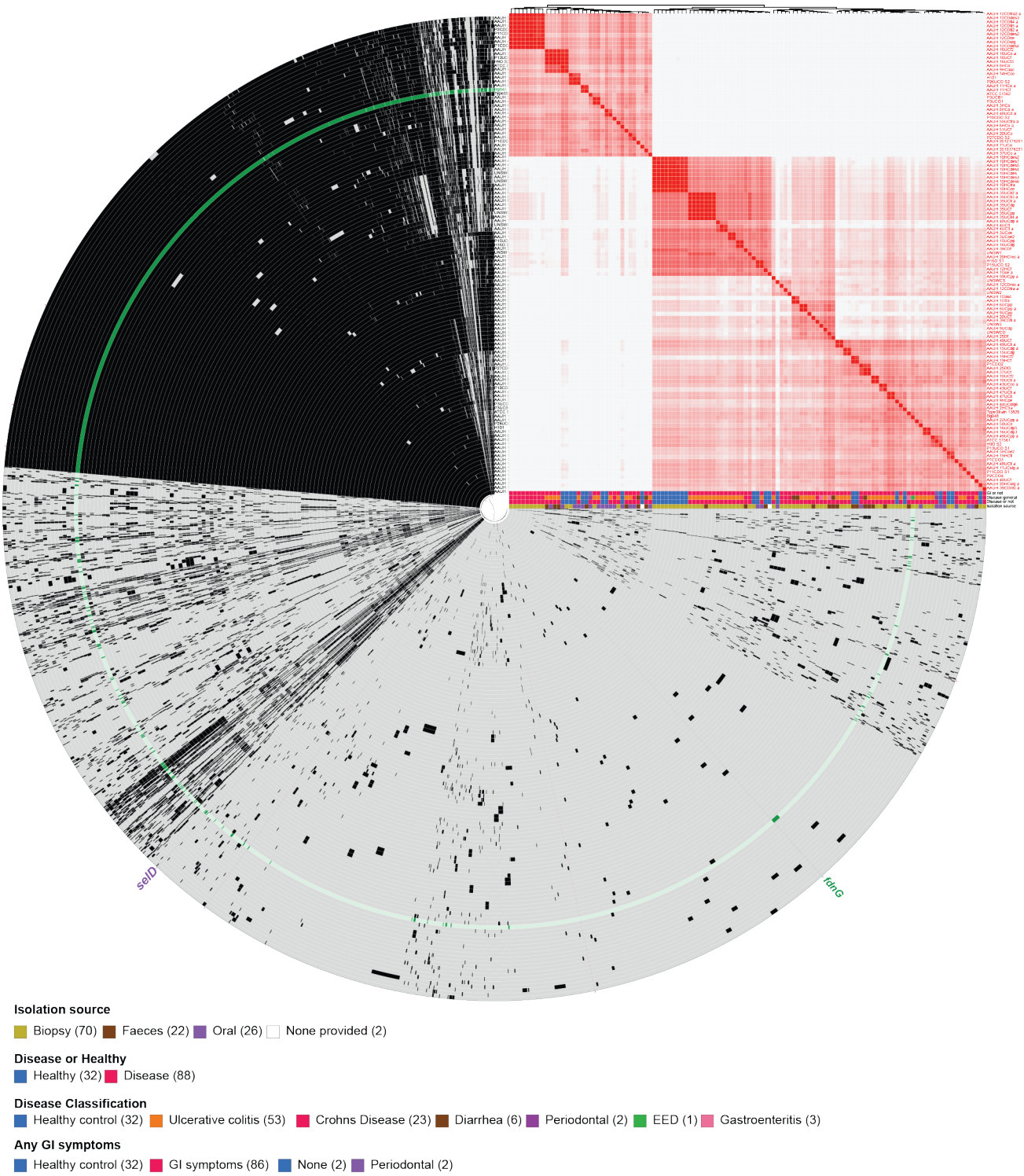

Extended Data Fig. 8. Comparative genomic analysis of *C. concisus* isolates. 120 whole *C. concisus* genomes are included in the circle phylogram that were isolated from intestinal biopsies, feces, or saliva

967 of healthy or diseased individuals. Genes that are present are shown in black; if genes are absent, in gray.
968 The Bangladeshi isolate from children with EED (Bg048) is highlighted in green. The nitrate-inducible
969 formate dehydrogenase (*fdnG*) unique to this Bangladeshi isolate and a selenate di-kinase (*selD*) unique to
970 the Bangladeshi isolate and one other genome are highlighted. Heatmap shows ANI comparisons between
971 all isolates.

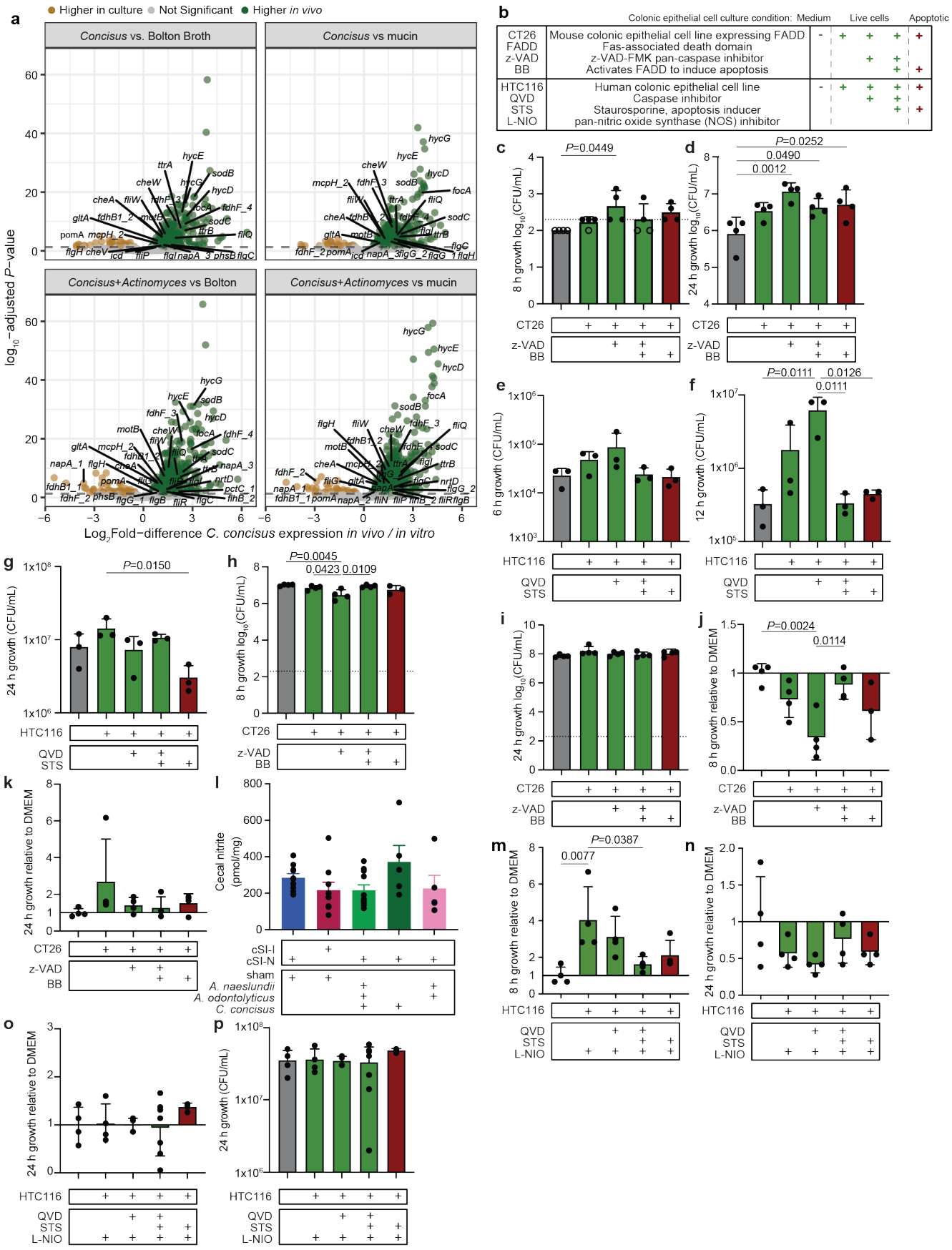
a
Higher in culture
Not Significant
Higher in vivo
Concisus vs. Bolton Broth
Concisus vs mucin
Concisus+Actinomyces vs Bolton
Concisus+Actinomyces vs mucin
log10−adjusted P−value
Log2Fold−difference C. concisus expression in vivo / in vitro
b
Colonic epithelial cell culture condition: Medium Live cells Apoptotic
CT26 Mouse colonic epithelial cell line expressing FADD
FADD Fas-associated death domain
z-VAD z-VAD-FMK pan-caspase inhibitor
BB Activates FADD to induce apoptosis
HTC116 Human colonic epithelial cell line
QVD Caspase inhibitor
STS Staurosporine, apoptosis inducer
L-NIO pan-nitric oxide synthase (NOS) inhibitor
c
P=0.0449
8 h growth log10(CFU/mL)
d
P=0.0252
0.0490
0.0012
24 h growth log10(CFU/mL)
e
6 h growth (CFU/mL)
f
P=0.0111
0.0126
0.0111
12 h growth (CFU/mL)
g
P=0.0150
24 h growth (CFU/mL)
h
P=0.0045
0.0423
0.0109
8 h growth log10(CFU/mL)
i
24 h growth log10(CFU/mL)
j
P=0.0024
0.0114
8 h growth relative to DMEM
k
24 h growth relative to DMEM
l
Cecal nitrite (pmol/mg)
cSI-I
cSI-N
sham
A. naeslundii
A. odontolyticus
C. concisus
m
P=0.0387
0.0077
8 h growth relative to DMEM
n
24 h growth relative to DMEM
o
24 h growth relative to DMEM
p
24 h growth (CFU/mL)
HTC116
QVD
STS
L-NIO
CT26
z-VAD
BB

973 **Extended Data Fig. 9. *C. concisus* growth in spent medium collected from colonic epithelial cells. a,**
974 *C. concisus* gene expression in the gut (*Concisus*, *Concisus+Actinomyces*) from the isolate 'add-in'
975 experiment (**Fig. 5**) compared to growth in rich medium (Bolton broth, or Bolton broth supplemented
976 with 1% mucin). Green, *P*-adj < 0.05 and higher expression in the gut; brown, *P*-adj < 0.05 and higher
977 expression *in vitro* (*DESeq2* Wald test, n=4 biological replicates per condition). Genes involved in
978 formate metabolism and anaerobic respiration are labelled. **b,** Abbreviations of cell lines and treatments
979 used to generate conditioned medium from mouse and human colonic epithelial cells that were live or
980 apoptotic. *C. concisus* growth in conditioned medium acquired from live cells are colored in green;
981 apoptotic cells, in red. QVD, Quinoline-Val-Asp-Difluorophenoxymethylketone (caspase inhibitor); L-
982 NIO, N^5-(1-Iminoethyl)-L-ornithine, dihydrochloride (nitric oxide synthase inhibitor). **c,d,**
983 Microaerophilic growth of *C. concisus* after 8 (**c**) or 24 hours (**d**) in conditioned medium from mouse
984 CT26 colonic epithelial cells that were live (CT26:FADD, z-VAD, z-VAD+BB) or treated with an
985 inducer of apoptosis (BB). Points shown with an open rather than filled circle denote abundances that
986 were below the limit of detection at the time of quantification and are presented at the limit of detection of
987 the assay. **e-g,** Microaerophilic growth of *C. concisus* after 6 (**e**), 12 (**f**), or 24 (**g**) hours in spent medium
988 from HTC116 human colonic epithelial cells that were live (QVD, QVD+STS) or that had been treated
989 with an inducer of apoptosis (STS). **h-k,** Anaerobic growth of *C. concisus* after 8 (**h, j**) or 24 hours (**i, k**)
990 in conditioned medium from live CT26 mouse colonic epithelial cells (CT26:FADD, z-VAD, z-
991 VAD+BB) or from cells treated with an inducer of apoptosis (BB). Panels **j** and **k** show growth relative to
992 (as a ratio to) growth in tissue culture medium. **l,** Levels of nitrite in cecal contents 9 days post-isolate
993 gavage (n=5-11 mice/condition, combined across two independent experiments). **m,n,** Microaerophilic
994 growth of *C. concisus* after 8 (**m**) or 24 (**n**) hours growth in conditioned medium from HTC116 human
995 colonic epithelial cells acquired from live cells (QVD, QVD+STS) or cells treated with an inducer of
996 apoptosis (STS). All cells were treated with an inhibitor of nitric oxide synthase (L-NIO). Growth shown
997 as a ratio to growth in cell culture medium alone. **o,p,** Anaerobic growth of *C. concisus* after 24 hours of
998 incubation in conditioned medium from HTC116 cells collected from live cells (QVD, QVD+STS) or
999 cells that had been treated with an inducer of apoptosis (STS). All cells were treated with an inhibitor of
1000 nitric oxide synthase (L-NIO). Panel **o** shows growth as a ratio to growth in tissue culture medium alone;
1001 **p**, total bacterial growth. For **c-p**, bars denote mean ± s.d., *P*-values determined with one-way ANOVA
1002 and Tukey's multiple comparisons. For **c,d**, **g-k**, **m-p**, n=4 biological replicates/condition; for **e,f**, n=3
1003 biological replicates/condition.
1004

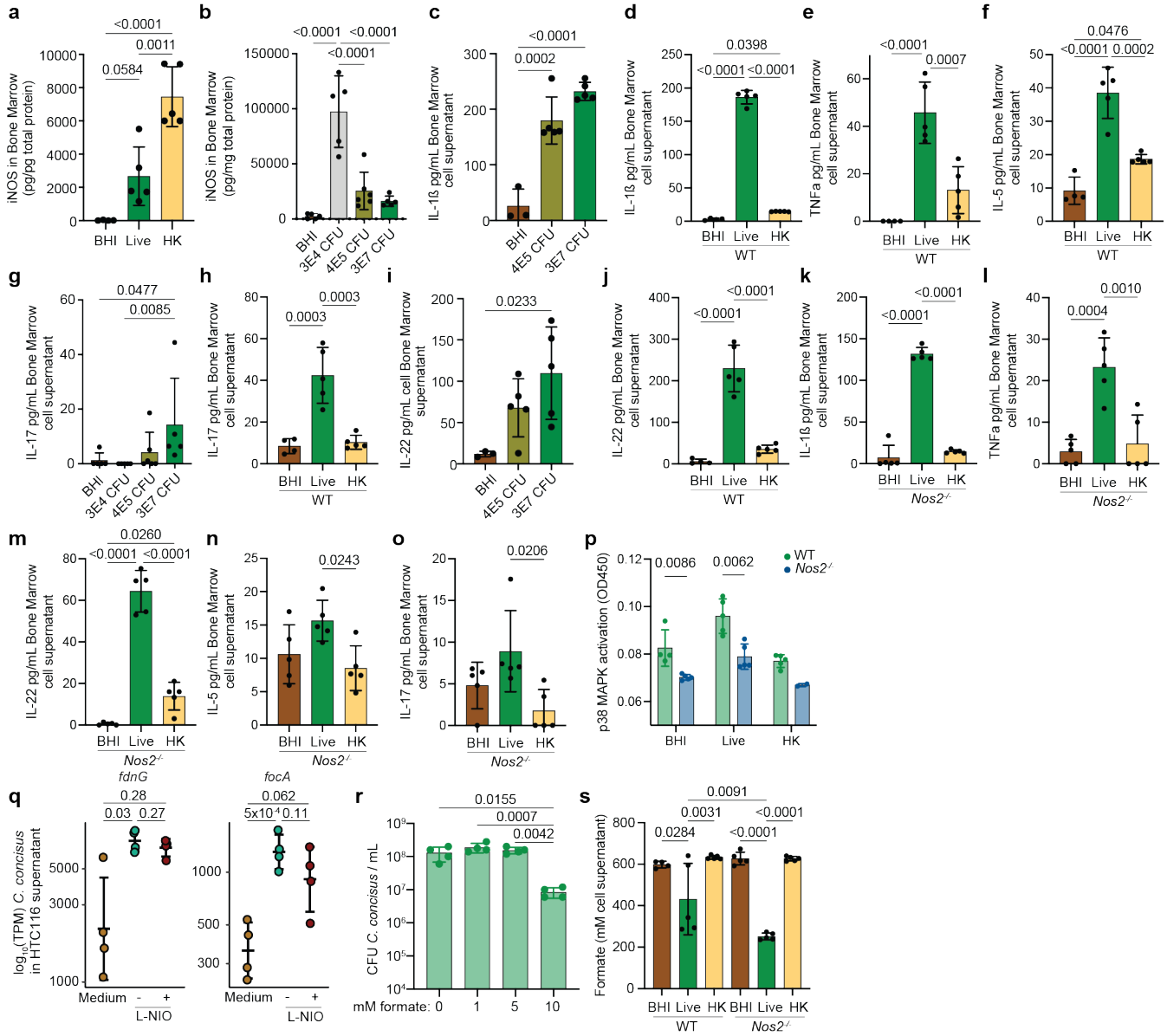

Extended Data Fig. 10. *C. concisus* induces iNOS and immune signaling. a,b, Bone marrow cells from wild-type (WT) mice were incubated for 48-hours with fresh (Live) or heat-killed (HK) *C. concisus* culture, or bacterial medium as a negative control. **b,** Bone marrow cells were co-cultured for 48-hours with increasing amounts of live *C. concisus* culture. Proteins were extracted from bone marrow cell pellets and iNOS levels were quantified. **c-j,** Bone marrow cells collected from wild-type (WT) mice were incubated for 48 hours with fresh *C. concisus* culture (Live, CFU), heat-killed *C. concisus* culture (HK), or bacterial medium as a negative control (BHI). IL-1ß (**c,d**), TNFa (**e**), IL-5 (**f**), IL-17 (**g,h**), and IL-22 (**i,j**) were quantified in cell supernatant. **k-o**, Bone marrow cells collected from *Nos2*$^{-/-}$ mice were incubated for 48 hours with fresh (Live) or heat-killed (HK) *C. concisus* culture. Again, IL-1ß (**k**), TNFa (**l**), IL-22 (**m**), IL-5 (**n**) and IL-17 (**o**) were quantified from cell culture supernatants. **p,** p38 MAPK activation was assessed in bone marrow cell lysates after 48 hours incubation bacterial medium (BHI), fresh *C. concisus* culture (Live), or heat-killed (HK) *C. concisus* culture (multiple unpaired t-tests with two-stage step-up FDR correction). **q,** Expression of the *C. concisus* nitrate-inducible formate dehydrogenase (*fdnG*) and formate transporter (*focA*) when cultured in supernatants collected from HTC116 cells that were or were not treated with the NOS inhibitor L-NIO or cell culture medium alone

1022 (statistics shown are unadjusted *P* values from the *DESeq2* Wald test, transcripts per million). **r,** *C.*
1023 *concisus* was cultured in Bolton broth supplemented with various levels of formate; growth was
1024 quantified after 24 hours. **s,** Formate was quantified in supernatants from bone marrow cells incubated for
1025 48 hours with bacterial culture medium (BHI), fresh *C. concisus* culture (Live), or heat-killed *C. concisus*
1026 culture (HK). For all panels, n=4-5 biological replicates/condition, bars denote mean ± s.d.. For **a-o**, **r**,**s**,
1027 *P*-values shown are the result of one-way ANOVA followed with Tukey's multiple comparisons.
1028

SUPPLEMENTARY TABLES

Supplementary Table 1. Diet and bacterial abundance information from gnotobiotic mouse experiments. a, Diets used in gnotobiotic mouse studies. Ingredients in and nutritional analysis of each diet. **b,** Cultured isolates and taxonomic classification from BEED study duodenal aspirates. **c,** MAG assembly information and MAG taxonomic classification. (i), Assembly and taxonomic classification. (ii), Sample metadata. **d,** Abundances of MAGs from gnotobiotic animal experiments. (i), Diet oscillation experiment, $\log_{10}$-tpm (**Extended Data Figs. 2f,g**). (ii), Intergenerational transmission experiment, absolute abundance: P37 animals (**Figs. 1c, 3j, Extended Data Figs. 2c, 3a**), P14 animals (**Extended Data Fig. 3a**) and adult mice (**Extended Data Figs. 2c-e**). (iii), Cohousing experiment, absolute abundance (**Figs. 3h,i**). (iv), Isolate add-in experiments, absolute abundance (**Fig. 4b, Extended Data Figs. 7a,b**). Abundance values are $\log_{10}$-transformed. *P*-adj values determined by Wilcoxon rank-sum tests and FDR correction.

Supplementary Table 2. Phenotypic data from gnotobiotic mouse experiments. a, Body weights from gnotobiotic animal experiments. (i) Preliminary test of consortia in recently weaned mice (**Extended Data Fig. 1a**); (ii), Intergenerational transmission experiment: P37 animals, P14 animals (**Extended Data Fig. 3e**) and conceptuses (**Fig. 1c, Extended Data Figs. 3b-d**) (Wilcoxon rank-sum tests). (iii), Cohousing experiments (linear mixed effects modeling). (iv), Gavage of pathology-associated isolates, 'add-in' experiments (**Extended Data Figs. 7c,d**) (repeated measures ANOVA). **b,** Protein levels in tissues from gnotobiotic animal experiments. (i), First test of consortia in recently weaned mice (**Extended Data Figs. 1b,c,f**). (ii), Diet oscillation experiment (**Extended Data Fig. 1h**). (iii), Intergenerational transmission experiment: P37 duodenum, ileum, colon, serum and cerebral cortex (**Figs. 1f-h, Extended Data Figs. 4b-e, Supplementary Fig. 2a**); P14 duodenum, ileum, colon and serum (**Extended Data Figs. 3f-m**); adult duodenum, ileum, colon, and serum. (iv), Cohousing experiments: duodenum, ileum, colon and serum (**Figs. 3b-c**). (v), Isolate add-in experiments: duodenum, colon and serum (**Fig. 4c-e, Extended Data Figs. 7e-f**). **c,** Histomorphometric analysis of small intestines of P37 animals from the intergenerational transmission experiment. (i), Duodenal (**Figs. 1d,e**) and (ii) ileal villus height, crypt depth, villus to crypt ratio (**Extended Data Fig. 4a**), and Ki67 quantification (**Fig. 2d, Extended Data Fig. 6b**). *P*-values determined using Tukey's post-hoc tests. **d,** Micro-computed tomography of femurs of P37 animals from the intergenerational experiment. *P*-values were determined using Wilcoxon rank-sum tests. **e,** Quantification of small intestinal acylcarnitines in P37 offspring ($\log_{10}$-μM) (**Extended Data Fig. 4f**). **f,** Immune cell profiling of tissues from gnotobiotic animal experiments. (i), Intergenerational transmission experiment: P37 duodenum, ileum, colon, spleen and meninges (**Figs. 1i,j, Extended Data Figs. 4g,h, Supplementary Figs. 1a-c**); duodenum, ileum, spleen and meninges of the dams. (ii), Cohousing experiment: bulk small intestinal tissue, spleen and meninges (**Figs. 4d-g**). *P*-values determined using Wilcoxon rank-sum tests. **g,** Quantification of ultrasonic vocalization metrics in P5-P9 pups (**Supplementary Figs. 1h,i**). **h,** Length of time for cSI-I and cSI-N dams to retrieve separated pups (**Supplementary Fig. 1j**).

Supplementary Table 3. Supplemental data for host RNA-sequencing. a, Bulk tissue RNA-Seq from gnotobiotic animal experiments. (i), Preliminary tests of consortia in recently weaned animals, significantly differentially expressed genes and results of GSEA between cSI-I and cSI-N-colonized mice 28 days after gavage in the duodenum, jejunum and ileum (**Extended Data Figs. 1d,e**). (ii), Intergenerational transmission experiment: gene set enrichment analysis (GSEA) of gene expression in the duodenum, ileum and colon of P37 animals. (iii), Cohousing experiment: differentially expressed genes in duodenal samples for: non-cohoused cSI-I controls versus non-cohoused cSI-N controls and cohoused versus non-cohoused cSI-N controls. There were no statistically significant differentially expressed genes between cohoused and cSI-I controls. GSEA of gene expression in the colon of non-cohoused cSI-I controls vs. non-cohoused cSI-N controls and cohoused vs. non-cohoused cSI-N controls (**Fig. 4f**). (iv), Add-in experiment: GSEA of gene expression in the colon. Pathways shown were enriched in all the following conditions: cohoused animals vs. cSI-N non-cohoused controls, *C.*

concisus+Actinomyces-gavaged animals vs. cSI-N sham-gavaged controls and *C. concisus*-gavaged animals vs. cSI-N sham-gavaged controls. Values provided (*P*- and *q*-values, enrichment scores, rank, leading edge, core enrichment) are for *C. concisus+Actinomyces*-gavaged vs. cSI-N sham-gavaged animals (**Fig. 4f**). **b,** Proportions of cell types quantified by snRNA-Seq in the duodenums (i) and ileums (ii) of P37 animals from the intergenerational transmission experiment (**Figs. 2a,b**) (n=3 mice/group, statistical significance determined by *edgeR*). **c,** snRNA-Seq analysis of duodenums and ileums of P37 offspring from intergenerational transmission experiment. (i) Pseudo-bulk differential expression of enterocyte clusters in the duodenum and ileum of cSI-I compared to cSI-N animals (n=3 mice/group; *DESeq2* Wald test). (ii) GSEA of gene expression along the crypt-villus axis (**Extended Data Fig. 5a**). (iii) GSEA and annotations for genes involved in efferocytosis (**Extended Data Fig. 5b**). (iv) 'Differential *NicheNet'* results (**Fig. 2c, Extended Data Fig. 6a**). (v) GSEA of homologues in the mouse gut (P37 duodenum and ileum) to LAZ-associated proteins quantified in the duodenal mucosa of children in the BEED study (**Fig. 2e, Extended Data Fig. 6c**). **d,** snRNA-Seq analysis of cerebral cortices of P37 offspring from the intergenerational transmission experiment. (i), Pseudobulk differential expression of glutamatergic neurons in the cerebral cortex (**Supplementary Fig. 1e**) (n=4 mice/group; *DESeq2* Wald test). (ii), GSEA of significantly (*P*-adj<0.05) differentially expressed genes in the cortex. (iii), Differential expression of S100A9-associated vs. background glutamatergic neurons. Positive $\log_2$-fold change indicates higher expression in S100A9-associated neurons (**Supplementary Fig. 2b**) (determined with the *FindMarkers* function in *Seurat*). Results of 'Differential *NicheNet*' analysis (**Supplementary Figs. 1g, 2c,d**) (iv). **e,** GSEA results in the duodenum and colon for bulk RNA-seq datasets of animals from cohousing and 'add-in' experiments; all treatment groups presented were compared to their cSI-N counterparts (**Fig. 4f**).

Supplementary Table 4. Comparative genomics analysis. a, Isolate genome assembly information and taxonomic classification. (i), Quality assessment and taxonomic classification of assembled isolate genomes. (ii), Average nucleotide identity (ANI) of isolate genomes with their related MAGs. (iii), Species-specific virulence factors in MAGs, their respective isolate genomes, and related reference genomes. **b,** *In silico* metabolic reconstructions of MAGs and isolate genomes. (i), mcSEED-based metabolic annotation for each MAG by gene. (ii), Annotations for pathology-associated MAGs and phylogenetically related organisms by gene. (iii) 'Metabolic phenotype' prediction key. **c,** *C. concisus* pan-genome analysis (**Extended Data Fig. 8**). (i), List of 120 isolate genomes included in pan-genomic analysis and their association with disease. Enrichment analyses performed on predicted genes (ii), COG20 functional annotations (iii) and COG Pathway annotations (iv). Enrichment results were included if functional groups were enriched in isolates from diseased conditions (Crohn's Disease, Ulcerative colitis, Gastroenteritis, Periodontitis) including EED, but not in isolates from healthy controls.

Supplementary Table 5. Supplemental data for microbial RNA-sequencing. a, Significantly differentially expressed *C. concisus* genes in the gut compared to growth in culture (**Extended Data Fig. 9a**) (*DESeq2* Wald test). (i,ii), *C. concisus* gene expression in the gut (single isolate 'add-in') compared to rich medium (Bolton broth ± 1% mucin). (iii,iv) *C. concisus* gene expression when gavaged concurrently with the *Actinomyces* strains (*C. concisus+Actinomyces*) compared to gene expression in rich medium (Bolton broth ± 1% mucin). **b,** *C. concisus* gene expression in the mouse gut in conditions where inflammation was produced [*C. concisus* (i), *C. concisus+Actinomyces* (ii), cSI-I (iii)] compared to cSI-N/mock-gavaged controls (**Figs. 5b,c**). **c,** *C. concisus* gene expression in spent medium collected from HTC116 cells compared to medium alone (**Fig. 5l**) (i). *C. concisus* gene expression in conditioned medium from HTC116 cells treated with the pan-nitric oxide inhibitor L-NIO compared to medium control (ii).

Supplementary Table 6. Antibody panels for flow cytometry analyses. Antibodies used for flow cytometry. (i), Antibodies used for flow cytometry of intestinal immune cells in intergenerational transmission and cohousing experiments (**Figs. 1i,j, Extended Data Figs. 4g,h**). (ii and iii), Antibodies

used for flow cytometry of splenic and meningeal immune cells in intergenerational transmission (ii, **Supplementary Figs. 1a-c**) and cohousing experiments (iii, **Figs. 3f,g**).

Supplementary Table 7. Metadata associated with sequencing datasets. Sequencing metadata from gnotobiotic animal and bacterial culture experiments. **a,** Bulk RNA-Seq collected from preliminary test of consortia (**Extended Data Figs. 1d,e**). **b,** Intergenerational transmission experiment: (i) short read shotgun DNA sequencing (**Figs. 1b,3j, Extended Data Figs. 2c-e, 3a**), (ii) snRNA-Seq (**Figs. 2a-c,e, Extended Data Fig. 5,6a,b, Supplementary Figs. 1d-g, 2b-d**), (iii) bulk tissue RNA-Seq (**Fig. 4f, Supplementary Fig. 2b**) and (iv) microbial RNA-Seq. **c,** Cohousing experiment: (i) short read shotgun DNA sequencing (**Figs. 3h,i**), (ii) bulk tissue RNA-Seq (**Fig. 4f**) and (iii) and microbial RNA-Seq. **d,** Isolate add-in experiments: (i) short read shotgun DNA sequencing (**Fig. 4b, Extended Data Figs. 7a,b**), (ii) and bulk tissue RNA-Seq and (iii) microbial RNA-Seq. **e,** *C. concisus* microbial RNA-Seq in culture medium and conditioned medium collected from HTC116 cells (**Fig. 5l, Extended Data Fig. 9a**).

METHODS

Mouse experiments

All experiments involving mice were performed using protocols approved by Washington University Animal Studies Committee. Mice were housed in plastic flexible film gnotobiotic isolators (Class Biologically Clean Ltd., Madison, WI) at 23 ºC under a strict 12-hour light cycle (lights on at 0600h). Autoclaved paper 'shepherd shacks' were kept in each cage to facilitate the natural nesting behaviors and for environmental enrichment.

Source of cSI-I and cSI-N bacterial consortia – The methods used for culturing bacterial strains from duodenal aspirates that were obtained from children enrolled in BEED study are described in a previous publication[5]. Strains were stored at -80 ºC in PBS containing 15% glycerol (v/v). For isolates originally isolated under anaerobic conditions, a 20 µL aliquot of each stock was used to inoculate a well in a 1 mL deep-well plate (Thermo Scientific) containing 600 µL LYBHI broth (Brain Heart Infusion [BHI] broth supplemented with 0.05% L-cysteine HCl [w/v] and 0.5% yeast extract [w/v]) followed by incubation under anaerobic conditions (atmosphere 75% N_2, 20% CO_2 5% H_2). For isolates originally isolated under microaerophilic conditions (85% N_2, 10% CO_2, 5% O_2), a 20 µL aliquot of each stock was inoculated into 600 µL BHI broth. After incubation for 48 hours at 37 ºC, a 20 µL aliquot of each anaerobic or microaerophilic culture was added to 600 µL of fresh medium which was incubated for an additional 24 hours at the same temperature under the same atmospheric conditions. Equal volumes of each isolate sub-culture were then pooled and a solution of PBS containing 30% glycerol (v/v) was added resulting in a final 15% glycerol pooled stock (v/v). Pooling was performed in the Coy chamber. The 15% glycerol pooled stock was sealed in multiple 1.8-mL crimp glass vials (Wheaton) and the vials were stored at -80 ºC prior to gavage into mice.

Diets – The 'Adult Mirpur' diet was designed based on 24-hour dietary recall surveys and food frequency questionnaires taken from adults enrolled in the BEED study living in an urban slum located in the Mirpur district of Dhaka City, Bangladesh[69]. A pelleted, sterile version of this diet was manufactured by Dyets, Inc. (Bethlehem, PA). The quantity of each ingredient used to prepare the diet is provided in **Supplementary Table 1a**. Rice (parboiled, long grain) and red lentils (masoor dal) were each cooked separately with an equal weight of water at 100 °C in a steam-jacketed kettle until the grains were cooked but still firm and then set aside. Tilapia filets (frozen) were steamed separately at 100 °C in a steam-jacketed kettle with a small amount of water until tender (15-20 minutes). Sweet pumpkin (Calabaza variety) was chopped, boiled in the steam-jacketed kettle until soft and then strained. Fresh market white potatoes, Daikon radish (moola), spinach, okra and yellow onions were washed, finely chopped and cooked together in the steam kettle without added water at 70 °C until soft. After cooling, all cooked ingredients were combined and mixed with the wheat flour (atta), soybean oil, salt, turmeric, garlic and coriander powder. The resulting diet was mixed extensively using a planetary mixer, spread on trays, dried overnight at 30 °C, and pelleted by extrusion (½ inch diameter; California Pellet Mill, CL5). Dried pellets were aliquoted into ~250 g portions and placed in a paper bag with an inner wax lining, which was

then placed in a plastic bag. Bags were subsequently vacuum-sealed, and their contents sterilized by gamma irradiation (30-50 kGy; Sterigenics).

The composition of the 'Mirpur-18' diet was based on Bangladeshi complementary feeding practices for 18-month-old children living in Mirpur, as defined by quantitative 24-hour dietary recall surveys conducted in the MAL-ED study[70]. This diet was manufactured according to a previously described protocol[2].

The sterility of irradiated diets was confirmed by culture in (i) BHI broth, (ii) Nutrient broth, and (iii) Sabouraud-dextran broth (all from Difco) for one week at 37 °C under aerobic conditions, and in reduced Tryptic Soy broth (Difco) supplemented with 0.05% L-cysteine HCl under anaerobic conditions. All diets were stored at -20 °C prior to use. Nutritional analysis of each irradiated diet was conducted by Nestlé Purina Analytical Laboratories (St. Louis, MO) (**Supplementary Table 1a**).

Husbandry for initial tests of bacterial consortia derived from children with EED – 4-5 week-old germ-free C57Bl/6J mice were given *ad libitum* access to a standard chow diet (Diet 2018S, Envigo). Three days prior to colonization, mice were switched to the Mirpur-18 diet. For initial comparisons of gnotobiotic mice that had been orally gavaged (oral gavage needle; Cadence Science; catalog no. 7901) with the cSI-I consortium, the cSI-N consortium or the cecal contents of conventionally-raised C57Bl/6J animals that had been maintained on the standard chow diet, one group of animals per treatment arm was euthanized 9 days after gavage, and the second group 28 days later (n=10 mice/group). All animals were weighed and fecal samples were collected three times per week during the experiment.

To test of the role of diet in mediating inflammation, adult female germ-free mice were given breeder chow (Lab Diet 5021) *ad libitum* prior to oral gavage with the cSI-I or cSI-N consortium. Mice maintained on breeder chow for one week prior to switching to the Adult Mirpur diet for the following week and then returned to breeder chow forthe final week. Blood was collected from all animals in their isolators retro-orbitally prior to a diet switch (n=3 animals/colonization group euthanized at the end of 7 days on a given diet; the remaining n=5 animals/group were euthanized at 28 days.

Husbandry for intergenerational transmission experiments – 6-8-week-old germ-free female C57Bl/6J mice were given *ad libitum* access to an autoclaved breeder chow (Lab Diet 5021; Purina Mills, Richmond, IN) until 3 days prior to colonization, at which time they were switched to the Adult Mirpur diet for the remainder of the experiment. Mice received 200 µL of the stock solutions of the cSI-I or cSI-N consortium via an oral gavage needle. Another group of mice received an oral gavage of clarified cecal contents pooled from conventionally raised C57Bl/6J animals maintained on the standard chow (200 µL/recipient animal).

One week after initial gavage, trio matings were performed (two colonized females with one germ-free C57Bl/6J male). Females were continued on the Adult Mirpur diet. Pups born to these mothers were maintained with their dams in the same cage until weaning, at which time pups from the same litter were transferred to new cages and weaned onto the Mirpur-18 diet. For dams and their pups, bedding was replaced every 7 days and diets were provided *ad libitum*. Following weaning of pups on postnatal day 21 (P21), trio matings were performed again using previously pregnant mice. Offspring were euthanized on P37 (first pregnancy) or P14 (subsequent pregnancies) without prior fasting. All biospecimens were flash-frozen in liquid nitrogen and stored at -80 °C until analyses were performed.

For additional matings to assess fetal weights, adult germ-free female C57Bl/6J mice were switched to the Adult Mirpur diet 3 days prior to gavage with 200 µL of the cSI-I or cSI-N consortium, as described above. Two weeks after gavage, female mice were mated in trios and pregnant dams were euthanized at embryonic day (E) 11.5 or E17.5.

Husbandry for cohousing experiments – Germ-free 4-5-week-old male C57Bl/6J mice were switched from a standard chow diet (Diet 2018S, Envigo) to the Mirpur-18 diet 3 days prior to colonization. Each mouse received 200 µL of the cSI-I or cSI-N bacterial consortium via a single oral gavage. Nine days later mice were either maintained in their cage and isolator (non-cohoused control groups; n=6-8/group/experiment) or were transferred to a new cage in a new isolator to be cohoused with an equal number of mice transferred from an isolator containing the other experimental group (n=6-8/group/experiment). Bedding was replaced every 7 days for all groups of animals and the Mirpur-18 diet was provided *ad libitum*. All animals were weighed three times a week and euthanized without prior

1236 fasting on experimental day 18. All biospecimens were flash-frozen in liquid nitrogen and stored at -80
1237 °C before use.
1238 ***Husbandry for tests of candidate mediators of EED ('add-in' experiments)*** – The design of this
1239 experiment was analogous to that of the cohousing experiment. Germ-free 4-5-week-old male C57Bl/6J
1240 mice were switched from a standard chow diet (Diet 2018S, Envigo) to the Mirpur-18 diet 3 days prior to
1241 initial colonization. Each mouse received 200 µL of the cSI-N consortium via a single oral gavage; all
1242 mice were maintained in a single gnotobiotic isolator. Nine days later, mice were distributed to new
1243 isolators and subsequently gavaged with 200 µL of either 15% PBS/glycerol alone (sham), the cSI-I
1244 bacterial consortium, or the cultured strains representing the *A. naeslundii*, *A. odontolyticus* and *C.*
1245 *concisus* MAGs. Mice received subsequent 200 µL gavages on days 10 and 11. Another reference control
1246 group of mice in their own isolator were initially gavaged with 200 µL of the cSI-I consortium, followed
1247 by gavage with medium alone on days 9 through 11. Bedding was replaced every 7 days and the Mirpur-
1248 18 diet was provided *ad libitum*. All animals were weighed three times a week and euthanized on
1249 experimental day 18 (first round of experiments) or 35 (follow-up more prolonged exposure experiment).
1250 ***Division of the intestine -*** At the time of euthanasia, the small intestine was removed and divided
1251 into thirds. Each third was then subdivided into two equal length subsegments ('proximal' and 'distal').
1252 The proximal subsegment was used for either histomorphometric analysis or flow cytometry. Intestinal
1253 contents were removed from the distal subsegment by gentle extrusion. The distal subsegment was then
1254 cut into three 1.5 cm-long pieces (labeled #1-3 based on their proximal-to-distal location) which were
1255 flash-frozen in liquid nitrogen and stored at -80 °C before use. These frozen pieces were used for bulk
1256 tissue RNA-Seq (piece #1), snRNA-Seq (piece #2), or ELISA and Luminex-based protein quantification
1257 (piece #3). From the proximal end of the colon, three 1.5 cm long pieces (labeled #1-3 based on their
1258 proximal-to-distal location) were flash-frozen for the same type of assays applied to small intestinal
1259 samples.
1260 ***Histomorphometric and immunocytochemical analyses of intestinal tissue*** – Proximal
1261 subsegments of the duodenum and ileum (see *"Division of the intestine"* above) were fixed in 10%
1262 neutral buffered formalin for 24h at 4 ºC followed by a 70% ethanol wash. These segments were the
1263 placed in parallel with one another and collectively embedded in paraffin. Five µm-thick sections were
1264 prepared and stained with hematoxylin and eosin and imaged using a Zeiss Axioscan 7 Slide Scanner.
1265 Ten well-oriented crypt-villus units were selected from each intestinal segment and villus height and crypt
1266 depth were quantified using *QuPath* (v0.2.3)[71]. Measurements were performed for 4-6 mice per group
1267 with the investigator blinded with respect to experimental group.
1268 Sections (5 µm-thick) were prepared from formalin-fixed, paraffin-embedded duodenal and ileal
1269 segments. Slides were de-paraffinized and heat-induced antigen retrieval was performed using Trilogy
1270 (Millipore Sigma). Slides were blocked in PBS containing 2% BSA, 5% donkey serum and 0.1% Triton-
1271 X (antibody buffer) for 30 minutes at room temperature and treated with primary antibodies (Ki67 anti-
1272 Rabbit, 1:300, Abcam AB16667; E-Cadherin anti-Mouse, 1:250, DB Sciences 610181) for 90 minutes at
1273 room temperature. Following three cycles of washing in PBS, slides were incubated with secondary
1274 antibodies (Alexa Fluor Donkey anti-Rabbit 488, 1:300, Invitrogen, catalog no. A32790; Alexa Fluor
1275 Donkey anti-Mouse, 1:300, Invitrogen, catalog no. A32731) for 30 minutes at room temperature,
1276 followed by a wash in PBS, incubation with DAPI (1:1000 dilution, Thermo Scientific, catalog no.
1277 62248) for 5 minutes, and a final wash in PBS. Slides were mounted with Prolong Gold Antifade
1278 Mountant (Invitrogen, catalog no. P36930) and imaged with a Zeiss Axio Scan 7 Brightfield/Fluorescence
1279 Slide Scanner. Data were analyzed using *QuPath* (v0.2.3)[71]; as with the histomorphometric analysis, the
1280 investigator was blinded with respect to treatment group.
1281 ***Micro-computed tomography (µCT) of bone*** – The femur was harvested from the left rear leg
1282 and cleaned of muscle and connective tissue. Femurs were stored in 10 mL 10% neutral buffered formalin
1283 at room temperature for 24 hours. Fixed femurs were then washed in 1X PBS for 15 minutes; this wash
1284 step was repeated two more times. Femurs were then subjected to a 30% ethanol wash for 30 minutes, a
1285 50% ethanol wash for 30 minutes and a final 70% ethanol wash for 30 minutes. Femurs were
1286 subsequently embedded in 2% agarose and scanned with a µCT 40 desktop cone beam instrument
1287 (ScanCO Medical, Brüttisellen, Switzerland). For analyses of cortical bone, 100 slices were taken for

each sample in the transverse plane, with a 6 µm voxel size (high resolution); slices began at the midpoint of the femur and extended toward the distal femur. The boundaries and thresholds for bone were drawn manually using µCT 40 software. Volumetric parameters were quantified using software associated with the ScanCO instrument.

Protein assays of serum, intestinal and brain tissue – Total intestinal protein was extracted by homogenizing a 1.5 cm-long piece of the duodenum, ileum or colon (piece #3, see *"Division of the intestine"* above) in 600 µL of a solution of ice-cold T-PER Buffer (Thermo Scientific) with Complete Ultra protease inhibitor (Roche), using Lysis Matrix F beads (MP Bio). The homogenate was centrifuged at 13,000 x *g* for 5 minutes at 4 ºC. Total protein concentration in the resulting supernatants was quantified using Micro BCA Protein Assay Kit (Thermo Scientific). Protein concentrations were normalized to 1 mg/mL in PBS with Complete Ultra protease inhibitor (Roche). Intestinal and/or serum levels of LCN2 and IGF-1 were quantified using Mouse Lipocalin-2/NGAL DuoSet ELISA and Mouse/Rat IGF-I/IGF-1 DuoSet ELISA (R&D Systems), respectively, following the manufacturer's instructions. Intestinal and/or serum levels of several other proteins were measured using a custom Mouse Pre-Mixed Multi-Analyte Kit (R&D Systems; CHI3L1, S100A9, MMP8, CXCL1, IL-17A, IL-17E) and the MILLIPLEX MAP Mouse Bone Magnetic Bead Panel (MilliporeSigma; DKK-1, FGF-23, OPG). Assays were performed on a FlexMap3D instrument (Luminex).

Ultrasonic vocalizations (USVs) – A separate set of cSI-I or cSI-N-colonized dams and their pups were used for measurement of USVs. One week prior to mating, non-virgin dams that were colonized with the cSI-I or cSI-N consortia were switched to the Adult Mirpur diet. Males were removed before dams gave birth. Litters with at least three pups were used for data collection and were culled to a maximum of six pups. USV assays were performed on postnatal days 5, 7 and 9. As maternal behavior varies throughout the day, we standardized these studies such that all recordings were performed between 1000 h and 1300 h.

Previous studies[72] utilized the use of a sound induction chamber, which served the dual purpose of diminishing background noise and maintaining the chamber at a temperature between 34-37 °C to reduce fluctuations in pup temperature through the experiment. However, standard induction chambers with heating elements are too large to fit into gnotobiotic isolators. We therefore created induction chambers by sterilizing lidded Styrofoam containers with Clidox. Within each box, an EtOH-sterilized microphone was placed approximately three inches above the pup holding pen. Data from the microphone were collected with Avisoft UltraSoundGate 116H recording interface at a sampling rate of 250,000 Hz and a gain of 6 to record USVs. Water recirculating heating pads were placed beneath the vinyl of the isolator, and an autoclaved 1 mL pipet tip box, which served as a pup holding pen, was placed on top of the heating pad within the isolator. The warmed holding pen allowed pups to maintain body temperature after separation from their dam. Body temperature was repeatedly monitored with a sterilized infrared temperature gun to ensure pup temperatures stayed between 34-37 °C.

Ultrasonic vocalizations were recorded for each pup sequentially for 3 minutes; pups that were not being recorded were maintained in the heated holding pen such that all pups were separated from the dam for the same amount of time. After all pups were recorded, the entire litter was returned to the dam.

Call spectra were analyzed using previously developed automated and blinded Matlab code[73] . Briefly, data were band-pass filtered between 25-110 Hz and a minimum spectral purity of 0.015 and spectral discontinuity of 1. Waveforms were divided into 512 samples per block, with 50% temporal overlap, resulting in a resolution of 1.02 ms. Number of calls, duration, mean frequency (Hz), mean peak dB, average pitch range (dB), and pause between calls were defined in recordings that had greater than 10 total calls. Data were analyzed with a mixed effects linear model in which the microbial community and postnatal day were fixed effects and dam and pup ID were random effects [(USV feature) ~ *Bacterial consortium* + *Postnatal Day* + (1|*Dam_ID/Pup_ID*)]. Post-hoc tests were performed on significantly different fixed effects in the model.

Pup retrieval assay – Pups were removed from their home cage and placed onto a heating pad kept between 34 and 37 °C for 10 minutes. One pup was placed into each of the three corners of a standard mouse cage at a location furthest from the dam's nest. Dam-pup behavior was recorded with a Logitech webcam suspended above the vinyl of the gnotobiotic isolator and the length of time for the dam

1340 to return all three pups to the nest was recorded. Data were analyzed with a linear model with bacterial
1341 consortium as a fixed effect [(*Length of time to retrieve pups*) ~ *Bacterial consortium* + (1|*Dam_ID*)].
1342
1343 **Flow cytometry of immune cell populations**
1344 ***Intergenerational transmission experiments*** – Subsegments of duodenum, ileum and/or colon
1345 (*See "Division of the intestine" above*) were digested and myeloid and lymphoid cells were collected
1346 according to methods previously described[5]. Briefly, each subsegment was immediately flushed with cold
1347 PBS after dissection to remove luminal contents. Each subsegment was then opened lengthwise and
1348 gently agitated for 20 minutes at room temperature in Hanks Balanced Salt Solution (HBSS)
1349 supplemented with 15mM HEPES, 10% bovine calf serum (BCS) and 5mM EDTA. Each sample was
1350 vortexed and the suspended cells were collected; the remaining tissue fragments were subjected to a
1351 second round of gentle agitation and vortexing. The tissue remaining after the second collection was
1352 rinsed with cold 1X HBSS prior to digestion with Collagenase IV (Sigma) in complete RPMI-1640 for 40
1353 minutes at 37 °C with gentle agitation. Digests were filtered through 100 µm mesh strainer (Falcon) and
1354 subjected to density gradient centrifugation using 40% and 70% Percol solutions (GE Healthcare).
1355 To dissect meninges, skin and muscle overlying the skull as well as the mandibles and bone
1356 rostral to maxillae were removed. The remaining skull was placed in Iscove's Modified Dulbecco's
1357 Medium (IMDM, Sigma Aldrich). The meninges were removed from the skull cap using fine forceps and
1358 visualization under a light microscope. Meninges were digested for 20 minutes at 37 °C with 1.4 U/mL of
1359 Collagenase VIII (Sigma Aldrich) and 35 U/mL of DNAse I (Sigma Aldrich) in IMDM. Following
1360 digestion, the tissue was gently pressed through a 70 µm mesh cell strainer (Falcon). The flow-through
1361 material was centrifuged at 450 x *g* at 4 °C for 4 minutes. Spleens were processed in a manner similar to
1362 what was used for the meninges with the exception that we performed an additional lysis step with
1363 ammonium-chloride-potassium (ACK) Lysis Buffer (Quality Biological) prior to staining.
1364 Cells collected from each sample type were resuspended in ice-cold FACS buffer (2 mM EDTA,
1365 25 mM HEPES, 1% BSA in 1X PBS) and stained for extracellular markers at 1:300 dilution. Dead cells
1366 were excluded using Zombie NIR fixable Viability kit. Cells were analyzed on a Cytek Aurora (Cytek
1367 Biosciences) and the results using FlowJo (v10.8.1). The fluorophore-labeled monoclonal antibodies used
1368 for flow cytometry are listed in **Supplementary Table 6** and gating strategies are presented in
1369 **Supplementary Information**.
1370 ***Cohousing and add-in experiments*** - Mice were injected retro-orbitally (under isoflurane
1371 anesthesia 2 minutes before euthanasia) with 2 µg of phycoerythrin (PE)–conjugated anti-CD45 antibody
1372 (Biolegend, clone 30-F11) to label intravascular leukocytes. Blood was collected from the retroorbital
1373 sinus following euthanasia, centrifuged and lysed using ACK lysis buffer (Quality Biological) for 1
1374 minute at room temperature, followed by addition of 2 mL 1X PBS to inactivate ACK lysis buffer. This
1375 lysis step was repeated two more times. The resulting material was subjected to centrifugation at 420 x *g*
1376 for 4 minutes. Cell pellets were resuspended in FACS buffer (PBS with 2% bovine serum albumin) and
1377 stained for extracellular markers at 1:300 dilution.
1378 Immune cells from intestines, spleen and meninges were collected as described above for the
1379 intergenerational experiment. Dead cells were excluded using Zombie NIR fixable Viability kit. Cells
1380 were analyzed on a Cytek Aurora (Cytek Biosciences) and the data assessed using FlowJo (v10.8.1). The
1381 fluorophore-labeled monoclonal antibodies used for flow cytometry are listed in **Supplementary Table**
1382 **6**.
1383
1384 **Metagenome-assembled genomes (MAGs)**
1385 ***Identification of MAGs*** - DNA was extracted from flash-frozen cecal contents obtained from P37
1386 cSI-I and cSI-N mice and their dams in the intergenerational experiment, as well as from non-cohoused
1387 and cohoused mice in the cohousing experiment. Cecal contents were subjected to bead beating and
1388 phenol-chloroform extraction to obtain crude genomic DNA, which was subsequently purified (QIAquick
1389 96 PCR Purification Kit) and quantified (Qubit). The final DNA fragment size distribution was
1390 determined using an Agilent Technologies 4200 TapeStation.

1391 Fragmented genomic DNA (400-1000 ng) was prepared for long-read sequencing using a
1392 SMRTbell Express Template Prep Kit 2.0 (Pacific Biosciences) adapted to a deep 96-well plate (Fisher
1393 Scientific) format. All DNA handling and transfer steps were performed with wide-bore, genomic DNA
1394 pipette tips (ART). Barcoded adapters were ligated to A-tailed fragments (overnight incubation at 20 °C)
1395 and damaged or partial SMRTbell templates were subsequently removed (SMRTbell Enzyme Cleanup
1396 Kit). High molecular weight templates were purified (the volume of added undiluted AMPure beads used
1397 was 0.45 times the volume of the DNA solution). A second round of size selection was performed by
1398 diluting AMPure beads to a final concentration of 40% (v/v) with SMRTbell elution buffer, after which
1399 the resulting mixture was added at 2.2 times the volume of the pooled libraries. DNA was eluted from the
1400 AMPure beads with 12 µL of SMRTbell elution buffer. Pooled libraries were quantified (Qubit) and their
1401 size distribution was assessed using a TapeStation (Agilent). Libraries were then sequenced to a depth of
1402 $1.85 \pm 1.5 \times 10^9$ reads/sample (mean ± SD) using a Sequel II System instrument (Sequel Binding Kit 3.0
1403 and Sequencing Primer v4, Pacific Biosystems). The resulting reads were demultiplexed and Q20 circular
1404 consensus sequencing (CCS) reads were generated (Cromwell workflow conFig.d in SMRT Link). CCS
1405 reads were assembled into contigs using *metaFlye* (v2.8.1;[74]) with hifi-error set to 0.003 and other options
1406 set to default. Contig quality was evaluated using *checkm* (v1.0.7;[75]). Any contig demonstrating *checkm*
1407 'Completeness' ≥85% and 'Contamination' ≤ 5% was nominated as a 'high quality' MAG. Remaining
1408 contigs were subjected to further MAG assembly efforts, first by calculating coverage using *CoverM*
1409 (v0.6.1, https://github.com/wwood/CoverM) and subsequently MAG reconstruction using *MaxBin*
1410 (v2.2.7;[76]). MAGs were cleaned using *MAGpurify* (v2.1.2;[77]) and subsequently evaluated for quality using
1411 *checkm*. In an iterative process, candidate MAGs demonstrating *checkm* Completeness ≥ 85% and
1412 Contamination ≤ 5% were again nominated as a MAG. High-quality MAGs from both primary and
1413 subsequent MAG assembly efforts were dereplicated using *dRep* (v2.3.2;[78]). Final MAG summary
1414 statistics were collected with *checkm* and *quast* (v4.5;[79]) (**Supplementary Table 1c**).
1415 ***Taxonomic classification of MAGs*** -Taxonomic assignments were initially made by employing
1416 the Genome Taxonomy Database Toolkit (*GTDB-Tk* v1.5.1;[80]) and corresponding database (release 95;
1417 *14*). Phylogenetic trees of MAGs and closely related reference genomes were generated using the
1418 Phylogenetic Tree Building service available from the Bacterial and Viral Bioinformatics Resource
1419 Center (BV-BRC;[81]). This service utilizes the Codon Tree method and universal protein families as
1420 homology group and analyzes alignments of these proteins identified in each genome using the program
1421 RAxML. The genome trees obtained were visualized via iTOL[82].
1422 ***Determination of the absolute abundances of MAGs and isolate genomes*** – The absolute
1423 abundances of MAGs were determined using previously described methods with minor modifications[83,84].
1424 In brief, 'spike-in' bacterial strains whose genomes are easily differentiated from those of gut bacteria
1425 were added to each weighed frozen sample of intestinal contents or feces prior to DNA isolation and
1426 preparation of barcoded libraries[85]. For intergenerational transmission and cohousing experiments,
1427 *Alicyclobacillus acidiphilus* spike-in was added (2.22×10^8 cells/mL suspension; DSM 14558; GenBank
1428 assembly accession: GCA_001544355.1)[84]. For isolate add-in experiments, a commercial 1:1 mix of
1429 *Imtechella halotolerans* and *Allobacillus halotolerans* was added (2×10^7 cells each per 20 µL
1430 suspension; Zymo product numbers LMG 26483 and LMG 24826, respectively).
1431 Intestinal contents and fecal samples were subjected to bead beating and phenol-chloroform
1432 extraction to obtain crude genomic DNA which was subsequently purified (QIAquick 96 PCR
1433 Purification Kit). Shotgun sequencing libraries were constructed using Nextera XT DNA Library Prep Kit
1434 and sequenced on an Illumina NovaSeq 6000 instrument [150 nt paired-end reads; $6.17 \times 10^6 \pm 3.75 \times 10^7$
1435 reads/sample (mean ± SD) from the intergenerational transmission experiment, $3.10 \times 10^6 \pm 7.94 \times 10^6$
1436 reads/sample from the cohousing experiments, and $3.03 \times 10^7 \pm 1.30 \times 10^8$ reads/sample from the isolate
1437 add-in experiment]. Sample metadata are listed in **Supplementary Table 7**. Due to increased host reads
1438 in small intestinal samples, libraries were balanced based on a host:microbe read ratio determined by
1439 preliminary shallow sequencing.
1440 Reads were demultiplexed (*bcl2fastq*), trimmed (*trimgalore,* v0.6.1;
1441 https://github.com/FelixKrueger/TrimGalore) and filtered to exclude host reads (*bowtie2*; v2.3.5;[86]).
1442 MAG abundances were determined by assigning reads to each MAG, followed by a normalization for

genome uniqueness in the context of a given community[85]. The resulting counts table was imported into R (v4.0.4). We calculated the absolute abundance of a given MAG *i* in sample *j* using the following equation:

$$strain_{i,j} = \left(\frac{counts_{i,j} \times spikein1\ cells\ added_j}{spikein1\ counts_j \times sample\ weight_j} + \frac{counts_{i,j} \times spikein2\ cells\ added_j}{spikein2\ counts_j \times sample\ weight_j} \right) \times 0.5$$

The statistical significance of observed differences in the abundances of a given MAG across different groups was tested using a non-parametric Wilcoxon-rank test with FDR corrections on calculated $\log_{10}$ absolute abundances. Final MAG abundances for all experiments are included in **Supplementary Table 1d**.

Identification and assembly of isolates genomes related to MAGs – Average nucleotide identity was calculated using *dRep* (v2.3.2;[78]) for all genomes assembled by shotgun sequencing (paired end 150 bp reads) of cultured isolates from the BEED study duodenal aspirates (**Supplementary Table 1b**)[2]. For cultured isolates displaying ANI $\geq$ 95% shared with MAGs of interest obtained from the intergenerational and cohousing experiments, monocultures of each isolate were grown in 10 mL broth overnight at 37 ºC under anaerobic conditions (atmosphere; 75% N_2, 20% CO_2 and 5% H_2) without shaking. Cells were recovered by centrifugation (5,000 x *g* for 10 minutes at 4 ºC) and high molecular weight genomic DNA was purified (QIAquick 96 PCR Purification Kit) and quantified (Qubit); the final fragment size distribution was determined using a TapeStation (Agilent). Fragmented genomic DNA (400-1000 ng) was prepared and long-read sequencing was performed as described above. The resulting reads were demultiplexed and Q20 circular consensus sequencing (CCS) reads were generated (Cromwell workflow conFig.d in SMRT Link). Genomes were assembled using *Flye* (v2.9;[87]) with hifi-error set to 0.003 and other options set to default. Assembly quality was evaluated using *checkm*. Taxonomic assignments were initially made by employing the Genome Taxonomy Database Toolkit (*GTDB-Tk* v1.5.1;[80]) and corresponding database (release 95; *14*). Final assembly summary statistics were collected with *checkM*, *quast* and *dRep* (**Supplementary Table 4a**). All isolates were of high quality based on marker gene analysis, consisted of one or two contigs, and shared >99.9999% ANI with their respective MAG (**Supplementary Table 4a**).

In silico metabolic reconstructions of MAGs and isolate genomes – MAGs and isolate genomes were initially annotated using *prokka* (v1.14;[88]); KEGG Orthology (KO) numbers were assigned to bacterial coding sequences using BlastKOALA[89]. MAGs were then subjected to *in silico* metabolic pathway reconstruction. Our approach for reconstruction is based on gene annotation using the microbial community SEED (mcSEED) database containing 2,856 reference bacterial genomes for which metabolic phenotypes have been inferred from expert curation and subsequent *in silico* predictions of the presence or absence of the pathway in each genome[90,91]. These results capture utilization and/or biosynthesis of 106 metabolites, including carbohydrates, amino acids, vitamins, and fermentation end-products[92–94].

For functional annotation of coding sequences in each genome, we used a combination of public domain tools (such as DBSCAN, DIAMOND, MMSeq2), custom scripts and the mcSEED reference database genes. These annotations were supplied to a 'Phenotype Predictor' pipeline that allows automated propagation of curated metabolic phenotypes over new microbial genomes and MAGs from represented phylogenetic groups using a consensus of three complementary approaches: (i) rule-based phenotype assignment using the genomic distribution of orthologs and a set of phenotype rules; (ii) machine learning models for binary phenotype prediction trained on reference sets of genes and phenotypes and (iii) a neighbor-based approach for phenotype assignment based on variability of metabolic phenotypes and genes within a group of phylogenetically close neighbors. The combination of all three approaches allows consensus phenotype assignment with >99% accuracy[95]. The mcSEED gene annotations are provided in **Supplementary Table 4b**.

Bulk RNA-Seq

1493 ***Intestinal tissue*** – RNA was extracted from 1.5 cm flash-frozen duodenum, ileum and/or colon
1494 (piece #1, *See "Division of the intestine" above*) using the Qiagen RNeasy 96 Kit. Total RNA was
1495 quantified (Qubit) and quality was assessed using a TapeStation (Agilent). cDNA libraries were generated
1496 using the Illumina Total RNA Prep with Ribo-Zero kit (Illumina). Barcoded libraries were sequenced on
1497 Illumina NovaSeq 6000 instrument [150 nt paired-end reads to a depth of $3.23 \times 10^7 \pm 3.54 \times 10^6$
1498 reads/sample (mean ± SD) from the intergenerational experiment and $7.13 \pm 3.08 \times 10^7$ reads/sample from
1499 the cohousing experiment)]. Sample metadata are provided in **Supplementary Table 7**.
1500 ***Brain*** - Flash-frozen cerebral cortical samples were homogenized by bead-beating for 30 seconds
1501 with RNAse-free stainless-steel beads (Midsci SSB14B-RNA) in 300 µL of lysis buffer provided by the
1502 NucleoSpin 96 RNA isolation and purification kit (Takara 740709.4). Lysates were centrifuged at 13,000
1503 x *g* for 5 minutes to remove beads and debris. RNA was isolated from the resulting supernatants
1504 following the manufacturer's protocol. cDNA libraries were generated using the Illumina Total RNA Prep
1505 with Ribo-Zero kit. Barcoded libraries were sequenced on Illumina NovaSeq 6000 instrument [150 nt
1506 paired-end reads to a depth of $2.41 \times 10^7 \pm 3.29 \times 10^6$ reads/sample (mean ± SD)]. Sample metadata are
1507 listed in **Supplementary Table 7**.
1508 ***Data analysis*** – Read quality was verified with *FastQC* (v0.11.7;
1509 http://www.bioinformatics.babraham.ac.uk/projects/fastqc/). Reads were then trimmed to remove adapters
1510 and low-quality read segments using *trimgalore* (v0.6.1). Trimmed reads were then pseudoaligned to a
1511 *kallisto* (v0.46.2[96]) index built from the Gencode v25 *Mus musculus* reference genome. Transcript counts
1512 were aggregated to gene counts. *Kallisto* 'estimated counts' values and transcripts per million (TPM)
1513 values were used to generate a gene-level expression matrix in R using *tximport* (v1.22.0;[97]) and *biomaRt*
1514 (v2.50.3;[98]). The 'lengthscaledTPM' function in *tximport* was used to adjust estimated counts by gene
1515 length and abundance. This resulting count matrix was imported into *limma-voom* (v3.50.3;[99,100]) to
1516 compare $\log_2$-cpm gene expression between groups. GSEA was performed using *clusterProfiler*
1517 (v4.2.2;[101]) and the Gene Ontology (GO) pathway database, with FDR-correction.
1518
1519 **snRNA-Seq**
1520 ***Isolation of nuclei from small intestinal tissue*** – Nuclei were extracted from flash-frozen 1.5 cm
1521 pieces of duodenum and ileum (piece #2, see *"Division of the intestine"* above) collected from P37 mice
1522 in the intergenerational transmission experiment. Briefly, the tissue piece was thawed and minced in lysis
1523 buffer (25 mM citric acid, 0.25 M sucrose, 0.1% NP-40, 1X protease inhibitor). Nuclei were released
1524 from cells using a Dounce homogenizer (Wheaton), then washed 3 times with buffer [25 mM citric acid,
1525 0.25 M sucrose, 1X protease inhibitor (Roche)] and filtered successively through 100 µm-, 70 µm-, 40
1526 µm-, 20 µm- and 5 µm-diameter strainers (pluriSelect) to obtain single nuclei. Following filtration, nuclei
1527 were pelleted by centrifugation (500 x *g* for 5 minutes) and resuspended in a buffer containing 5 mM
1528 KCl, 3 mM $MgCl_2$, 50 mM Tris, 1 mM DTT, 0.4 U/µL RNase inhibitor (Sigma), plus 0.4 U/µL Superase
1529 inhibitor (ThermoFisher)[102].
1530 ***Isolation of nuclei from the cerebral cortex***– Brains were removed from the skull, placed on ice,
1531 and hemisected in the sagittal plane. The cerebellum, thalamus and midbrain were removed while
1532 retaining the cortex from the left hemibrain. The left cortex was split into six equal coronal sections along
1533 the rostral-caudal axis; segments #1 and #4 along that axis were used for bulk RNA-Seq, while segments
1534 #2 and #5 were used for snRNA-Seq. All segments of the left cortex were flash-frozen in liquid nitrogen
1535 immediately after dissection.
1536 Nuclei from flash-frozen cortical tissue were initially harvested using a 2 mL Dounce
1537 homogenizer in a Tris-based lysis buffer (10 mM Tris, 146 mM NaCl, 1 mM $CaCl_2$, 21 mM $MgCl_2$, 40
1538 U/mL RNAse inhibitor, 1% BSA, 0.1% NP40). Nuclei were passed through a 30 µm filter (Miltenyi 130-
1539 041-407), washed once for 5 minutes in a Tris-based wash buffer (10 mM Tris, 146 mM NaCl, 1 mM
1540 $CaCl_2$, 21 mM $MgCl_2$, 40 U/mL RNAse inhibitor, 1% BSA), and then incubated in 1 µg/mL of Hoechst
1541 33342 (Thermo 62249) for 5 minutes at 4 ºC. Nuclei were washed again for 5 minutes with wash buffer,
1542 passed through a 20 µm filter (Miltenyi 130-101-812) and subjected to fluorescent activated nuclear
1543 sorting (FANS). A total of 200,000 Hoechst-positive nuclei were collected from each sample based on
1544 their forward and side-scatter properties.

1545 ***Generation and sequencing of snRNA-Seq libraries*** **–** We used approximately 7,000 nuclei per
1546 intestinal sample and 6,000 nuclei per brain sample for gel bead-in-emulsion (GEM) generation. Reverse
1547 transcription and library construction were performed according to the protocol provided in the 3' gene
1548 expression v3.1 kit manual (10X Genomics PN-1000121). Balanced libraries were sequenced on Illumina
1549 NovaSeq 6000 instrument [150 nt paired-end reads; $2.95 \times 10^8 \pm 2.02 \times 10^7$ reads/sample (mean ± SD)].
1550 Sample metadata are listed in **Supplementary Table 7**.
1551
1552 **Analysis of snRNA-Seq datasets**
1553 ***Preprocessing and quality control*** - Read alignment, feature-barcode matrices and quality
1554 controls were performed using the *CellRanger* 5.0 pipeline with the flag '--include-introns'
1555 (GRCm38/mm10). 'Ambient' RNA was removed using the *remove-background* module from
1556 CellBender[103]. Sample integration, count normalization, cell clustering and marker gene identification
1557 were performed using Seurat 4.0[104]. Briefly, filtered feature-barcode matrices from CellRanger were
1558 imported as a Seurat object using *CreateSeuratObject*. Matrices were filtered to remove low quality
1559 nuclei (defined as nuclei with < 200 or > 5000 genes or < 400 UMIs). For intestinal samples, nuclei with
1560 over 5% reads from mitochondrial genes or over 5% reads from ribosomal protein genes were excluded.
1561 For brain cortex samples, the corresponding thresholds were 4% and 2.5%, respectively. Each sample was
1562 then normalized using *SCTransform*[105,106] and predicted doublets were removed using *DoubletFinder*[107].
1563 Samples of the same tissue type (duodenum, ileum, or cerebral cortex) were integrated using
1564 *SelectIntegrationFeatures*, *PrepSCTIntegration*, *FindIntegrationAnchors* and *IntegrateData* from the
1565 Seurat software package. Each integrated dataset was subjected to unsupervised clustering using
1566 *FindNeighbors* (dimensions = 1:30) and *FindClusters* (resolution = 0.8 and 1.2 for duodenum and ileum,
1567 respectively) from the Seurat package.
1568 ***Cell type annotation*** - Cell type annotation for duodenal and ileal snRNA-Seq objects was
1569 performed using the *FindMarkers* function in Seurat. Manual cell type assignments were conducted based
1570 on expression of reported markers[108]. For cell type annotation in the cerebral cortex, the integrated Seurat
1571 object was converted to a *SingleCellExperiment* object[109]. Nuclei were then annotated using *SingleR*[110],
1572 with manual adjustments to ensure that nuclei belonging to a cell type all resided in the same cluster (self-
1573 organizing map clustering implemented with 40 centers implemented with *bluster*[109]).
1574 ***Pseudo-bulk analysis of differential gene expression*** – Genes defined as having low levels of
1575 expression (read count < 4) were filtered out prior to count aggregation across nuclei for a given cell type
1576 (cluster) within each biological sample. Each pseudo-bulked sample served as input for *DESeq2*-based
1577 differential gene expression analysis (likelihood ratio test, minimum=1e-6[111]). Genes with differential
1578 expression (adjusted $P < 0.05$) were used as input for GSEA with *clusterProfiler*[101].
1579 ***Trajectory inference analysis*** – Trajectory inference analysis was conducted with *Slingshot*[112].
1580 Briefly, genes were removed whose read count did not exceed 3; remaining counts were quantile-
1581 normalized prior to principal components analysis, which was performed with *prcomp*. Gaussian mixture
1582 modeling was performed to cluster cells with *mclust*[113] and pseudotime was inferred with *slingshot*. A
1583 negative binomial model was fit with *tradeSeq*[114]; n=30 knots was used for fitting the negative binomial
1584 generalized additive model (*fitGAM*) based on optimizing the number of genes with optimal K
1585 (*evaluateK*). Subsequently, differential expression testing across pseudotime between the cSI-I and cSI-N
1586 treatment groups was performed with *conditionTest*. As the results of *conditionTest* do not include
1587 directionality between conditions, we aggregated overall expression for cSI-I or cSI-N astrocytes to
1588 determine whether a gene that was significantly differently expressed across pseudotime at a higher or
1589 lower level in cSI-I compared to cSI-N animals. Over-enrichment analysis was performed on genes
1590 whose expression was significantly different between cSI-I versus cSI-N animals over pseudotime using
1591 *conditionTest* and querying the Panther database[115].
1592 ***Intercellular signaling*** – Signaling within each tissue (duodenum, ileum or cerebral cortex) was
1593 inferred with *NicheNet*[35]. Briefly, log-transformed counts were used for as input for the wrapper function
1594 *nichenet_seratobj_aggregate*. Default ligands, receptors and target matrices were used. In the duodenum
1595 and ileum, all cell clusters were designated as 'sender' cells to stem and transit amplifying (TA) 'receiver'
1596 cells. In the cerebral cortex, all cell clusters were defined as sender cells to either glutamatergic or

1597 GABA-ergic receiver neurons (separately). *Differential NicheNet* analysis was performed as described[36].
1598 Default ligand and receptor matrices were used; read counts were log-transformed. While both *NicheNet*
1599 algorithms predict ligand-receptor links within a tissue, *Differential NicheNet* includes differential
1600 expression of ligands within a given 'sender' cell type between conditions (cSI-I vs. cSI-N) in the ranking
1601 of ligand-receptor pairs, while the *NicheNet* algorithm does not.
1602 ***Selection of inflammation-correlated nuclei in the cerebral cortex*** – We used *Scissor*[116] to select
1603 nuclei in the cerebral cortex that were associated with serum levels of the inflammation-associated protein
1604 S100A9 across all P37 animals from the intergenerational experiment. *Seurat_preprocessing* was run on
1605 raw snRNA-Seq counts. *First*, a Pearson correlation matrix was calculated for the single nucleus and bulk
1606 RNA-Seq expression matrices from the cerebral cortex of (i) P37 cSI-I mice (n=16 animals from n=4
1607 litters; n=5 females and n=11 males), cSI-N mice (n=18 from n=4 litters, n=11 females and n=7 males)
1608 and CONV-D animals (n=16 from n=4 litters, n=10 females and n=6 males). *Second*, a gaussian
1609 regression model was optimized on the correlation matrix with serum levels of the protein S100A9. A
1610 grid search with alpha = (0.001, 0.01, 0.1, 0.2, 0.3, 0.5, 0.7, 0.8, 0.9, 1.0) was performed; the analysis
1611 described in the text used alpha = 0.7. The *FindMarkers* from *Seurat* was used to determine differential
1612 expression between (i) Scissor-selected (S100A9-negatively associated) astrocytes versus background
1613 (non-selected) astrocytes or (ii) Scissor-selected (S100A9-positively associated) glutamatergic neurons
1614 versus background glutamatergic neurons.
1615
1616 ***C. concisus* comparative genomics analysis**
1617 Published *C. concisus* whole genomes (97 from refs[51], 14 from ref[52], 8 from NCBI taxid=199) were
1618 downloaded from NCBI through *anvi'o* (v8, ref[117]). A typical pan-genomic workflow was conducted.
1619 Briefly, whole genomes (.gbff files) and associated metadata were downloaded through their NCBI
1620 BioProject accessions or taxid numbers. Contig databases were generated with default config settings
1621 using the anvi'o snakemake workflow[118]; NCBI-PGAP was used as the gene caller to create a genomes
1622 storage database. For the pangenome analysis[119], ncbi-blast was used with *mcl-inflation*=10 and
1623 *minbit*=0.5. Genome similarity was computed with *pyANI*. Disease-associated metadata were manually
1624 curated and used to compute functional enrichment (*anvi-compute-functional-enrichment-in-pan*[118]. The
1625 statistical approach used to define enrichment scores for functions or genes fits a generalized linear model
1626 to the occurrence of each module and computes a Rao test statistic with multiple hypothesis correction;
1627 this approach has been described previouslyd[118].
1628
1629 **Epithelial cell death induction assay**
1630 HCT116 cells were cultured at 37 ºC in DMEM medium supplemented with 10% FBS at 4 x 10^5 cells per
1631 ml. Cells were washed with 1xPBS and selected controls were pre-treated with DMSO (0.1%) or 30 µM
1632 caspase inhibitor (QVD, Quinoline-Val-Asp-Difluorophenoxymethylketone) for 1h before inducing
1633 apoptosis with administration of 1 µM staurosporine (STS; Abcam) for 24 h.
1634 CT26:FADD cells were seeded at 2 x 10^6 cells per 10 cm culture dish. The next day, cultures
1635 were incubated with 1 µg/ml doxycycline for 16 h to induce expression of the FADD construct (Fas-
1636 associated death domain). Doxycycline was removed by washing with 1x PBS before 1 h pre-treatment
1637 with 20 µM z-VAD-FMK (z-VAD, pan-caspase inhibitor, MedChem Express) or DMSO (0.1%). Cell
1638 death was induced by adding 10 nM B/B homodimerizer for 5 h after which time supernatants were
1639 collected and centrifuged at 350 x *g* for 5 minutes to remove cellular debris. The resulting supernatants
1640 were filtered using 0.2µm syringe filter (SFCA; Corning) and then frozen at -20 ºC for later use in *C.*
1641 *concisus* growth assays.
1642 ***C. concisus growth in conditioned medium from intestinal epithelial cells*** – *C. concisus* isolate
1643 Bg048 was routinely cultured in Bolton Broth supplemented with 10% FBS (autoclaved and subsequently
1644 filter-sterilized) and on BHI-agar plates supplemented with 7.5-10% (v/v) horse or sheep blood. For
1645 growth in spent medium collected from colonic epithelial cell lines, 25 µL of a 24-hour culture of *C.*
1646 *concisus* in Bolton Broth with 10% FBS was sub-cultured into a 1:1 (v/v) mixture of Bolton Broth with
1647 10% FBS and intestinal epithelial cell culture spent medium or blank cell culture medium as a control
1648 (DMEM). After a 6-24 h incubation at 37 ºC, a 30 µL aliquot of the resulting culture was removed for

1649 serial dilutions and the determination of CFU using blood agar plates incubated under micro-aerophilic
1650 conditions (5% O_2, 10% CO_2, 85% N_2) or anaerobic conditions (5% H_2, 20% CO_2, 75% N_2). After 48
1651 hours of growth, *C. concisus* colonies were counted and growth relative to DMEM was evaluated.
1652
1653 **Microbial RNA-Seq**
1654 **C. concisus *gene expression in the mouse gut* –** RNA was isolated from cecal contents harvested
1655 from cSI-I and cSI-N sham-gavaged controls, and 'cSI-N plus isolate-add in' mice described in **Fig. 4** and
1656 **Extended Data Fig. 7**. cDNA libraries were generated from isolated RNA samples using the Total RNA
1657 Prep with Ribo-Zero Plus kit (Illumina). Barcoded libraries were sequenced on an Illumina NovaSeq
1658 6000 instrument [150 nt paired-end reads to a depth of $1.93 \times 10^8 \pm 7.94 \times 10^7$ reads/sample (mean ± SD);
1659 n=6 samples/treatment group]. Sample metadata are listed in **Supplementary Table 7**. Raw reads were
1660 trimmed (*trimgalore*; v0.6.1), filtered to exclude host reads (*bowtie2*; v2.3.5), and mapped to MAGs
1661 (*kallisto*; v0.46.2) and the *C. concisus* isolate genome (see section of *Methods* titled ***Identification and***
1662 ***assembly of isolates genomes related to MAGs*)**. The resulting *kallisto* pseudocounts tables were
1663 imported into R (v4.0.4). The geometric mean of absolute abundance (see ***Determination of the absolute***
1664 ***abundances of MAGs and isolate genomes*)** was used to set *sizeFactors* for the *DESeq2* object prior to
1665 differential expression with the *DESeq2 Wald* test.
1666 **C. concisus *gene expression in vitro* –** *C. concisus* was grown anaerobically on solid BHI agar
1667 supplemented with 10% sheep blood. After 48 hours, single colonies were picked into rich medium
1668 (Bolton broth supplemented with 10% FBS); after 24 hours of anaerobic growth at 37 ºC, an aliquot was
1669 diluted 1:32 into media used for assessing gene expression; these conditions included (i) Bolton broth
1670 supplemented with 10% FBS ± 1% mucin, grown anaerobically and (ii) Bolton broth supplemented with
1671 10% FBS mixed 1:1 (v/v) with conditioned medium from HTC116 colonic epithelial cells, grown under
1672 microaerophilic conditions. The colonic epithelial cell media conditions used were as follows; (i)
1673 conditioned medium from HTC116 cells grown in DMEM, (ii) conditioned medium from HTC116 cells
1674 treated with L-NIO and (iii) DMEM cell culture medium control. After 24 hours, these broth cultures
1675 were transferred to 5 mL snap-top microcentrifuge tubes and centrifuged at 20,000 x *g* for 30 minutes at
1676 10 ºC to pellet *C. concisus* cells. Supernatant was removed and cell pellets were frozen at -20 ºC. RNA
1677 was extracted with the Qiagen RNeasy UCP Micro kit. Briefly, 200 µL of acid-washed glass beads were
1678 added to the bacterial pellets on ice with 350 µL buffer RULT containing 2-mercaptoethanol. Bead
1679 beating was performed for 5 minutes, and followed by a protocol described in the kit, including on-
1680 column DNase treatment. Quality was assessed with RNA High Sensitivity ScreenTape using an Agilent
1681 Technologies 4200 TapeStation and quantified with Qubit RNA High Sensitivity. ERCC RNA Spike-In
1682 Mix (Invitrogen, 4456740) was added prior to library prep which was performed using the Total RNA
1683 Prep with Ribo-Zero Plus kit (Illumina). Barcoded libraries were sequenced [AVITI instrument (Element
1684 Biosciences); 150 nt paired-end reads; $1.03 \times 10^7 \pm 7.4 \times 10^6$ reads/sample (mean±SD)]. Demultiplexed
1685 reads were quality-trimmed (*trimgalore*) and mapped to the *C. concisus* isolate genome Bg048 and ERCC
1686 transcripts (*kallisto*). Kallisto pseudocounts tables were imported into R, and ERCC counts were extracted
1687 to create a *DESeq2* object from which*ESeq2 sizeFactors* were calculated and centered. These *sizeFactors*
1688 were used to normalize the *C. concisus DESeq2* object prior to differential expression testing (Wald test).
1689 To facilitate comparison of gene expression between the *in vivo* and *in vitro* experimental
1690 conditions, reads from housekeeping genes (*rpoA, gyrB, recA, dnaK, atpA*) were extracted; the geometric
1691 mean of these five housekeeping genes was calculated per sample and centered for the *DESeq2*
1692 *sizeFactors* in a manner analogous to the ERCC spike-in control.
1693
1694 ***C. concisus* co-culture with mouse immune cells**
1695 Conventionally raised 8-12 week old female wild-type C57Bl6/J or *Nos2*$^{-/-}$ (B6.129P2-*Nos2*^{tm1Lau}/J) mice
1696 fed standard mouse diet (LabDiet 5010) were euthanized. Femurs were collected and placed into RPMI
1697 1640 supplemented with 2 mM L-glutamine and 10% FBS and kept on ice. Bone marrow was extracted
1698 from each femur by centrifugation and resuspended in 1 mL RPMI. Briefly, femurs were placed vertically
1699 into a 0.65 mL snap-top tube (Avant 2924) with a puncture hole created by an 18 gauge needle. The tube
1700 was placed within a 1.5 mL microcentrifuge tube (Eppendorf) and samples were centrifuged >10,000 x *g*

1701 for 15 seconds. Bone marrow cells were resuspended in RPMI and pooled between mice (n=2
1702 animals/genotype per experiment) and 200 µL aliquots were placed into wells of a 24-well tissue culture
1703 plate. Live *C. concisus* cultures grown anaerobically in Bolton broth for 24 hours or heat-killed at 100 ºC
1704 for 2.5 hours 400 µl was added to each well containing bone marrow from WT or iNOS$^{-/-}$ mice. Cells
1705 were cultured under an atmosphere of 5% CO_2 at 37 ºC for 48 hours. Tissue culture plates were
1706 centrifuged at 500 x *g* to pellet cells and collect cell supernatants, which were aliquoted into PCR plates
1707 and stored at -20 ºC. Cell pellets were washed with 1 mL PBS, centrifuged at 1000 x *g*, and stored at -20
1708 ºC until protein extraction and quantification.
1709 ***Quantification of cytokines with ELISAs*** – Bone marrow cell supernatants were thawed and
1710 cytokines were assayed using 50 µL of undiluted following the manufacturer's instructions (IL-1B,
1711 Abcam 197742; IL-17, Abcam 199081; IL-22, Abcam 223857; IL-5, Abcam 204523; TNFa, Abcam
1712 208348; MAPK signaling, Invitrogen, 85-86195-11). To quantify levels of iNOS in bone marrow cell
1713 pellets, protein was extracted using the cell lysis buffer provided in the iNOS ELISA kit (Abcam
1714 253219). The cell extract was diluted 1:3 to quantify protein concentration using the Micro BCA Protein
1715 Assay Kit (Thermo Scientific 23235). 50 µL of cell extract was used quantify iNOS following
1716 instructions provided with the ELISA kit; final iNOS concentration was normalized to total protein
1717 concentration.
1718
1719
1720
1721 **REFERENCES**

1722 1. Lindenbaum, J., Kent, T. H. & Sprinz, H. Malabsorption and jejunitis in American Peace Corps
1723 volunteers in Pakistan. *Annals of internal medicine* **65**, 1201–1209 (1966).

1724 2. Chen, R. Y. *et al.* Duodenal microbiota in stunted undernourished children with enteropathy. *New*
1725 *England Journal of Medicine* **383**, 321–333 (2020).

1726 3. Hossain, Md. S. *et al.* Environmental enteric dysfunction and small intestinal histomorphology of
1727 stunted children in Bangladesh. *PLOS Neglected Trop. Dis.* **17**, e0010472 (2023).

1728 4. Owino, V. *et al.* Environmental enteric dysfunction and growth failure/stunting in global child health.
1729 *Pediatrics* **138**, e20160641 (2016).

1730 5. Cowardin, C. A. *et al.* Environmental enteric dysfunction: gut and microbiota adaptation in pregnancy
1731 and infancy. *Nature Reviews Gastroenterology and Hepatology* **20**, 223–237 (2022).

1732 6. Martorell, R. & Zongrone, A. Intergenerational influences on child growth and undernutrition.
1733 *Paediatric and Perinatal Epidemiology* **26**, 302–314 (2012).

1734 7. Ramakrishnan, U., Martorell, R., Schroeder, D. G. & Flores, R. Role of intergenerational effects on
1735 linear growth. *Symposium: Causes and etiology of stunting role of intergenerational effects on linear*
1736 *growth* **129**, 544–549 (1999).

1737 8. Soliman, A. *et al.* Early and long-term consequences of nutritional stunting: From childhood to
1738 adulthood. *Acta Bio Med.* **92**, e2021168 (2021).

1739 9. Coley, E. J. L. & Hsiao, E. Y. Malnutrition and the microbiome as modifiers of early
1740 neurodevelopment. *Trends in Neurosciences* **44**, 753–764 (2021).

1741 10. Yan, X., Zhao, X., Li, J., He, L. & Xu, M. Effects of early-life malnutrition on neurodevelopment and
1742 neuropsychiatric disorders and the potential mechanisms. *Progress in Neuro-Psychopharmacology and*
1743 *Biological Psychiatry* **83**, 64–75 (2018).

1744 11. Georgieff, M. K., Ramel, S. E. & Cusick, S. E. Nutritional influences on brain development. *Acta*
1745 *Paediatrica* **107**, 1310–1321 (2018).

1746 12. Lunn, P. G., Northrop-Clewes, C. A. & Downes, R. M. Intestinal permeability, mucosal injury, and
1747 growth faltering in Gambian infants. *The Lancet* **338**, 907–910 (1991).

1748 13. Campbell, D. I., Elia, M. & Lunn, P. G. Growth faltering in rural Gambian infants is associated with
1749 impaired small intestinal barrier function, leading to endotoxemia and systemic inflammation. *Journal of*
1750 *Nutrition* **133**, 1332–1338 (2003).

1751 14. Harper, K. M., Mutasa, M., Prendergast, A. J., Humphrey, J. & Manges, A. R. Environmental enteric
1752 dysfunction pathways and child stunting: A systematic review. *PLoS Neglected Tropical Diseases* **12**,
1753 e00062051 (2018).

1754 15. Mahfuz, M. *et al.* Bangladesh Environmental Enteric Dysfunction (BEED) study: Protocol for a
1755 community-based intervention study to validate non-invasive biomarkers of environmental enteric
1756 dysfunction. *BMJ Open* **7**, e017768 (2017).

1757 16. Bhattacharjee, A. *et al.* Environmental enteric dysfunction induces regulatory T cells that inhibit local
1758 CD4 + T cell responses and impair oral vaccine efficacy. *Immunity* **54**, 1–13 (2021).

1759 17. Malique, A. *et al.* NAD+ precursors and bile acid sequestration treat preclinical refractory
1760 environmental enteric dysfunction. *Sci. Transl. Med.* **16**, eabq4145 (2024).

1761 18. Perruzza, L. *et al.* Protection from environmental enteric dysfunction and growth improvement in
1762 malnourished newborns by amplification of secretory IgA. *Cell Rep. Med.* **5**, 101639 (2024).

1763 19. Salameh, E. *et al.* Modeling undernutrition with enteropathy in mice. *Sci. Rep.* **10**, 15581 (2020).

1764 20. Klune, C. B., Jin, B. & DeNardo, L. A. Linking mPFC circuit maturation to the developmental
1765 regulation of emotional memory and cognitive flexibility. *eLife* **10**, e64567 (2021).

1766 21. Semba, R. D. *et al.* Environmental enteric dysfunction is associated with carnitine deficiency and
1767 altered fatty acid oxidation. *EBioMedicine* **17**, 57–66 (2017).

1768 22. Lemons, J. M. S. *et al.* Enterobacteriaceae growth promotion by intestinal acylcarnitines, a biomarker
1769 of dysbiosis in inflammatory bowel disease. *Cell. Mol. Gastroenterol. Hepatol.* **17**, 131–148 (2024).

1770 23. Dambrova, M. *et al.* Acylcarnitines: Nomenclature, biomarkers, therapeutic potential, drug targets,
1771 and clinical trials. *Pharmacol. Rev.* **74**, 506–551 (2022).

1772 24. Rutkowsky, J. M. *et al.* Acylcarnitines activate proinflammatory signaling pathways. *Am. J. Physiol.-*
1773 *Endocrinol. Metab.* **306**, E1378–E1387 (2014).

1774 25. Veitch, A. M., Kelly, P., Zulu, I. S., Segal, I. & Farthing, M. J. G. Tropical enteropathy: A T-cell-
1775 mediated crypt hyperplastic enteropathy. *European Journal of Gastroenterology and Hepatology* **13**,
1776 1175–1181 (2001).

1777 26. Liu, T. C. *et al.* A novel histological index for evaluation of environmental enteric dysfunction
1778 identifies geographic-specific features of enteropathy among children with suboptimal growth. *PLoS*
1779 *Neglected Tropical Diseases* **14**, 1–21 (2020).

1780 27. Mulenga, C. *et al.* Epithelial abnormalities in the small intestine of Zambian children with stunting.
1781 *Front. Med.* **9**, 849677 (2022).

1782 28. Lee, C. S. *et al.* Boosting apoptotic cell clearance by colonic epithelial cells attenuates inflammation
1783 in vivo. *Immunity* **44**, 807–820 (2016).

1784 29. Shankman, L. S. *et al.* Efferocytosis by Paneth cells within the intestine. *Current Biology* **31**, 2469-
1785 2476.e5 (2021).

1786 30. Mehrotra, P. & Ravichandran, K. S. Drugging the efferocytosis process: concepts and opportunities.
1787 *Nature Reviews Drug Discovery* **21**, 601–620 (2022).

1788 31. Anderson, C. J. *et al.* Microbes exploit death-induced nutrient release by gut epithelial cells. *Nature*
1789 **596**, 262–267 (2021).

1790 32. Morioka, S. *et al.* Efferocytosis induces a novel SLC program to promote glucose uptake and lactate
1791 release. *Nature* **563**, 714–718 (2018).

1792 33. Perry, J. S. A. *et al.* Interpreting an apoptotic corpse as anti-inflammatory involves a chloride sensing
1793 pathway. *Nature Cell Biology* **21**, 1532–1543 (2019).

1794 34. Maschalidi, S. *et al.* Targeting SLC7A11 improves efferocytosis by dendritic cells and wound healing
1795 in diabetes. *Nature* **606**, 776–784 (2022).

1796 35. Browaeys, R., Saelens, W. & Saeys, Y. NicheNet: modeling intercellular communication by linking
1797 ligands to target genes. *Nature Methods* **17**, 159–162 (2020).

1798 36. Guilliams, M. *et al.* Spatial proteogenomics reveals distinct and evolutionarily conserved hepatic
1799 macrophage niches. *Cell* **185**, 379-396.e38 (2022).

1800 37. Takahashi, T. & Shiraishi, A. Stem cell signaling pathways in the small intestine. *International*
1801 *Journal of Molecular Sciences* **21**, 2032 (2020).

1802 38. Vanuytsel, T., Senger, S., Fasano, A. & Shea-Donohue, T. Major signaling pathways in intestinal
1803 stem cells. *Biochimica et Biophysica Acta - General Subjects* **1830**, 2410–2426 (2013).

1804 39. Yu, X. M. *et al.* Wnt5a inhibits hypoxia-induced pulmonary arterial smooth muscle cell proliferation
1805 by downregulation of β-catenin. *American Journal of Physiology - Lung Cellular and Molecular*
1806 *Physiology* **304**, L103–L111 (2013).

1807 40. Zhang, L. *et al.* Isolation and detection of *Campylobacter concisus* from saliva of healthy individuals
1808 and patients with inflammatory bowel disease. *Journal of Clinical Microbiology* **48**, 2965–2967 (2010).

1809 41. Liu, F., Ma, R., Wang, Y. & Zhang, L. The clinical importance of *Campylobacter concisus* and other
1810 human hosted Campylobacter species. *Frontiers in Cellular and Infection Microbiology* **8**, 243 (2018).

1811 42. Kirk, K. F., Nielsen, H. L., Thorlacius-Ussing, O. & Nielsen, H. Optimized cultivation of
1812 *Campylobacter concisus* from gut mucosal biopsies in inflammatory bowel disease. *Gut Pathogens* **8**, 27
1813 (2016).

1814 43. Vielkind, P., Jentsch, H., Eschrich, K., Rodloff, A. C. & Stingu, C.-S. Prevalence of *Actinomyces spp*.
1815 in patients with chronic periodontitis. *Int. J. Méd. Microbiol.* **305**, 682–688 (2015).

1816 44. Iablokov, S. N., Novichkov, P. S., Osterman, A. L. & Rodionov, D. A. Binary metabolic phenotypes
1817 and phenotype diversity metrics for the functional characterization of microbial communities. *Frontiers in*
1818 *Microbiology* **12**, 653314 (2021).

1819 45. Zhang, Y. *et al.* Neutrophil infiltration leads to fetal growth restriction by impairing the placental
1820 vasculature in DENV-infected pregnant mice. *eBioMedicine* **95**, 104739 (2023).

1821 46. Göhring, K. *et al.* Neutrophil CD177 (NB1 gp, HNA-2a) expression is increased in severe bacterial
1822 infections and polycythaemia vera. *Br. J. Haematol.* **126**, 252–254 (2004).

1823 47. Nattramilarasu, P. K., Sá, F. D. L. de, Schulzke, J. D. & Bücker, R. Immune-mediated aggravation of
1824 the *Campylobacter concisus*-induced epithelial barrier dysfunction. *International Journal of Molecular*
1825 *Sciences* **22**, 2043 (2021).

1826 48. Aagaard, M. E. Y., Kirk, K. F., Nielsen, H. L., Steffensen, R. & Nielsen, H. *Campylobacter concisus*
1827 from chronic inflammatory bowel diseases stimulates IL-8 production in HT-29 cells. *Gut Pathogens* **15**,
1828 5 (2023).

1829 49. Mahendran, V. *et al.* The prevalence and polymorphisms of zonula occluden toxin gene in multiple
1830 *Campylobacter concisus* strains isolated from saliva of patients with inflammatory bowel disease and
1831 controls. *PLoS ONE* **8**, e77525 (2013).

1832 50. Liu, B., Zheng, D., Zhou, S., Chen, L. & Yang, J. VFDB 2022: a general classification scheme for
1833 bacterial virulence factors. *Nucleic Acids Res.* **50**, D912–D917 (2021).

1834 51. Kirk, K. F. *et al.* Molecular epidemiology and comparative genomics of *Campylobacter concisus*
1835 strains from saliva, faeces and gut mucosal biopsies in inflammatory bowel disease. *Sci. Rep.* **8**, 1902
1836 (2018).

1837 52. Liu, F. *et al.* Analysis of complete *Campylobacter concisus* genomes identifies genomospecies
1838 features, secretion systems and novel plasmids and their association with severe ulcerative colitis. *Microb.*
1839 *Genom.* **6**, mgen000457 (2020).

1840 53. Khangulov, S. V., Gladyshev, V. N., Dismukes, G. C. & Stadtman, T. C. Selenium-containing
1841 formate dehydrogenase H from *Escherichia coli*: A molybdopterin enzyme that catalyzes formate
1842 oxidation without oxygen transfer. *Biochemistry* **37**, 3518–3528 (1998).

1843 54. Yeow, M. *et al.* Analyses of energy metabolism and stress defense provide insights into
1844 *Campylobacter concisus* growth and pathogenicity. *Gut Pathogens* **12**, 13 (2020).

1845 55. Litvak, Y., Byndloss, M. X. & Bäumler, A. J. Colonocyte metabolism shapes the gut microbiota.
1846 *Science* **362**, eaat9076 (2018).

1847 56. Rivera-Chávez, F. & Bäumler, A. J. The pyromaniac inside you: *Salmonella* metabolism in the host
1848 gut. *Annual Review of Microbiology* **69**, 31–48 (2015).

1849 57. Rivera-Chávez, F. *et al.* Energy taxis toward host-derived nitrate supports a *Salmonella* pathogenicity
1850 island 1-independent mechanism of invasion. *mBio* **7**, e00960-16 (2016).

1851 58. Winter, S. E. *et al.* Host-derived nitrate boosts growth of *E. coli* in the inflamed gut. *Science* **339**,
1852 708–711 (2013).

1853 59. Faber, F. *et al.* Host-mediated sugar oxidation promotes post-antibiotic pathogen expansion. *Nature*
1854 **534**, 697–699 (2016).

1855 60. McCall, T. B., Feelisch, M., Palmer, R. M. J. & Moncada, S. Identification of N-iminoethyl-l-
1856 ornithine as an irreversible inhibitor of nitric oxide synthase in phagocytic cells. *Br. J. Pharmacol.* **102**,
1857 234–238 (1991).

1858 61. Huang, Y., Suyemoto, M., Garner, C. D., Cicconi, K. M. & Altier, C. Formate acts as a diffusible
1859 signal to induce *Salmonella* invasion. *J. Bacteriol.* **190**, 4233–4241 (2008).

1860 62. Wang, K.-C., Lerche, M. H., Ardenkjær-Larsen, J. H. & Jensen, P. R. Formate metabolism in *Shigella*
1861 *flexneri* and its effect on HeLa cells at different stages during the infectious process. *Microbiol. Spectr.*
1862 **11**, e00631-22 (2023).

1863 63. Kassem, I. I., Candelero-Rueda, R. A., Esseili, K. A. & Rajashekara, G. Formate simultaneously
1864 reduces oxidase activity and enhances respiration in *Campylobacter jejuni*. *Sci. Rep.* **7**, 40117 (2017).

1865 64. Rogawski, E. T. *et al.* Use of quantitative molecular diagnostic methods to investigate the effect of
1866 enteropathogen infections on linear growth in children in low-resource settings: longitudinal analysis of
1867 results from the MAL-ED cohort study. *The Lancet Global Health* **6**, e1319–e1328 (2018).

1868 65. Vonaesch, P. *et al.* Stunted children display ectopic small intestinal colonization by oral bacteria,
1869 which cause lipid malabsorption in experimental models. *Proceedings of the National Academy of*
1870 *Sciences* **119**, e2209589119 (2022).

1871 66. Vonaesch, P. *et al.* Stunted childhood growth is associated with decompartmentalization of the
1872 gastrointestinal tract and overgrowth of oropharyngeal taxa. *Proceedings of the National Academy of*
1873 *Sciences of the United States of America* **115**, E8489–E8498 (2018).

1874 67. Dinh, D. M. *et al.* Longitudinal analysis of the intestinal microbiota in persistently stunted young
1875 children in south India. *PLoS ONE* **11**, e0155405 (2016).

1876 68. Hossain, M. S. *et al.* Alterations in the histological features of the intestinal mucosa in malnourished
1877 adults of Bangladesh. *Scientific Reports* **11**, 2355 (2021).

1878 69. Fahim, S. M. *et al.* Evidence of gut enteropathy and factors associated with undernutrition among
1879 slum-dwelling adults in Bangladesh. *American Journal of Clinical Nutrition* **111**, 657–666 (2020).

1880 70. Acosta, A. M. *et al.* Relationship between growth and illness, enteropathogens and dietary intakes in
1881 the first 2 years of life: Findings from the MAL-ED birth cohort study. *BMJ Global Health* **2**, e000370
1882 (2017).

1883 71. Bankhead, P. *et al.* QuPath: Open source software for digital pathology image analysis. *Scientific*
1884 *Reports* **7**, 16878 (2017).

1885 72. Rieger, M. A. & Dougherty, J. D. Analysis of within subjects variability in mouse ultrasonic
1886 vocalization: Pups exhibit inconsistent, state-like patterns of call production. *Front. Behav. Neurosci.* **10**,
1887 182 (2016).

1888 73. Barnes, T. D., Rieger, M. A., Dougherty, J. D. & Holy, T. E. Group and individual variability in
1889 mouse pup isolation calls recorded on the same day show stability. *Front. Behav. Neurosci.* **11**, 243
1890 (2017).

1891 74. Kolmogorov, M. *et al.* metaFlye: scalable long-read metagenome assembly using repeat graphs.
1892 *Nature Methods* **17**, 1103–1110 (2020).

1893 75. Parks, D. H., Imelfort, M., Skennerton, C. T., Hugenholtz, P. & Tyson, G. W. CheckM: Assessing the
1894 quality of microbial genomes recovered from isolates, single cells, and metagenomes. *Genome Research*
1895 **25**, 1043–1055 (2015).

1896 76. Wu, Y. W., Simmons, B. A. & Singer, S. W. MaxBin 2.0: An automated binning algorithm to recover
1897 genomes from multiple metagenomic datasets. *Bioinformatics* **32**, 605–607 (2016).

1898 77. Nayfach, S., Shi, Z. J., Seshadri, R., Pollard, K. S. & Kyrpides, N. C. New insights from uncultivated
1899 genomes of the global human gut microbiome. *Nature* **568**, 505–510 (2019).

1900 78. Olm, M. R., Brown, C. T., Brooks, B. & Banfield, J. F. DRep: A tool for fast and accurate genomic
1901 comparisons that enables improved genome recovery from metagenomes through de-replication. *ISME*
1902 *Journal* **11**, 2864–2868 (2017).

1903 79. Mikheenko, A., Saveliev, V. & Gurevich, A. MetaQUAST: Evaluation of metagenome assemblies.
1904 *Bioinformatics* **32**, 1088–1090 (2016).

1905 80. Chaumeil, P. A., Mussig, A. J., Hugenholtz, P. & Parks, D. H. GTDB-Tk: A toolkit to classify
1906 genomes with the genome taxonomy database. *Bioinformatics* **36**, 1925–1927 (2020).

1907 81. Olson, R. D. *et al.* Introducing the Bacterial and Viral Bioinformatics Resource Center (BV-BRC): A
1908 resource combining PATRIC, IRD and ViPR. *Nucleic acids research* **51**, D678–D689 (2023).

1909 82. Letunic, I. & Bork, P. Interactive tree of life (iTOL) v5: An online tool for phylogenetic tree display
1910 and annotation. *Nucleic Acids Research* **49**, W293–W296 (2021).

1911 83. Stämmler, F. *et al.* Adjusting microbiome profiles for differences in microbial load by spike-in
1912 bacteria. *Microbiome* **4**, 28–13 (2016).

1913 84. Wolf, A. R. *et al.* Bioremediation of a common product of food processing by a human gut bacterium.
1914 *Cell Host and Microbe* **26**, 463-477.e8 (2019).

1915 85. McNulty, N. P. *et al.* The impact of a consortium of fermented milk strains on the gut microbiome of
1916 gnotobiotic mice and monozygotic twins. *Science Translational Medicine* **3**, 106ra106 (2011).

1917 86. Langmead, B. & Salzberg, S. L. Fast gapped-read alignment with Bowtie 2. *Nature Methods* **9**, 357–
1918 359 (2012).

1919 87. Kolmogorov, M., Yuan, J., Lin, Y. & Pevzner, P. A. Assembly of long, error-prone reads using repeat
1920 graphs. *Nature Biotechnology* **37**, 540–546 (2019).

1921 88. Seemann, T. Prokka: Rapid prokaryotic genome annotation. *Bioinformatics* **30**, 2068–2069 (2014).

1922 89. Kanehisa, M., Sato, Y. & Morishima, K. BlastKOALA and GhostKOALA: KEGG tools for
1923 functional characterization of genome and metagenome sequences. *Journal of Molecular Biology* **428**,
1924 726–731 (2016).

1925 90. Overbeek, R. *et al.* The subsystems approach to genome annotation and its use in the project to
1926 annotate 1000 genomes. *Nucleic Acids Research* **33**, 5691–5702 (2005).

1927 91. Aziz, R. K. *et al.* SEED servers: High-performance access to the SEED genomes, annotations, and
1928 metabolic models. *PLoS ONE* **7**, e48053 (2012).

1929 92. Rodionov, D. A. *et al.* Micronutrient requirements and sharing capabilities of the human gut
1930 microbiome. *Frontiers in Microbiology* **10**, 1316 (2019).

1931 93. Ashniev, G. A., Petrov, S. N., Iablokov, S. N. & Rodionov, D. A. Genomics-based reconstruction and
1932 predictive profiling of amino acid biosynthesis in the human gut microbiome. *Microorganisms* **10**, 740
1933 (2022).

1934 94. Frolova, M. S., Suvorova, I. A., Iablokov, S. N., Petrov, S. N. & Rodionov, D. A. Genomic
1935 reconstruction of short-chain fatty acid production by the human gut microbiota. *Frontiers in Molecular*
1936 *Biosciences* **9**, 949563 (2022).

1937 95. Hibberd, M. C. *et al.* Bioactive glycans in a microbiome-directed food for malnourished children.
1938 *Nature* **In press**, (2023).

1939 96. Bray, N. L., Pimentel, H., Melsted, P. & Pachter, L. Near-optimal probabilistic RNA-seq
1940 quantification. *Nature Biotechnology* **34**, 525–527 (2016).

1941 97. Soneson, C., Love, M. I. & Robinson, M. D. Differential analyses for RNA-seq: Transcript-level
1942 estimates improve gene-level inferences. *F1000Research* **4**, 1521 (2016).

1943 98. Durinck, S., Spellman, P. T., Birney, E. & Huber, W. Mapping identifiers for the integration of
1944 genomic datasets with the R/ Bioconductor package biomaRt. *Nature Protocols* **4**, 1184–1191 (2009).

1945 99. Law, C. W., Chen, Y., Shi, W. & Smyth, G. K. Voom: Precision weights unlock linear model analysis
1946 tools for RNA-seq read counts. *Genome Biology* **15**, R29 (2014).

1947 100. Ritchie, M. E. *et al.* Limma powers differential expression analyses for RNA-sequencing and
1948 microarray studies. *Nucleic Acids Research* **43**, e47 (2015).

1949 101. Yu, G., Wang, L. G., Han, Y. & He, Q. Y. ClusterProfiler: An R package for comparing biological
1950 themes among gene clusters. *OMICS A Journal of Integrative Biology* **16**, 284–287 (2012).

1951 102. Chang, H.-W. *et al. Prevotella copri* and microbiota members mediate the beneficial effects of a
1952 therapeutic food for malnutrition. *Nat. Microbiol.* **9**, 922–937 (2024).

1953 103. Fleming, S. J., Marioni, J. C. & Babadi, M. CellBender remove-background: A deep generative
1954 model for unsupervised removal of background noise from scRNA-seq datasets. *bioRxiv* (2019)
1955 doi:10.1101/791699.

1956 104. Hao, Y. *et al.* Integrated analysis of multimodal single-cell data. *Cell* **184**, 3573–3587 (2021).

1957 105. Hafemeister, C. & Satija, R. Normalization and variance stabilization of single-cell RNA-seq data
1958 using regularized negative binomial regression. *Genome Biology* **20**, 296 (2019).

1959 106. Choudhary, S. & Satija, R. Comparison and evaluation of statistical error models for scRNA-seq.
1960 *Genome Biology* **23**, 27 (2022).

1961 107. McGinnis, C. S., Murrow, L. M. & Gartner, Z. J. DoubletFinder: Doublet detection in single-cell
1962 RNA-sequencing data using artificial nearest neighbors. *Cell Systems* **8**, 329-337.e4 (2019).

1963 108. Moor, A. E. *et al.* Spatial reconstruction of single enterocytes uncovers broad zonation along the
1964 intestinal villus axis. *Cell* **175**, 1156–1167 (2018).

1965 109. Amezquita, R. A. *et al.* Orchestrating single-cell analysis with Bioconductor. *Nature Methods* **17**,
1966 137–145 (2020).

1967 110. Aran, D. *et al.* Reference-based analysis of lung single-cell sequencing reveals a transitional
1968 profibrotic macrophage. *Nature Immunology* **20**, 163–172 (2019).

1969 111. Love, M. I., Huber, W. & Anders, S. Moderated estimation of fold change and dispersion for RNA-
1970 seq data with DESeq2. *Genome biology* **15**, 550 (2014).

1971 112. Street, K. *et al.* Slingshot: cell lineage and pseudotime inference for single-cell transcriptomics.
1972 *BMC Genomics* **19**, 477 (2018).

1973 113. Scrucca, L., Fop, M., Murphy, B. T. & Raftery, A. E. Mclust 5: clustering, classification, and density
1974 estimation using gaussian finite mixture models. *The R Journal* **8**, 289–317 (2016).

1975 114. Berge, K. V. den *et al.* Trajectory-based differential expression analysis for single-cell sequencing
1976 data. *Nature Communications* **11**, 1201 (2020).

1977 115. Mi, H. *et al.* Protocol update for large-scale genome and gene function analysis with the PANTHER
1978 classification system (v.14.0). *Nature Protocols* **14**, 703–721 (2019).

1979 116. Sun, D. *et al.* Identifying phenotype-associated subpopulations by integrating bulk and single-cell
1980 sequencing data. *Nature Biotechnology* **40**, 527–538 (2022).

1981 117. Eren, A. M. *et al.* Community-led, integrated, reproducible multi-omics with anvi'o. *Nat. Microbiol.*
1982 **6**, 3–6 (2021).

1983 118. Shaiber, A. *et al.* Functional and genetic markers of niche partitioning among enigmatic members of
1984 the human oral microbiome. *Genome Biol.* **21**, 292 (2020).

1985 119. Delmont, T. O. & Eren, A. M. Linking pangenomes and metagenomes: the Prochlorococcus
1986 metapangenome. *PeerJ* **6**, e4320 (2018).